

國立臺北大學統計學系
碩士論文

指導教授：陳秉洋 博士

以合成最佳化演算法生成加速壽命試驗之
模型辨識設計

Model Discrimination Design Generation
for Accelerated Life Testing Experiments
via Hybridized Optimization Algorithms

研究生：林貫原

中華民國 一 一 四 年 六 月

國立臺北大學碩士學位論文

考試委員會審定書

以合成最佳化演算法生成加速壽命試驗之模型辨識設計
Model Discrimination Design Generation for Accelerated Life Testing
Experiments via Hybridized Optimization Algorithms

本論文係 林貫原 於國立臺北大學統計學系完成之
碩士學位論文，於中華民國 114 年 6 月 6 日承下列考試委
員審查通過及口試合格，特此證明

論文考試委員簽名：

委員(召集人)

張升乾

委員(指導教授)

陳秉璋

委員

李宜真

委員

楊鈞樞

委員

系(所)主任簽名：

蘇南誠

國立臺北大學一一三學年度第二學期碩士學位論文提要

論文題目: 以合成最佳化演算法生成加速壽命試驗之模型辨識設計

論文頁數: 115

所組別: 統計學系碩士班 系(所) 組(學號: 711233119)

研究生: 林貫原 指導教授: 陳秉洋

論文提要內容: 本研究旨在探討加速壽命試驗中，當存在多個候選模型可描述產品失效機制時，如何建構最適模型辨識設計。在此，於實驗設計的考量上，相較於對各候選模型參數的精準估計，如何能夠有效區分模型，確保所選模型貼近產品真實的失效機制，應為首要目標。加速壽命試驗透過施加高於正常使用條件的應力，以加速產品失效並在有限時間內取得壽命資料。然而，儘管進行加速，試驗結束時仍可能有樣本未發生失效，導致資料中出現設限現象。此類設限資料的特性，在既有模型辨識實驗設計的文獻中尚缺乏系統性的探討。本研究首先探討在樣本可能為設限資料的情況下，如何建構最適模型辨識準則，基於改良後的 Kullback-Leibler 散度、Lin-Wong 散度、Chi-Square 距離與 Bhattacharyya 距離，提出 CKL-、CLW-、 $C\chi^2$ - 及 CB-最適模型辨識設計準則，以因應不同資料特性與應用需求。另外，由於設計準則之數學結構複雜且為最大最小化的巢狀優化問題，不易推導最適設計之封閉解，本研究結合粒子群優化與梯度下降優化方法，構建一套高效的數值搜尋演算法，以尋找具最大模型辨識效力的實驗配置。為驗證方法之穩定性與有效性，本研究舉可靠度研究中常用的失效模型為案例進行數值實驗，考慮不同情境的失效機制與機率分布假設之候選模型，比較所提出之各種設計準則之模型辨識設計結果及效果，期望為後續可靠度試驗的實驗設計提供理論依據與實務參考。

關鍵詞: 模型辨識設計、加速壽命試驗模型、粒子群優化演算法

ABSTRACT

MODEL DISCRIMINATION DESIGN GENERATION FOR ACCELERATED LIFE TESTING EXPERIMENTS VIA HYBRIDIZED OPTIMIZATION ALGORITHMS

by

LIN, KUAN-YUAN

June 2025

ADVISOR: Dr. CHEN, PING-YANG

DEPARTMENT: DEPARTMENT OF STATISTICS

MAJOR: STATISTICS

DEGREE: MASTER OF SCIENCE

This study aims to investigate the construction of optimal model discrimination designs in Accelerated Life Testing (ALT) when multiple candidate models are available to describe the product's failure mechanism. In this context, rather than focusing on the precise estimation of parameters within each candidate model, the primary objective of experimental design should be to effectively distinguish between competing models and ensure that the selected model closely reflects the true underlying failure behavior of the product. Accelerated Life Testing accelerates product failure by applying stress levels beyond normal use conditions, thereby enabling lifespan data to be collected within a limited timeframe. However, even under such accelerated conditions, some units may not fail by the end of the test, resulting in Type I censored data. The presence of censoring introduces unique data characteristics that have not been systematically addressed in the existing literature on model discrimination design. To address this gap, the present study first explores how to construct optimal model discrimination criteria under the possibility of Type I censored observations. Based on modified forms of Kullback–Leibler divergence, Lin–Wong divergence, Chi-square distance, and Bhattacharyya distance, we propose four new design criteria tailored for model discrim-

ination under censoring: the CKL-, CLW-, $C\chi^2$ -, and CB-optimal criteria. These criteria are designed to accommodate varying data characteristics and practical application needs. Due to the mathematical complexity of the proposed design criteria, each involving a nested max – min optimization problem, deriving closed-form solutions is generally intractable. To this end, we develop a computationally efficient numerical algorithm that combines Particle Swarm Optimization with gradient-based optimization methods to search for the optimal model discrimination designs. To validate the effectiveness of the proposed approach, we conduct numerical studies using commonly adopted failure models in reliability research. Through various scenarios of failure behavior and underlying probability distribution assumption of the candidate models, we show for each proposed criterion the resulting model discrimination designs and discuss their performances. The results are intended to provide both theoretical guidance and practical reference for experimental planning in future reliability studies.

KEY WORDS: Model Discrimination Design, Accelerated Life Testing Model, Particle Swarm Optimization



Contents

1	Introduction	1
2	Literature Review	5
2.1	Accelerated Life Testing	5
2.2	Model Discrimination Design	11
2.3	Numerical Methods in Finding Model Discrimination De- signs	14
2.4	Existing Approach of Model Discrimination Design for ALT	18
3	Methodology	27
3.1	KL-optimal Criterion	28
3.2	Model Discrimination Criteria for Type I Censored Data . .	33
3.3	Numerical Integration for Criterion Computation	37
3.4	The PSO-QN Algorithm for Model Discrimination Design Generation	38
4	Numerical Studies	41
4.1	The Comparison of Integration Methods via non-Censored Example	41
4.2	Type I Censoring Model Discrimination Designs with Fixed Variance for Rival Model	52

4.3	Type I Censoring Model Discrimination Designs with Parameterized Variance for Rival Model	62
4.3.1	Competing Mean Responses, Equal Distribution Assumption with Parameterized Variance	62
4.3.2	Equal Mean Response, Competing Distribution Assumptions with Stress-Dependent Variance	68
5	Conclusion and Future Works	73
5.1	Summary and Key Contributions	73
5.2	Limitations and Future Directions	75
	References	77
A	The Directional Derivative Plots of the Resulting Model Discrimination Designs	81
B	R Implementation Example	97
C	Demonstration of the Shiny Interface	107

List of figure

2.1	PSO velocity components visualization	17
2.2	PSO concept diagram	18
2.3	Conceptual diagram of Accelerated Life Testing (Nasir and Pan, 2015)	20
4.1	The directional derivative plots of the resulting designs discriminating for the MMM vs. MM case assuming Log-Normal response.	46
4.2	The directional derivative plots of the resulting designs discriminating for the MMM vs. MM case assuming Weibull response.	51
4.3	The directional derivative plots of the resulting designs ξ_{CKL}^* discriminating for the cases of Quadratic vs. Linear means assuming Log-Normal response.	64
4.4	The directional derivative plots of the resulting designs ξ_{CKL}^* discriminating for the cases of Quadratic vs. Linear means assuming Weibull response.	65
A.1	The directional derivative plots of the resulting ξ_{CKL}^* designs discriminating for cases of Quadratic vs. Linear means with equal variance. Results are shown in Table 4.1	82

A.2	The directional derivative plots of the resulting ξ_{CKL}^* designs discriminating for cases of Quadratic vs. Linear means with unequal variance assuming Log-Normal response. Results are shown in Table 4.2.	83
A.3	The directional derivative plots of the resulting ξ_{CKL}^* designs discriminating for cases of Quadratic vs. Linear means with unequal variance assuming Weibull response. Results are shown in Table 4.2.	84
A.4	The directional derivative plots of the resulting ξ_{CLW}^* designs discriminating for cases of Quadratic vs. Linear means with equal variance. Results are shown in Table 4.3.	85
A.5	The directional derivative plots of the resulting ξ_{CLW}^* designs discriminating for cases of Quadratic vs. Linear means with unequal variance assuming Log-Normal response. Results are shown in Table 4.4.	86
A.6	The directional derivative plots of the resulting ξ_{CLW}^* designs discriminating for cases of Quadratic vs. Linear means with unequal variance assuming Weibull response. Results are shown in Table 4.4.	87
A.7	The directional derivative plots of the resulting ξ_{CB}^* designs discriminating for cases of Quadratic vs. Linear means with equal variance. Results are shown in Table 4.5.	88
A.8	The directional derivative plots of the resulting ξ_{CB}^* designs discriminating for cases of Quadratic vs. Linear means with unequal variance assuming Log-Normal response. Results are shown in Table 4.6.	89

A.9	The directional derivative plots of the resulting ξ_{CB}^* designs discriminating for cases of Quadratic vs. Linear means with unequal variance assuming Weibull response. Results are shown in Table 4.6.	90
A.10	The directional derivative plots of the resulting $\xi_{C\chi^2}^*$ designs discriminating for cases of Quadratic vs. Linear means with equal variance. Results are shown in Table 4.7.	91
A.11	The directional derivative plots of the resulting $\xi_{C\chi^2}^*$ designs discriminating for cases of Quadratic vs. Linear means with unequal variance assuming Log-Normal response. Results are shown in Table 4.8.	92
A.12	The directional derivative plots of the resulting $\xi_{C\chi^2}^*$ designs discriminating for cases of Quadratic vs. Linear means with unequal variance assuming Weibull response. Results are shown in Table 4.8.	93
A.13	The directional derivative plots of the resulting ξ_{CKL}^* designs for Meeker cases, under the same mean response structure but assuming the true model follows a Log-Normal distribution with variance depending on stress. Results are shown in Table 4.12.	94
A.14	The directional derivative plots of the resulting ξ_{CKL}^* designs for Meeker cases, under the same mean response structure but assuming the true model follows a Weibull distribution with variance depending on stress. Results are shown in Table 4.12.	95
B.1	Directional derivative plot generated from the example code to verify design optimality	106
C.1	Overview of the main User Interface panel	108

C.2	Divergence calculation method selection	109
C.3	Distribution assumption selection	109
C.4	Algorithm configuration options	110
C.5	Summary table of User-Defined settings	112
C.6	Censoring threshold configuration	112
C.7	Selection of divergence criteria in Arrhenius tab	113
C.8	Model distribution options in Meeker tab	113



List of table

4.1	Summary of CKL-optimal design results for cases of Quadratic vs. Linear means under with equal variance	58
4.2	Summary of CKL-optimal design results for cases of Quadratic vs. Linear means under with unequal variance	58
4.3	Summary of CLW-optimal design results for cases of Quadratic vs. Linear means under with equal variance	59
4.4	Summary of CLW-optimal design results for cases of Quadratic vs. Linear means under with unequal variance	59
4.5	Summary of CB-optimal design results for cases of Quadratic vs. Linear means under with equal variance	60
4.6	Summary of CB-optimal design results for cases of Quadratic vs. Linear means under with unequal variance	60
4.7	Summary of $C\chi^2$ -optimal design results for cases of Quadratic vs. Linear means under with equal variance	61
4.8	Summary of $C\chi^2$ -optimal design results for cases of Quadratic vs. Linear means under with unequal variance	61
4.9	Comparison of design points, weights, and cumulative failure probabilities under different model assumptions ($\sigma = 0.9780103$)	67

4.10 Comparison of design points, weights, and cumulative failure probabilities under different model assumptions ($\sigma = 1.4780103$)	67
4.11 Simulation settings for Meeker cases including mean and dispersion parameters of the true and rival models	70
4.12 Summary of CKL-optimal design results for Meeker cases, under the same mean response structure but assuming the true model follows a Weibull distribution with variance depending on stress.	71



Chapter 1

Introduction

In the study of Accelerated Life Testing (ALT), the primary goal of experimental design has traditionally focused on improving the precision of parameter estimation—for instance, through the use of c -optimal design to minimize estimation variance. However, when multiple candidate life models are considered, focusing solely on parameter estimation may not suffice to ensure model adequacy. The core question addressed in this research is: how can an experiment be designed such that the data collected effectively discriminate among competing models and allow the selection of the one that best describes product failure behavior? This is the key challenge that model discrimination design aims to resolve.

Reliability testing plays a crucial role in product life analysis, and ALT accelerates the observation of failure events by applying stress conditions beyond normal usage (e.g., temperature, humidity, vibration). Most ALT models are based on the Arrhenius equation, which assumes an exponential relationship between stress (typically temperature) and failure time. However, in real-world applications, multiple structurally distinct models may appear plausible. As the actual failure mechanism

is not directly observable, designing experiments that help distinguish between these models becomes essential. Another practical issue arises from censoring. Even under accelerated stress conditions, some products may not fail within the study duration. As a result, a censoring time must be defined to limit the test duration while ensuring that the data remain informative. Hence, model discrimination design in ALT must also account for the presence of Type I censored observations when constructing design strategies.

Although model discrimination has been widely studied in other areas of statistics, its application in ALT remains limited. For instance, [Nasir and Pan \(2015\)](#) proposed a Bayesian-based model discrimination strategy using the Hellinger distance to measure model separability. However, their approach faces challenges in computational cost and result stability, and is limited to specific scenarios and criteria. To address this gap, we aim to extend model discrimination design within the ALT framework by incorporating the effects of Type I censored data.

Our first major contribution to this research is the proposal of four model discrimination design criteria—CKL-, CLW-, CB-, and $C\chi^2$ -optimal criteria—each based on a different divergence measures and adapted for use with Type I censored data. These criteria aim to improve the flexibility and accuracy of model selection under varied experimental conditions.

How to generate a model discrimination is another key to this research. Since the optimization problems involved are nested and generally lack closed-form expression of the objective function, we further propose an efficient hybrid search algorithm combining Particle Swarm Optimization (PSO) and the Newton-based approach such as the L-BFGS algorithm to enhance computational efficiency and convergence stability.

We demonstrate how this approach can identify experimental designs with high model discrimination power within a reasonable computation time and validate its performance through numerical simulations.

This thesis is organized as follows: Chapter 2 reviews relevant literature, discussing the development of model discrimination design and existing optimization criteria. Chapter 3 presents our proposed design criteria and optimization methodology. Chapter 4 presents numerical experiment results and compares the performance of different design criteria under various scenarios. Chapter 5 summarizes key findings and suggests possible future research directions.





Chapter 2

Literature Review

2.1 Accelerated Life Testing

Producing high-reliability products has always been a critical goal in the manufacturing industry. During the initial stages of product development, it is essential to determine whether the product's lifespan meets established standards. However, when the expected lifespan significantly exceeds the feasible testing duration, a common approach is to conduct Accelerated Life Testing (ALT). This method accelerates the aging process by altering environmental conditions, such as increasing temperature or vibration frequency, and collects data under various stress conditions. These data are then combined with mathematical models to extrapolate the product's lifespan under normal usage conditions. For example, pharmaceutical stability testing often needs to be completed within weeks. According to the [Guideline et al. \(2003\)](#), accelerated tests are recommended under high-temperature and high-humidity conditions. Pfizer, for instance, employs accelerated stability testing during drug development to simulate 2 to 5 years of storage conditions. Similarly, the target lifespan of electric vehicle (EV) batteries is typically 8 to 10 years or over 100,000 kilometers. Since actual testing cannot span such long dura-

tions, researchers estimate the degradation curve of battery capacity over time to further extrapolate the lifespan under real-world conditions. [Uddin et al. \(2017\)](#) used accelerated testing results under different temperatures and charge-discharge rates to simulate long-term usage scenarios for predicting lithium-ion battery performance degradation under real-world driving conditions.

[Arrhenius \(1889\)](#) proposed the Arrhenius model, which laid the theoretical foundation for chemical reaction kinetics and has been widely applied in reliability analysis and ALT. It describes the effect of temperature on reaction rates or product lifespan and assumes that the failure process follows the Arrhenius equation, which is expressed as:

$$t(T) = A \cdot \exp\left(\frac{E_a}{K \cdot Temp}\right), \quad (2.1)$$

where:

- $t(T)$: The product's lifespan at temperature $Temp$.
- A : The pre-exponential factor, a constant related to the intrinsic properties of the product.
- E_a : The activation energy, which represents the energy required to drive the failure process, typically measured in electron volts (eV).
- K : The Boltzmann constant ($8.617 \times 10^{-5} eV/K$).
- $Temp$: Absolute temperature in Kelvin (K), where $Temp = ^\circ C + 273.15$.

The model assumes an exponential relationship between failure rate and temperature, indicating that the failure rate accelerates significantly at higher temperatures. This characteristic makes the Arrhenius model a fundamental tool in ALT, where high-temperature data are collected

to extrapolate the product's lifespan under normal operating conditions. However, in practical applications, the accuracy of the model is influenced by multiple factors, particularly in experimental design, parameter estimation, and model discrimination.

First, the selection of temperature points is a critical factor affecting the accuracy of results in ALT. If the chosen test temperature is too low, it requires a significant amount of time and cost to observe product failures, making it difficult to effectively shorten the testing cycle. On the other hand, excessively high temperatures, while accelerating failures, may create conditions that deviate too far from actual usage environments, thereby reducing the relevance and applicability of the extrapolated results. Therefore, determining the optimal selection of temperature points within a limited number of tests is an important challenge.

Second, in parameter estimation, the accuracy of activation energy (E_a) and the pre-exponential factor (A) is crucial for lifespan prediction. Traditionally, parameters are estimated using Least Squares Estimation (LSE) or Maximum Likelihood Estimation (MLE). However, in ALT, Type I censored data is inevitable, as some products will not fail within the test duration due to time constraints. As a result, standard estimation methods may not be applicable. Instead, a modified likelihood function that accounts for Type I censored data must be used to ensure statistical validity under the ALT framework.

Under the MLE framework, consider that we conduct tests at j different temperature levels (T_j), each with n individual samples, we record the lifespan of the i -th sample at temperature T_j as t_{ij} . We assume that the lifespan (t_{ij}) follows $Weibull(\lambda, \beta)$, where λ_j is the scale parameter corresponding to temperature T_j , determined via the Arrhenius model, and β is the shape parameter (often assumed to be constant across differ-

ent temperature conditions):

$$f(t_{ij}; \lambda_j, \beta) = \beta \lambda_j t_{ij}^{\beta-1} \exp(-\lambda_j t_{ij}^\beta),$$

where:

1. λ_j is determined by the Arrhenius model:

$$\lambda_j = A^{-1} \exp\left(-\frac{E_a}{KT_j}\right).$$

2. β is the Weibull shape parameter (typically known or estimated separately).

If all tested samples fail (i.e., no Type I censored data), the likelihood function is:

$$L(A, E_a, \beta) = \prod_j \prod_{i=1}^{n_j} f(t_{ij}; \lambda_j, \beta).$$

Taking the logarithm, the log-likelihood function becomes:

$$\ell(A, E_a, \beta) = \sum_j \sum_{i=1}^{n_j} \left[\ln \beta + (\beta - 1) \ln t_{ij} - \ln A - \frac{E_a}{KT_j} - A^{-1} e^{-\frac{E_a}{KT_j}} t_{ij}^\beta \right].$$

However, in ALT, due to limited test time, some samples may not fail by the end of the experiment, resulting in Type I censored data. In such cases, the survival function must be incorporated:

$$S(t; \lambda_j, \beta) = \exp(-\lambda_j t^\beta).$$

Thus, the modified likelihood function considering both failures and Type I censored observations is:

$$\begin{aligned} L(A, E_a, \beta) &= \prod_j \prod_{i \in \text{failures}} f(t_{ij}; \lambda_j, \beta) \times \prod_{i \in \text{censored}} S(t_{ij}; \lambda_j, \beta) \\ &= \prod_j \prod_{i \in \text{failures}} \beta \lambda_j t_{ij}^{\beta-1} \exp(-\lambda_j t_{ij}^\beta) \times \prod_{i \in \text{censored}} \exp(-\lambda_j t_{ij}^\beta). \end{aligned}$$

Taking the logarithm, the modified log-likelihood function becomes:

$$\begin{aligned} \ell(A, E_a, \beta) = & \sum_j \sum_{i \in \text{failures}} \left[\ln \beta + (\beta - 1) \ln t_{ij} - \ln A - \frac{E_a}{KT_j} - A^{-1} e^{-\frac{E_a}{KT_j}} t_{ij}^\beta \right] \\ & - \sum_j \sum_{i \in \text{censored}} A^{-1} e^{-\frac{E_a}{KT_j}} t_{ij}^\beta. \end{aligned}$$

In other words, parameter estimation in ALT must be adjusted in accordance with the likelihood function that accounts for Type I censored data to obtain robust results. The objective is to estimate the key parameters affecting product lifespan, namely A , E_a , and β . We seek the parameter estimates \hat{A} , \hat{E}_a , $\hat{\beta}$ that maximize the modified log-likelihood function.

To obtain the most suitable parameter estimates for the ALT data, we solve the following system of equations:

$$\frac{\partial \ell}{\partial A} = 0, \quad \frac{\partial \ell}{\partial E_a} = 0, \quad \frac{\partial \ell}{\partial \beta} = 0.$$

The parameters \hat{A} , \hat{E}_a , $\hat{\beta}$, obtained through the MLE method, ensure the accuracy of the ALT model and enable effective prediction of product lifespan under normal operating conditions.

In previous studies, c -optimal design has been widely applied to minimize the variance of key parameter estimates by selecting optimal experimental conditions (e.g., temperature levels). Particularly in ALT, c -optimal design is frequently used to improve the estimation accuracy of activation energy E_a , ensuring the reliability of the lifespan model.

For example:

1. [Lu et al. \(2019\)](#) proposed a Bayesian sequential design approach based on dual objectives, integrating both D-optimality and c -optimality

criteria. The former is utilized in the early phase of experimentation to rapidly improve the precision of model parameter estimation, while the latter is applied in later stages to minimize the variance of specific lifespan quantiles (e.g., the p -th percentile lifespan), ensuring robust and accurate lifespan prediction.

2. [Abd El-Raheem \(2020\)](#) investigated the application of c -optimal design in Multiple Accelerated Life Tests (Multiple ALT) and compared the efficiency of different optimality criteria (D-, c -, and A-optimality) through experimental design evaluation and sensitivity analysis.
3. [Newer et al. \(2024\)](#) explored the use of c -optimal design in ALT, particularly under Progressive Type-I Censoring (PTIC) conditions. They compared multiple optimality criteria (D-, E-, T-, c -, R-, and P-optimality) and found that c -optimality effectively minimizes the variance in estimating specific lifespan distribution parameters, such as the scale parameter λ_0 in the Weibull distribution. Their results indicate that in Step-stress Accelerated Life Testing (SALT), c -optimal design enhances the estimation accuracy of critical lifespan distribution parameters, even under limited testing resources.

Finally, in ALT research, model discrimination has often been overlooked. Although the Arrhenius model is widely used in temperature-accelerated testing, its applicability should be validated based on real-world data. While it assumes a specific exponential relationship between temperature and failure rate, whether this relationship accurately captures product behavior in a given application must be carefully examined. As such, experimental design should not only aim to estimate parameters efficiently but also evaluate whether the Arrhenius model remains appropriate, or if alternative models are needed.

However, existing research has predominantly focused on improving parameter estimation accuracy, often through techniques such as c -optimal design to enhance the efficiency of parameter estimation. Comparatively, less attention has been given to how to effectively design experiments to distinguish between competing models, particularly when both models are based on the Arrhenius framework but differ in their structural formulations. This raises an important question: can an experimental design be structured so that future data can effectively discriminate between competing models? This approach, known as model discrimination design, aims to identify optimal experimental conditions that induce noticeable differences in model behavior within the observed data. By doing so, it enhances the accuracy of model selection, ensuring both the reliability and applicability of lifespan predictions.

2.2 Model Discrimination Design

In practical applications, whether in the technology industry, manufacturing, or other rapidly evolving fields, the pace of change often exhibits exponential growth. In this context, previously adopted models may gradually lose their applicability due to environmental changes, leading to a decline in predictive accuracy and, in some cases, reduced decision-making effectiveness. As a result, determining whether to continue using an existing model or transition to a new one that better reflects the current conditions becomes a critical issue. To make optimal decisions, model discrimination design can be employed to assess the applicability of different models. When adapting to new environmental challenges, decision-makers should not blindly discard old models or fully adopt new ones. Instead, a rigorous statistical approach should be used to objectively evaluate the suitability of various models, ensuring that the

chosen model accurately represents the current context and enhances decision-making accuracy and reliability.

Atkinson and Fedorov (1975a,b) proposed an experimental design method for distinguishing between two rival models, assuming that the models follow a Normal distribution. They introduced the T-optimal design, which is specifically aimed at optimizing model discrimination. Consider two Gaussian models with the same variance σ^2 but different mean response functions, denoted as $\eta_1(x, \theta_1)$ and $\eta_2(x, \theta_2)$, respectively. The objective is to compare these two models. In practice, the first model is often assumed to be known, as it may be based on expert opinions or prior experiences reflecting the current state of knowledge. Therefore, we assume the first model to be the true model, with known parameters $\theta_1 = \theta_{tr}$, such that $\eta_{tr}(x) = \eta_1(x, \theta_{tr})$. The second model, on the other hand, is a rival model, represented as $\eta_r(x, \theta_2) = \eta_2(x, \theta_2)$, where $\theta_2 \in \Theta_2$ is unknown.

To conduct model discrimination in the absence of prior data, the T-optimal design criterion is employed, with its objective function defined as shown in Equation (2.2):

$$T_{2,tr}(\xi) = \min_{\theta_2 \in \Theta_2} \int_X \Delta_{2,tr}(x, \theta_2) \xi(dx), \quad (2.2)$$

where $\Delta_{2,tr}(x, \theta_2) = [\eta_{tr}(x) - \eta_r(x, \theta_2)]^2$, and ξ is the experimental design distribution. Our goal is to select a design distribution ξ such that the difference between the two models, after minimizing with respect to θ_2 , remains sufficiently large to clearly discriminate between the two models in subsequent data analysis.

However, the T-optimal criterion focuses solely on minimizing the difference between the two models with respect to θ_2 . We aim to ensure that the selected design further amplifies the difference between the two

models after data is collected. Thus, we propose a maximization-based design approach, which leads to the adjustment of the objective function, as described in the equation (2.3):

$$\max_{\xi \in \Xi} T_{2,tr}(\xi) = \max_{\xi \in \Xi} \min_{\theta_2 \in \Theta_2} \int_X \Delta_{2,tr}(x, \theta_2) \xi(dx). \quad (2.3)$$

The core idea of this approach is to select a design distribution ξ such that, for every possible θ_2 , the minimum difference between the models is maximized across all designs. This ensures that regardless of how future data may influence the estimation of θ_2 , the actual difference between the models will always be greater than the minimum difference considered during the design phase. Therefore, this design approach not only addresses the current model discrimination problem but also enhances the efficiency of future experimental data, providing stronger support for model selection.

Theorem 1. *To verify whether the selected design ξ_T^* is optimal, we apply the Equivalence Theorem (Atkinson and Fedorov, 1975a,b). As shown in Equation (2.4):*

$$\psi_T(x, \xi_T^*) = \Delta_{2,tr}(x, \hat{\theta}_2(\xi_T^*)) - T_{2,tr}(\xi_T^*) \leq 0, \quad (2.4)$$

where:

- The first term $\Delta_{2,tr}(x, \hat{\theta}_2(\xi_T^*))$ represents the minimum model difference across all possible $\theta_2 \in \Theta_2$ for each point x in the design space \mathcal{X} .
- The second term $T_{2,tr}(\xi_T^*)$ represents the minimum model discrepancy calculated based on the selected design ξ_T^* , which is determined as the global optimal criterion through the max-min optimization process.

If the inequality $\psi_T(x, \xi_T^*) \leq 0$ holds for all $x \in \mathcal{X}$, then ξ_T^* can be confirmed as the T-optimal design. This indicates that, at any design

point, the maximum local model difference does not exceed the globally minimized model difference, thereby ensuring the optimality of the design.

However, the T-optimal design, proposed by [Atkinson and Fedorov \(1975a,b\)](#), aims to achieve effective model discrimination by maximizing the sum of the squared differences between competing models. Nevertheless, this method has certain limitations in specific application scenarios. For instance, when models do not have homoscedastic or the error terms deviate from normality, merely considering the sum of squared differences may not sufficiently capture the disparity between models. In such cases, the overall shape of the distributions should be accounted for, which can be measured using the Kullback-Leibler (KL) divergence to quantify the information loss between models. [López-Fidalgo et al. \(2007\)](#) addressed these scenarios by proposing KL-optimal designs and conducted simulations under various conditions to identify effective designs for model discrimination.

2.3 Numerical Methods in Finding Model Discrimination Designs

In the process of optimization, [Atkinson and Fedorov \(1975a,b\)](#) adopted an incremental design approach similar to the exchange algorithm. However, when applied to continuous design spaces, this method typically starts by specifying a baseline design—such as randomly selecting three initial support points. It then iteratively explores candidate points from a discretized version of the design space (e.g., using intervals of 50 or 100 units), testing whether adding each point improves the design criterion. If improvement is observed, the candidate point is incorporated into the design. Over multiple iterations, this can lead to a final design with more

support points than originally intended, often clustered in specific regions. For example, nearby points like 99, 100, and 101 may all carry small weights, creating the appearance of multiple points within a narrow stress region. Such characteristics reduce interpretability and make it difficult to control the number of support points.

Moreover, building upon the findings and analyses of previous studies, both T-optimal and KL-optimal designs often involve computationally intensive optimization processes, posing significant challenges to efficiency. Adopting more efficient continuous optimization algorithms presents a promising direction. Over the past decade, research has shown that Particle Swarm Optimization (PSO) demonstrates significant advantages in addressing experimental design problems, effectively overcoming limitations that traditional theories or algorithms have struggled to resolve. Therefore, this study will employ PSO as a solution method to enhance computational efficiency and accuracy. Notably, [Chen et al. \(2020\)](#) successfully applied PSO to model discrimination problems, inspiring this study to explore the potential of applying this approach to the Arrhenius model, one of the most commonly used models in the field of reliability.

[Eberhart and Kennedy \(1995\)](#) first introduced the PSO method, a heuristic optimization algorithm inspired by the collective behavior of bird flocks and fish schools in nature. In PSO, each bird or fish is treated as a particle, representing a candidate solution. By combining information from its own historical best solution (Local Best) and the swarm-wide best solution (Global Best), by continuously updating its velocity and position, eventually converging to the global optimal solution. Numerous studies have applied PSO to solve various types of optimal design problems. For example, [Chen et al. \(2011\)](#) explored A-optimal, D-

optimal, and Minimax designs; [Lukemire et al. \(2016\)](#) applied PSO to search for D-optimal designs; and [Walsh and Borkowski \(2022\)](#) investigated G-optimal designs.

The iterative process of PSO consists of two main steps. First, initializing the velocity and position of the particles, and then calculating the particle velocities using Equation (2.5) and updating their positions with Equation (2.6). During this process, the motion of a particle is governed by three key components, as shown in the Figure 2.1 :

- (A): The inertia term, which represents the particle's momentum and influences its current velocity by continuing its previous velocity.
- (B): The cognitive learning term, which guides the particle toward its personal best position (ξ_L^t , LBest), encouraging individual exploration.
- (C): The social learning term, which directs the particle toward the global best position (ξ_G^t , GBest), leveraging the collective knowledge of the swarm to approach the global optimum.

The motion of particle i at time t and $t + 1$ is controlled by the following equations:

$$v_i^{t+1} = \underbrace{\varphi_t v_i^t}_{(A)} + \underbrace{\gamma_1 \beta_1 \otimes [\xi_L^t - \xi_i^t]}_{(B)} + \underbrace{\gamma_2 \beta_2 \otimes [\xi_G^t - \xi_i^t]}_{(C)}, \quad (2.5)$$

and

$$\xi_i^{t+1} = \xi_i^t + v_i^{t+1}, \quad \text{for } i = 1, \dots, N. \quad (2.6)$$

In Equation (2.5), v_i^t and v_i^{t+1} represent the velocity of particle i at time t and $t + 1$, respectively. The parameter φ_t , known as the inertia weight, ranges between 0 and 1. It can either be a constant or a time-

decreasing function. Typically, a larger inertia weight is used in the early stages of the algorithm to enhance global exploration and prevent premature convergence to local optima. In contrast, a smaller inertia weight is employed in the later stages to refine local searches, improve solution precision, and accelerate convergence. The learning factors γ_1 and γ_2 correspond to cognitive and social learning, respectively, and determine the weight of the particle's movement toward LBest and GBest. Both are typically constants. The random numbers β_1 and β_2 , sampled from a uniform distribution $U(0, 1)$, are introduced to add stochasticity to the search process, thereby enhancing the diversity of the particles exploration.

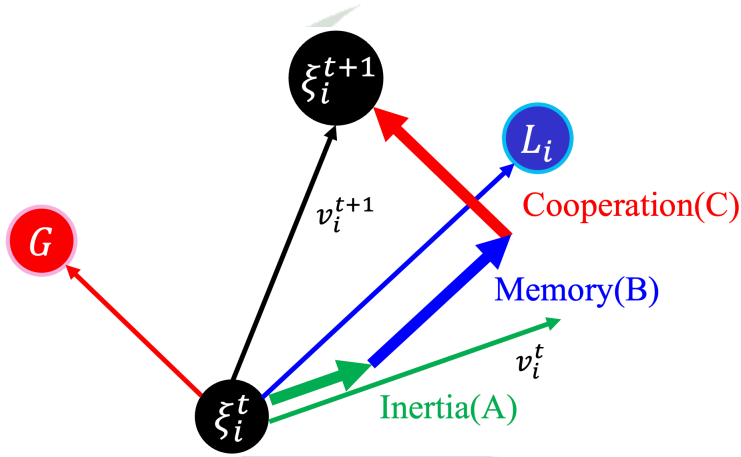


Figure 2.1: PSO velocity components visualization

PSO Algorithm Process:(Refer to Figure 2.2)

1. Initialization of particles:

- Generate a swarm of n particles.
- Initialize the position ξ_i and velocity v_i of each particle, where $i = 1, \dots, n$.
- Identify each particle's local best solution (ξ_L^t , LBest) and the global best solution of the swarm (ξ_G^t , GBest).

2. Iterative process:

- Calculate each particle's velocity using Equation (2.5).
- Update each particle's position using Equation (2.6).
- Evaluate the fitness value of each particle based on the optimization objective function, and update its LBest and the GBest.
- Check if the stopping criteria are met (e.g., reaching the maximum number of iterations or convergence of the fitness value).
If not, repeat the above steps.

3. Output results:

- Return the global best solution (GBest) as the final result.

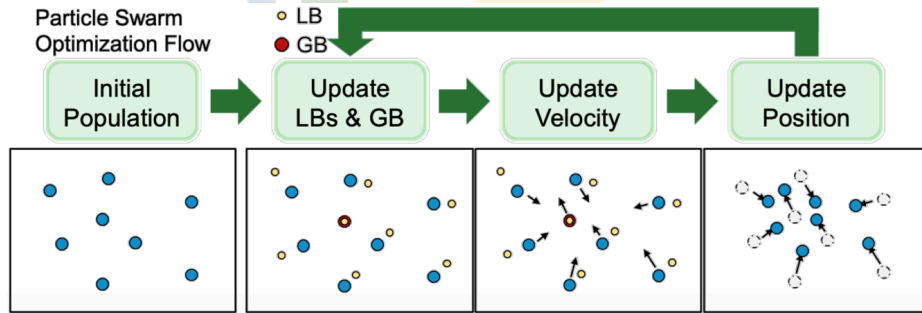


Figure 2.2: PSO concept diagram

2.4 Existing Approach of Model Discrimination Design for ALT

In ALT research, the issue of model discrimination has been relatively underexplored, and [Nasir and Pan \(2015\)](#) is one of the more representative studies in this area. This study addresses model discrimination in ALT by proposing an optimal experimental design strategy based on the Bayesian approach, focusing on how to distinguish between competing models through experimental design, particularly in scenar-

ios where the relationship between lifespan and stress variables may be linear or nonlinear, and the model structure remains uncertain. They employ Hellinger distance to measure the differences between the predictive distributions of competing models and validate the effectiveness of their design through numerical simulations.

To illustrate the concept of ALT, we refer to Figure 2.3. Suppose we have two models, M_1 and M_2 , and our objective is to predict the p -th quantile of product lifespan (τ_p). However, when the actual product takes an extended period to fail under normal usage conditions, the best approach is to increase stress levels to accelerate failure and reduce testing time.

In the experiment, two stress levels are defined: low stress (S_{Low}) and high stress (S_{High}), and failure data distributions are obtained under these conditions. Using an extrapolation method, the failure distribution under actual usage stress (S_{UC}) is then estimated to predict product lifespan.

In the figure, the x-axis represents stress, and the y-axis represents product lifespan, with both being log-transformed primarily because many lifespan models, such as the Arrhenius model, exhibit a nonlinear relationship. Taking the logarithm transforms this into a linear form, facilitating statistical inference. Additionally, under high-stress conditions, product lifespan tends to have high variability, often resulting in a skewed distribution. Log transformation helps normalize the data, making it more compatible with statistical models and improving estimation stability. Consequently, the same ALT procedure is applied to both M_1 and M_2 to examine their p -th quantile of lifespan (τ_p) under different stress conditions. The log-transformed lifespan distribution shift ($\Delta\hat{\tau}_p$) across different stress levels provides a clearer view of model behavior, facili-

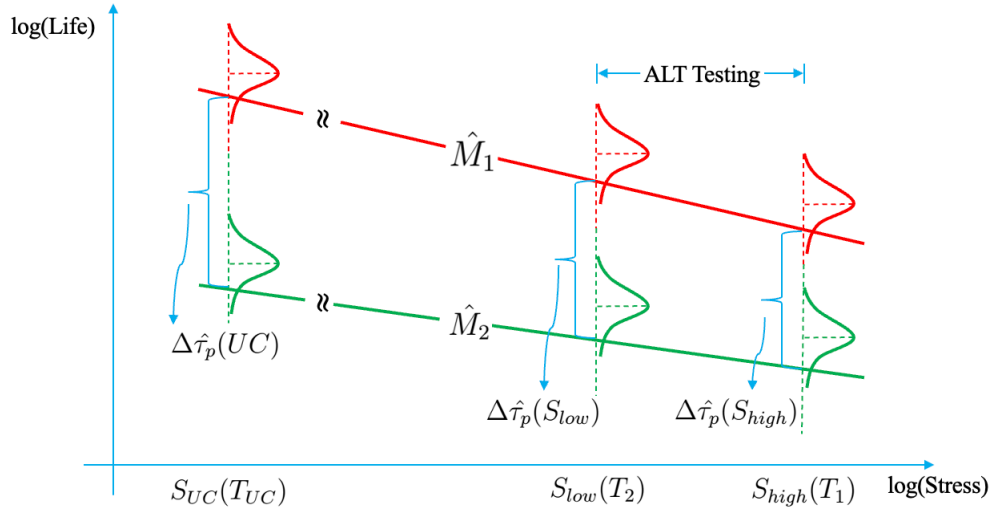


Figure 2.3: Conceptual diagram of Accelerated Life Testing (Nasir and Pan, 2015)

tating model discrimination. The following will sequentially describe the details of the simulation steps in this study.

In this context, a reliability engineer is interested in studying the growth of Intermetallic Compounds (IMC) at the Au-Al interface in semiconductor assemblies. It is known that the failure mechanism is influenced by temperature stress, necessitating an Accelerated Life Testing to estimate the device's operational lifespan. The objective is to design an experimental plan capable of distinguishing between linear acceleration model M_1 and quadratic acceleration model M_2 under temperature stress, with parameters θ_1 and θ_2 , respectively. The experimental setup and testing conditions are as follows:

- Baking Chamber Duration: The maximum test time is 42 days, equivalent to 1008 hours.
- Two Types of Ovens Available:
 - Low-Stress Oven: Temperature range from 60°C to 115°C.

- High-Stress Oven: Temperature range from 100°C to 250°C.
- Experimental Cost Constraint: A maximum of 20 tests can be conducted.

This study is based on a real industrial example from their paper and provides a detailed simulation setup, which includes all the following aspects.

I. Model Adjustment and Definition of Models for Comparison:

We begin by linearizing the Arrhenius model (Equation (2.1)) to define the model:

$$\begin{aligned}
 t(T) &= A \exp\left(\frac{E_a}{K \times Temp}\right) \\
 \Rightarrow \log(t(T)) &= \log(A) + \frac{E_a}{K \times Temp} \\
 \Rightarrow \underbrace{\log(t(T))}_{\mu} &= \underbrace{\log(A)}_{\beta_0} + \underbrace{\frac{E_a}{K}}_{\beta_1} \times \underbrace{\frac{1}{Temp}}_x.
 \end{aligned} \tag{2.7}$$

Next, by standardizing the accelerating variable, Equation (2.7) can be expanded as:

$$\underbrace{\log(t(T))}_{\mu} = \underbrace{(\beta_0 + \beta_1 x_{low})}_{\gamma_0} + \underbrace{[\beta_1(x_{high} - x_{low})]}_{\gamma_1} \underbrace{\left(\frac{x - x_{low}}{x_{high} - x_{low}}\right)}_{\xi}. \tag{2.8}$$

Adding a quadratic term to capture potential nonlinear acceleration effects:

$$\mu = \beta_0 + \beta_1 x + \beta_2 x^2. \tag{2.9}$$

After standardizing the accelerating variable in Equation (2.9), it

expands to:

$$\begin{aligned} \overbrace{\log(t(T))}^{\mu} &= \overbrace{(\beta_0 + \beta_1 x_{low})}^{\gamma_0} + \overbrace{[\beta_1(x_{high} - x_{low})]}^{\gamma_1} \overbrace{\left(\frac{x - x_{low}}{x_{high} - x_{low}}\right)}^{\xi} \\ &\quad + \underbrace{[\beta_2(x_{high}^2 - x_{low}^2)]}_{\gamma_2} \underbrace{\left(\frac{x - x_{low}}{x_{high} - x_{low}}\right)^2}_{\xi^2}. \end{aligned} \quad (2.10)$$

Based on the above derivation, Equation (2.8) is embedded within Equation (2.10), meaning that M_2 is a special case of M_1 . Thus, we define M_1 and M_2 as follows:

$$M_1 : \mu_1 = \gamma_0 + \gamma_1 \xi + \gamma_2 \xi^2, \quad (2.11)$$

$$M_2 : \mu_2 = \gamma_0 + \gamma_1 \xi. \quad (2.12)$$

Additionally, the reliability engineer believes that the Weibull distribution adequately describes the growth life and failure mechanism of Au-Al intermetallic compounds in semiconductor packaging. Therefore, it is assumed that the lifespan T follows a Weibull distribution, $T \sim Weibull(\alpha, \beta)$, where α is the scale parameter and β is the shape parameter. A logarithmic transformation is then applied, resulting in a Smallest Extreme Value (SEV) distribution, $\log(t) \sim SEV(\mu, \sigma)$, where $\sigma = \frac{1}{\beta}$ and $\mu = \log(\alpha)$.

For both models, when handling Type I censored data, the survival probability beyond time t_c is given by:

$$Pr(t > t_c) = \exp \left[- \left(\frac{t_c}{\alpha} \right)^\beta \right], t_c > 0.$$

II. Distance Measure Between Probability Distributions: This study uses the Hellinger distance to measure the differences between $\Delta \hat{\tau}_p(S_{Low})$ and $\Delta \hat{\tau}_p(S_{High})$ as illustrated in Figure 2.3. Suppose the lifespan

data from two models are given by $Y_1 = (y_{11}, y_{21}, \dots, y_{N1})$ and $Y_2 = (y_{12}, y_{22}, \dots, y_{N2})$, each with N observations. The Hellinger distance is defined as:

$$D_H(Y_1, Y_2) = \frac{1}{\sqrt{2}} \sqrt{\sum_{i=1}^N (\sqrt{y_{i1}} - \sqrt{y_{i2}})^2}.$$

III. Utility Function Definition: The utility function to be maximized considers the scenarios under both low and high-stress conditions, using data from both models Y_1 and Y_2 :

$$u_{2|1} = D_{S_{Low}}(\hat{\tau}_{p,(M_2|Y_1)}, \hat{\tau}_{p,(M_1|Y_1)}) + D_{S_{High}}(\hat{\tau}_{p,(M_2|Y_1)}, \hat{\tau}_{p,(M_1|Y_1)}),$$

$$u_{1|2} = D_{S_{Low}}(\hat{\tau}_{p,(M_1|Y_2)}, \hat{\tau}_{p,(M_2|Y_2)}) + D_{S_{High}}(\hat{\tau}_{p,(M_1|Y_2)}, \hat{\tau}_{p,(M_2|Y_2)}).$$

IV. Expectation of the Utility Function: Since the actual data has not yet been observed during the experimental design stage, the study computes the expected utility by integrating over the data sampling distributions $p(y_1|\theta_1)$ and $p(y_2|\theta_2)$, along with the prior distributions of the parameters $\pi(\theta_1)$ and $\pi(\theta_2)$:

$$E(u_{2|1}) = \int \int u_{2|1} p(y_1|\theta_1) \pi(\theta_1) d_{y_1} d_{\theta_1},$$

$$E(u_{1|2}) = \int \int u_{1|2} p(y_2|\theta_2) \pi(\theta_2) d_{y_2} d_{\theta_2}.$$

V. Model Weights and Final Utility Function: Since the true underlying model is unknown, prior probabilities $\tau(M_1)$ and $\tau(M_2)$ are assigned to each model. The overall utility function $U(\xi)$ is defined as:

$$U(\xi) = \tau(M_1)E(u_{2|1}) + \tau(M_2)E(u_{1|2}) \quad (2.13)$$

Maximizing $U(\xi)$ ensures that the experimental design maximizes the distinguishability between the two competing models.

VI. Given Prior Distributions:

- Both models are initially considered equally likely, with $\tau(M_1) = \tau(M_2) = 0.5$.
- The activation energy is assumed to follow a uniform distribution, $E_a \sim U(1.0, 1.05)$, indicating equal probability across the range 1.0 to 1.05 eV.
- The intercept term is assumed to follow a normal distribution with mean 0 and a large variance, $\beta_0 \sim N(0, 1000^2)$, reflecting high uncertainty about its value.
- Similarly, the quadratic term in model M_2 is assumed to follow $\beta_2 \sim N(0, 1000^2)$, allowing for a wide range of potential values.
- The lifespan data are assumed to follow a Weibull distribution with the shape parameter β drawn from a Gamma distribution, $\beta \sim \text{Gamma}(1, 2)$.

They adopted a Bayesian simulation approach, where data were repeatedly sampled to estimate the shape of the empirical distribution and calculate the differences between various distributions. In this process, they utilized Gibbs sampling—a technique within the Markov Chain Monte Carlo (MCMC) framework—and employed WinBUGS software to compute $\hat{\tau}_p$, while also simulating the maximization of the utility function to identify the optimal design ξ^* .

However, this method presents two major drawbacks. First, the computational process is highly time-consuming, especially when dealing with high-dimensional data or large sample sizes, which significantly increases computational costs. Second, due to the stochastic nature of the method, each simulation run may yield different results, leading to

challenges in reproducing previous outcomes. This further limits the method's practical applicability.

[Nasir and Pan \(2015\)](#) explored the application of model discrimination design in reliability testing. However, as outlined above, their approach still leaves considerable room for improvement. Therefore, this study will build upon the gaps identified in their work to conduct further in-depth investigations.





Chapter 3

Methodology

This study focuses on approximation designs, which are widely recognized for their practicality in experimental design. Approximation designs are probability measures defined over the design space \mathcal{X} , used to allocate limited observations across specific design points. Let the response variable y follow a conditional probability distribution $f(y \mid x, \theta, \sigma^2)$, where x represents a design point (support point) from the design space, such that $x \in \mathcal{X}$, θ denotes all unknown parameters, and σ^2 is the variance of the errors, treated as a nuisance parameter.

When the design points are $x_1, x_2, \dots, x_n \in \mathcal{X}$, an approximation design ξ can be expressed as:

$$\xi = \begin{Bmatrix} x_1 & x_2 & \dots & x_n \\ w_1 & w_2 & \dots & w_n \end{Bmatrix}.$$

Here, w_i represents the weight assigned to the design point x_i , satisfying $0 < w_i < 1$ and $\sum_{i=1}^n w_i = 1$, where $i = 1, 2, \dots, n$. If the total sample size is N , the number of observations allocated to the design point x_i is approximately $N \cdot w_i$, typically rounded to the nearest integer in practice. The objective of approximation designs is often based on convex or concave functions, allowing optimization algorithms to efficiently

identify the best designs, which is denoted as ξ^* . Additionally, to confirm whether the obtained design is optimal, this study will employ the Equivalence Theorem as a verification tool.

3.1 KL-optimal Criterion

When the two models have different variances or the error terms do not follow a Normal distribution, [López-Fidalgo et al. \(2007\)](#) proposed the KL-optimal design to address such cases. This design measures the information loss between models using Kullback-Leibler divergence (KL divergence), which is also referred to as relative entropy, information divergence, or information gain. As the name suggests, it is closely related to entropy. The following sections will introduce different related metrics in sequence.

[Shannon \(1948\)](#) proposed information entropy as a measure of the uncertainty or information content in a probability distribution. Information content, $I(x)$, can be viewed as a surprise index: when the probability $P(x)$ of an event occurring is low, the occurrence of the event surprises us (high information content); conversely, when $P(x)$ is high, the occurrence of the event is expected, resulting in lower information content.

For example:

- A sunny day in the desert tomorrow \rightarrow This is expected, as the probability is high (close to 1), so the information content is low.
- Rain in the desert tomorrow \rightarrow This is a rare event, with a low probability (close to 0), so the information content is high.

Therefore, when $P(x)$ approaches 0, indicating the event is highly

unlikely to occur and the surprise level is high, the information content value must be large; when $P(x)$ approaches 1, the information content value must be small.

The definition of information content is:

$$I(x) = -\log P(x). \quad (3.1)$$

Entropy represents the average information content, as events usually do not occur in isolation and require comprehensive consideration. Assuming we consider the first model (true model) $f_{tr}(y \mid x, \sigma_1^2)$, its information entropy is defined as:

$$H(f_{tr}) = - \int f_{tr}(y \mid x, \sigma_1^2) \log \{f_{tr}(y \mid x, \sigma_1^2)\} dy. \quad (3.2)$$

A higher value of $H(f_{tr})$ indicates greater variability in the distribution, meaning that more information is obtained when an event occurs. Intuitively, information entropy can be interpreted as the amount of information gained after an event takes place. Since probability values range between 0 and 1, taking the logarithm results in negative values. Therefore, a negative sign is introduced in the formula to ensure that $H(f_{tr})$ remains non-negative. A larger entropy value suggests greater variability in the probability distribution and a higher amount of information provided by the occurrence of an event, whereas a smaller entropy value indicates less information.

Cross entropy measures the difference between the observed predicted probability distribution and the true probability distribution. Intuitively, it quantifies the additional information loss incurred when using one model to describe the true distribution. Consider the first model (true model) $f_{tr}(y \mid x, \sigma_1^2)$ and the second model (rival model) $f_r(y \mid$

x, θ_2, σ_2^2). The cross entropy is defined as:

$$H(f_{tr}, f_r) = - \int f_{tr}(y | x, \sigma_1^2) \log \{f_r(y | x, \theta_2, \sigma_2^2)\} dx. \quad (3.3)$$

Cross entropy measures the average information loss when we approximate the true distribution $f_{tr}(y | x, \sigma_1^2)$ with a rival model $f_r(y | x, \theta_2, \sigma_2^2)$. A larger cross entropy value indicates a greater discrepancy between the two distributions, implying higher uncertainty and requiring more information to describe $f_{tr}(y | x, \sigma_1^2)$. Conversely, if the two distributions are similar, the cross entropy value will be lower, indicating that the rival model describes the true distribution more accurately. It is important to note that the minimum value of cross entropy is usually not zero; when the two models are identical, the cross entropy $H(f_{tr}, f_r)$ equals the entropy $H(f_{tr})$.

Kullback-Leibler (KL) divergence is used to measure the similarity between two probability distributions. Essentially, it can be derived from information entropy and cross entropy. Since cross entropy always has a minimum value equal to entropy, their difference remains non-negative, allowing KL divergence to quantify the additional information loss when approximating the true model $f_{tr}(y | x, \sigma_1^2)$ using an rival model $f_r(y | x, \theta_2, \sigma_2^2)$. This property ensures that the minimum of KL divergence is constrained at zero, providing an interpretable measure of how much extra information is lost due to model approximation. The derivation process of KL divergence is as follows:

$$\begin{aligned} KL \text{ Divergence} &= \text{Cross Entropy} - \text{Information Entropy} \\ D_{KL}(f_{tr}, f_r, x, \theta_2) &= (3.3) - (3.2) \\ &= H(f_{tr}, f_r) - H(f_{tr}) \\ &= \int f_{tr}(y | x, \sigma_1^2) \log \left\{ \frac{f_{tr}(y | x, \sigma_1^2)}{f_r(y | x, \theta_2, \sigma_2^2)} \right\} dy. \end{aligned} \quad (3.4)$$

The KL divergence value reflects the difference between the two probability distributions:

- If the two models have similar probability distributions, $D_{KL}(f_{tr}, f_r, x, \theta_2)$ will be small.
- If the two models are identical, then $D_{KL}(f_{tr}, f_r, x, \theta_2) = 0$, indicating no information loss.

Since KL divergence is asymmetric (i.e., $D_{KL}(f_{tr}, f_r, x, \theta_2) \neq D_{KL}(f_r, f_{tr}, x, \theta_2)$), it does not satisfy the properties of a true distance metric. However, it remains a widely used measure in probability distribution comparisons.

The KL-optimal design criterion, proposed by [López-Fidalgo et al. \(2007\)](#), is formulated using Equation (3.4), with its objective function defined in Equation (3.5):

$$KL_{2,tr}(\xi) = \min_{\theta_2 \in \Theta_2} \int_X D_{KL}(f_{tr}, f_r, x, \theta_2) \xi(dx). \quad (3.5)$$

Unlike T-optimal designs, the KL-optimality criterion does not rely solely on model error differences to measure discrimination power. Instead, it utilizes the Kullback-Leibler (KL) divergence to evaluate the informational disparity between the probability distributions of the two models. This design approach is particularly advantageous when the models have different variances or when the error distributions deviate from normality, allowing for greater flexibility in experimental design.

The objective of KL-optimal design is to select a design distribution ξ that maximizes the ability to discriminate between models, even under the least favorable estimation of θ_2 . To achieve this, we reformulate the

objective function, as shown in Equation (3.6):

$$\max_{\xi \in \Xi} KL_{2,tr}(\xi) = \max_{\xi \in \Xi} \min_{\theta_2 \in \Theta_2} \int_X D_{KL}(f_{tr}, f_r, x, \theta_2) \xi(dx). \quad (3.6)$$

This formulation follows a similar rationale to T-optimal designs, where the optimality criterion seeks to maximize the minimum discrepancy. However, KL-optimal designs achieve model identifiability by maximizing the KL divergence, ensuring stronger discrimination between competing models.

Theorem 2. *To verify whether the selected design ξ_{KL}^* is optimal, we apply the Equivalence Theorem (Atkinson and Fedorov, 1975a,b), as expressed in Equation (3.7):*

$$\psi_{KL}(x, \xi_{KL}^*) = D_{KL}(f_{tr}, f_r, x, \hat{\theta}_2(\xi_{KL}^*)) - KL_{2,tr}(\xi_{KL}^*) \leq 0. \quad (3.7)$$

where:

- The first term, $D_{KL}(f_{tr}, f_r, x, \hat{\theta}_2(\xi_{KL}^*))$, represents the minimum KL divergence computed at each design point x over all possible values of $\theta_2 \in \Theta_2$ in the design space \mathcal{X} .
- The second term, $KL_{2,tr}(\xi_{KL}^*)$ represents the global minimum KL divergence obtained for the entire design ξ_{KL}^* , which is determined as the global optimal criterion through the max-min optimization process.

If the inequality $\psi_{KL}(x, \xi_{KL}^*) \leq 0$ holds for all $x \in \mathcal{X}$, then ξ_{KL}^* is confirmed as the KL-optimal design. This ensures that at any design point, the maximum local KL divergence does not exceed the global minimum KL divergence, guaranteeing that the selected design can effectively discriminate between the models.

3.2 Model Discrimination Criteria for Type I Censored Data

In the context of reliability and survival analysis, where Type I censored data is common, the original mathematical formulations often fail to accommodate this constraint. Park & Shin (2013) refined the computation of KL divergence and proposed two alternative formulations tailored to Type I censored data. They conducted comparative analyses to evaluate the performance of these formulations under different scenarios, demonstrating that they preserved the non-negativity, monotonicity, and other core properties of KL divergence. Building on this, Pakgohar et al. (2019) introduced additional divergence measures, including Kullback-Leibler (KL) divergence, Lin-Wong (LW) divergence, Bhattacharyya distance (B), and the Chi-squared (χ^2) measure. They systematically compared these measures with KL divergence in the context of Type I censored data and demonstrated their consistency and reliability in practical applications. Among these measures, KL divergence, closely tied to Shannon entropy, serves as a fundamental tool in information theory to quantify the relative information loss between two distributions. Its core concept lies in assessing the additional information required to describe one distribution relative to another, making it essential for model discrimination and information theory. However, KL divergence is sensitive to skewed data and may yield infinite values in extreme cases, posing limitations in certain applications. To address these issues, the LW divergence was developed. This measure refines the application of logarithmic functions, incorporating the differences between distributions and survival functions in Type I censored data. It is characterized by its finiteness and non-negativity, effectively avoiding the potential issue of infinite values in KL divergence while providing greater

robustness. The Bhattacharyya distance, on the other hand, focuses on the overlap between distributions, making it suitable for measuring similarity but less sensitive to subtle changes in distributions compared to KL divergence and LW divergence. Lastly, the χ^2 measure evaluates distributional differences through a ratio-based approach, proving effective for large sample sizes but may underestimate differences when the distributions are very similar. This study will adopt the more effective KL divergence formulation proposed by [Park and Shin \(2014\)](#), along with the three measures introduced by [Pakgohar et al. \(2019\)](#), for use in experimental designs aimed at model discrimination.

In the results presented in the next section, Div denotes the divergence criterion. We consider four different divergence measures, assuming that the *firstmodel* (true model, M_1) has a conditional probability density function $f_{tr}(y | x, \sigma_1^2)$, while the second model (rival model, M_2) has a conditional probability density function $f_r(y | x, \theta_2, \sigma_2^2)$. The corresponding cumulative probability density functions are given by $F_{tr}(C | x, \sigma_1^2)$ and $F_r(C | x, \theta_2, \sigma_2^2)$, where C represents the censoring threshold. Furthermore, the survival functions are defined as:

$$\bar{F}_{tr}(C) = 1 - F_{tr}(C), \quad \bar{F}_r(C) = 1 - F_r(C).$$

Divergence Measures:

- Censored Kullback-Leibler (CKL) divergence:

$$D_{CKL}(f_{tr}, f_r) = \int_{-\infty}^C f_{tr} \log \left\{ \frac{f_{tr}}{f_r} \right\} dy + \bar{F}_{tr}(C) \log \left\{ \frac{\bar{F}_{tr}(C)}{\bar{F}_r(C)} \right\}. \quad (3.8)$$

- Censored Lin-Wong (CLW) divergence:

$$D_{CLW}(f_{tr}, f_r) = \int_{-\infty}^C f_{tr} \log \left\{ \frac{2f_{tr}}{f_{tr} + f_r} \right\} dy + \bar{F}_{tr}(C) \log \left\{ \frac{2\bar{F}_{tr}(C)}{\bar{F}_{tr}(C) + \bar{F}_r(C)} \right\}. \quad (3.9)$$

- Censored Bhattacharyya (CB) distance measure:

$$D_{CB}(f_{tr}, f_r) = \int_{-\infty}^C \sqrt{f_{tr} \cdot f_r} dy + \sqrt{\bar{F}_{tr}(C) \cdot \bar{F}_r(C)}. \quad (3.10)$$

- Censored Chi-Square ($C\chi^2$) distance measure:

$$D_{C\chi^2}(f_{tr}, f_r) = \int_{-\infty}^C \frac{(f_{tr})^2}{f_r} dy + \frac{(\bar{F}_{tr}(C))^2}{\bar{F}_r(C)} - 1. \quad (3.11)$$

To further extend this framework, we propose four new optimal designs that explicitly incorporate the impact of Type I censored time (C) into the optimization process: CKL-, CLW-, $C\chi^2$ -, and CB-optimal designs. These designs correspond to the Type I censored versions of KL divergence, Lin-Wong divergence, Chi-Square (χ^2) distance measure, and Bhattacharyya (B), respectively. By integrating censoring considerations into the optimization framework, these new formulations aim to provide more robust and practically meaningful experimental designs, particularly in scenarios where censoring plays a crucial role.

Define C^* is the optimal criterion value obtained via optimization algorithms (e.g., PSO, L-BFGS), serving as an evaluation metric for design effectiveness. Meanwhile, \hat{C} is the recalculated criterion value based on the optimized design ξ^* and estimated parameters $\hat{\theta}$, used to assess the stability of the optimization process. The optimization criterion value is formally defined as:

$$C^* = \max_{\xi \in \Xi} \min_{\theta_r \in \Theta_r} \left\{ \int_X \text{Div} (M_1(x, \theta_{tr}), M_2(x, \theta_r)) \xi(dx) \right\}. \quad (3.12)$$

where:

- $\xi \in \Xi$ represents all possible experimental designs. Our goal is to find the optimal design ξ^* within this set.

- $\min_{\theta_r \in \Theta_r}$ represents the rival model parameter in the worst-case scenario, meaning that among all possible values of θ_r , we select the one that minimizes the model's distinguishability.
- $\text{Div}(M_1, M_2)$ is the divergence measure that quantifies the difference between the true model M_1 and the competing model M_2 . This measure can be the CKL divergence, CLW divergence, CB distance, or $C\chi^2$ distance.

The criterion in equation (3.12) follows a max-min strategy. First, for each design ξ , the minimum model distinguishability is computed (i.e., the worst-case discriminability under the least favorable θ_r). Then, the design ξ^* that maximizes this minimum value is selected. In other words, this approach ensures that even in the worst-case scenario, the collected experimental data will still provide the highest level of model distinguishability.

Conjecture 1. *Let $\xi^* \in \Xi$ be a regular divergence-optimal design.*

- (a) *A necessary and sufficient condition for the design ξ^* to be divergence-optimal is $\psi(x; \xi^*) \leq 0$ for all $x \in \mathcal{X}$, where*

$$\psi(x; \xi) = \text{Div}(M_1(x, \theta_{tr}), M_2(x, \hat{\theta}_r)) - \int_{\mathcal{X}} \text{Div}(M_1(x, \theta_{tr}), M_2(x, \hat{\theta}_r)) \xi(dx) \quad (3.13)$$

and $\hat{\theta}_r$ is the unique solution to the inner optimization problem:

$$\hat{\theta}_r = \arg \min_{\theta_r \in \Theta_r} \int_{\mathcal{X}} \text{Div}(M_1(x, \theta_{tr}), M_2(x, \theta_r)) \xi(dx) \quad (3.14)$$

- (b) *The function $\psi(x; \xi^*)$ achieves its maximum value at the support points of the optimal design ξ^* .*

This conjecture generalizes the well-known equivalence theorem under KL-optimality to the broader family of divergence-based design

criteria, such as CKL divergence, CLW divergence, CB distance, or $C\chi^2$ distance.

In practical applications, this optimization problem is typically solved using numerical methods such as Particle Swarm Optimization (PSO) or L-BFGS, allowing us to obtain the most suitable ξ^* . The next section will present numerical simulation results based on this design criterion.

3.3 Numerical Integration for Criterion Computation

In this study, numerical integration serves as the core computational tool for evaluating model discrimination criteria. The integral expressions derived—such as Equations (3.8) through (3.11)—involve censoring adjustments and logarithmic terms, which make them analytically intractable and difficult to solve in closed-form. As a result, closed-form expression of the objective function are often unavailable or impractical. Therefore, we employ numerical approximation methods, specifically using the built-in `integrate()` function in R for efficient and accurate computation.

The fundamental idea of numerical integration originates from the concept of the Riemann sum, which approximates the integral by dividing the integration interval into multiple subintervals and summing the product of the function values and the corresponding subinterval widths. Classical methods such as the trapezoidal rule and Simpson's rule are direct extensions of this idea. However, in practical applications, uniform subdivision may be insufficient when the integrand exhibits rapid variation, sharp peaks, or censoring effects. To address these challenges and improve both accuracy and efficiency, the `integrate()` function adopts

an adaptive quadrature strategy, which dynamically adjusts the subdivision of the interval and the evaluation points according to the local behavior of the integrand ([Davis and Rabinowitz, 2007](#)).

The algorithm first performs a coarse estimation over the entire interval and then recursively subdivides regions where the estimated error exceeds a threshold, forming a set of unequally spaced subintervals. This approach significantly reduces unnecessary computation and concentrates computational effort on regions with high variability. In R, the implementation of `integrate()` combines Romberg integration techniques with recursive partitioning logic, providing robust and accurate approximations in practical scenarios ([Stoer et al., 1980](#)).

In the context of this study, the integrals associated with model discrimination criteria can be reduced to one-dimensional definite integrals through appropriate transformation and truncation handling. As such, the `integrate()` function can be directly applied. Its concise syntax, fast computation, and support for customizable error tolerance and integration bounds make it a practical and efficient tool for the numerical calculations required in this research.

3.4 The PSO-QN Algorithm for Model Discrimination Design Generation

In this study, we employ the PSO-QN algorithm, which integrates Particle Swarm Optimization (PSO) with the Limited-memory Broyden-Fletcher-Goldfarb-Shanno (L-BFGS) method to solve nested optimization problems. This approach was first introduced by [Chen et al. \(2020\)](#) to address the high computational costs associated with the traditional Nested-PSO ([Chen et al., 2015](#)) framework.

The conventional Nested-PSO (Chen et al., 2015) applies PSO to both the outer and inner optimization layers. While effective in exploring the global optimum, this approach becomes computationally expensive, especially when dealing with high-dimensional data or large sample sizes. To overcome this limitation, Chen et al. (2020) proposed the PSO-QN algorithm, which modifies the inner optimization process by combining PSO for outer global search and L-BFGS for inner local optimization. This hybrid approach significantly improves computational efficiency while maintaining strong optimization performance.

In our study, we observe that the optimization criterion function has a nested mathematical structure:

- Inner Problem: Differentiable with respect to parameter θ_2 and convex.
- Outer Problem: Potentially non-convex, with multiple local extrema.

Due to the favorable mathematical properties of the inner function, gradient-based numerical optimization methods can be applied to efficiently determine the optimal solution. For instance, L-BFGS leverages first-order and approximate second-order derivative information to accelerate convergence and is particularly efficient for high-dimensional problems with lower memory requirements. Therefore, after PSO identifies candidate solutions for the global optimum, we further refine them using L-BFGS, ensuring faster and more stable convergence.

This type of nested optimization problem can be exemplified by a KL-optimality criterion under Type-I censoring conditions, represented

as Equation (3.15):

$$\max_{\xi \in \Xi} CKL_{2,tr}(\xi) = \overbrace{\max_{\xi \in \Xi} \min_{\theta_2 \in \Theta_2} \int_X D_{CKL}(f_{tr}, f_r, x, \theta_2) \xi(dx)}^{PSO \text{ (outer)} \quad L-BFGS \text{ (inner)}} \quad (3.15)$$

In this formulation:

- Outer Problem (solved by PSO): $\max_{\xi \in \Xi} CKL_{2,tr}(\xi)$ searches for the global optimal design ξ^* .
- Inner Problem (handled by L-BFGS): $\min_{\theta_2 \in \Theta_2} \int_X D_{CKL}(f_{tr}, f_r, x, \theta_2) \xi(dx)$ performs local minimization of the differentiable inner objective function to evaluate the fitness for the outer problem.

In summary, PSO is responsible for the global search to handle the outer optimization, while L-BFGS refines the local search for the differentiable inner function. This hybrid approach enhances optimization efficiency and ensures robust results.

This method has been successfully applied to model discrimination design problems, particularly in distinguishing between two competing models. However, further simulation tests are required to evaluate its performance across different divergence measures and assess its robustness.

Chapter 4

Numerical Studies

4.1 The Comparison of Integration Methods via non-Censored Example

Before proceeding to the main objectives of this study, we begin by validating the stability of our numerical integration approach through a benchmark example with a known closed-form expression of the objective function. Specifically, we reproduce the KL-optimal design example proposed by [López-Fidalgo et al. \(2007\)](#), in which the authors derived an explicit analytical expression to guide model discrimination. By applying our numerical integration framework under the same conditions, we aim to confirm whether our method can recover consistent results. This verification serves as a foundational check to ensure computational reliability for subsequent simulation studies. The following introduces the experimental background and model specifications of that example.

In practical applications, the errors in pharmacokinetic models are often assumed to follow a Log-Normal distribution. The study considers two competing models: the classical Michaelis–Menten (MM) model and a Modified Michaelis–Menten (MMM) model, which has been adjusted for specific application scenarios. Their definitions are given as

follows:

$$\begin{cases} \text{MMM} : y = \frac{Vx}{K+x} + Fx + \epsilon \\ \text{MM} : y = \frac{Vx}{K+x} + \epsilon \end{cases}, x \in X = [aK, bK].$$

where:

- x represents the substrate concentration, such as drug concentration in plasma or drug dosage.
- y represents the rate of product formation in the chemical reaction.
- V denotes the maximum reaction rate.
- K represents the Michaelis constant (Km), which is the value of x when the reaction rate reaches half of the maximum rate.
- ϵ is the error term, which is assumed to follow a Log-Normal distribution in this context.

[López-Fidalgo and Wong \(2002\)](#) suggested setting $b = 5$, and under this condition, $a = 0.1$ is typically considered the minimum concentration value. Since the original study used a closed-form expression of the objective function to compute the KL divergence, we first conduct a mathematical derivation using the most fundamental notation to establish a general formula, ensuring that key steps are clearly understood. Then, to better align with the application context of this study, we adapt the formula to the model discrimination framework. For instance, σ_1 is further specified as $\sigma_1(x, \theta_1)$. This approach maintains the readability of the mathematical derivation while making its subsequent application more intuitive.

Suppose we have two random variables, P and Q , which follow Log-Normal distributions with means μ_1 and μ_2 and standard deviations σ_1

and σ_2 , respectively. Their probability density functions (PDF) are given as:

$$p(y) = \frac{1}{y\sigma_1\sqrt{2\pi}} e^{-\frac{(\log y - \mu_1)^2}{2\sigma_1^2}},$$

$$q(y) = \frac{1}{y\sigma_2\sqrt{2\pi}} e^{-\frac{(\log y - \mu_2)^2}{2\sigma_2^2}}.$$

The Kullback-Leibler (KL) divergence can be written as:

$$\begin{aligned} D_{KL}(P \parallel Q) &= \int_{-\infty}^{\infty} p(y) \log \left(\frac{p(y)}{q(y)} \right) dy \\ &= \int_0^{\infty} \frac{1}{y\sigma_1\sqrt{2\pi}} e^{-\frac{(\log y - \mu_1)^2}{2\sigma_1^2}} \log \left(\frac{\frac{1}{y\sigma_1\sqrt{2\pi}} e^{-\frac{(\log y - \mu_1)^2}{2\sigma_1^2}}}{\frac{1}{y\sigma_2\sqrt{2\pi}} e^{-\frac{(\log y - \mu_2)^2}{2\sigma_2^2}}} \right) dy \quad (4.1) \\ &= \int_0^{\infty} \frac{1}{y\sigma_1\sqrt{2\pi}} e^{-\frac{(\log y - \mu_1)^2}{2\sigma_1^2}} \left(\log \left(\frac{\sigma_2}{\sigma_1} \right) + \frac{(\log y - \mu_2)^2}{2\sigma_2^2} - \frac{(\log y - \mu_1)^2}{2\sigma_1^2} \right) dy \\ &= \log \left(\frac{\sigma_2}{\sigma_1} \right) \underbrace{\int_0^{\infty} \frac{1}{y\sigma_1\sqrt{2\pi}} e^{-\frac{(\log y - \mu_1)^2}{2\sigma_1^2}} dy}_1 + \frac{1}{2\sigma_2^2} \underbrace{\int_0^{\infty} \frac{1}{y\sigma_1\sqrt{2\pi}} e^{-\frac{(\log y - \mu_1)^2}{2\sigma_1^2}} (\log y - \mu_2)^2 dy}_{\sigma_1^2 + (\mu_1 - \mu_2)^2} \\ &\quad - \frac{1}{2\sigma_1^2} \underbrace{\int_0^{\infty} \frac{1}{y\sigma_1\sqrt{2\pi}} e^{-\frac{(\log y - \mu_1)^2}{2\sigma_1^2}} (\log y - \mu_1)^2 dy}_{\sigma_1^2} \\ &= \log \left(\frac{\sigma_2}{\sigma_1} \right) + \frac{\sigma_1^2 + (\mu_1 - \mu_2)^2}{2\sigma_2^2} - \frac{1}{2} \\ &= \log \left(\frac{\sigma_2}{\sigma_1} \right) + \frac{\sigma_1^2 - \sigma_2^2 + (\mu_1 - \mu_2)^2}{2\sigma_2^2} \\ &= \log \left(\frac{\sigma_2}{\sigma_1} \right) - \frac{\sigma_2^2 - \sigma_1^2 + (\mu_2 - \mu_1)^2}{2\sigma_2^2}. \end{aligned}$$

For the first term of the integral evaluates to:

$$\int_0^{\infty} \frac{1}{y\sigma_1\sqrt{2\pi}} e^{-\frac{(\log y - \mu_1)^2}{2\sigma_1^2}} dy = 1,$$

which follows from the fact that the probability density function of a Log-Normal distribution integrates to 1.

For the second term of the integral evaluates to:

$$\begin{aligned}
& \int_0^\infty \frac{1}{y\sigma_1\sqrt{2\pi}} e^{-\frac{(\log y - \mu_1)^2}{2\sigma_1^2}} (\log y - \mu_2)^2 dy \\
&= E[(\log y - \mu_2)^2] \\
&= E[(\log y - \mu_1 + \mu_1 - \mu_2)^2] \\
&= E(\log y - \mu_1)^2 + 2E[(\log y - \mu_1)(\mu_1 - \mu_2)] + E[(\mu_1 - \mu_2)^2] \\
&= \sigma_1^2 + 2(\mu_1 - \mu_2)E(\log y - \mu_1) + (\mu_1 - \mu_2)^2 \\
&= \sigma_1^2 + 2(\mu_1 - \mu_2) \underbrace{[E(\log y) - \mu_1]}_{= \mu_1 - \mu_1 = 0} + (\mu_1 - \mu_2)^2 \\
&= \sigma_1^2 + (\mu_1 - \mu_2)^2.
\end{aligned}$$

Finally, we apply the derived results to the original model discrimination setting, comparing the discriminative ability of two competing models, MMM and MM, at different design points x . Let $\eta_j(x, \theta_j)$ and $v_j^2(x, \theta_j)$ be the means and variances of the two competing Log-Normal models, and let $\mu_j(x, \theta_j)$ and $\sigma_j^2(x, \theta_j)$ be the mean and variance of the Normal distributions of the logarithm of the observations, where $j = 1, 2$. These quantities are defined as:

$$\begin{aligned}
E(y) &= \eta_j(x, \theta_j) = \exp\left\{\frac{\sigma_j^2(x, \theta_j)}{2} + \mu_j(x, \theta_j)\right\}, \\
Var(y) &= v_j^2(x, \theta_j) = \eta_j^2(x, \theta_j) [\exp\{\sigma_j^2(x, \theta_j)\} - 1].
\end{aligned}$$

Thus, we can further express $\mu_j(x, \theta_j)$ and $\sigma_j^2(x, \theta_j)$ as:

$$\begin{aligned}
\mu_j(x, \theta_j) &= \log \left[\frac{\eta_j(x, \theta_j)}{\{1 + v_j^2(x, \theta_j)\eta_j(x, \theta_j)^{-2}\}^{1/2}} \right], \\
\sigma_j^2(x, \theta_j) &= \log \{1 + v_j^2(x, \theta_j)\eta_j(x, \theta_j)^{-2}\}.
\end{aligned}$$

Following the previous derivation, the KL divergence can be expressed as:

$$D_{KL}(M_1, M_2, x, \theta_1, \theta_2) = \log \left(\frac{\sigma_2(x, \theta_2)}{\sigma_1(x, \theta_1)} \right) - \frac{\sigma_2^2(x, \theta_2) - \sigma_1^2(x, \theta_1) + (\mu_2(x, \theta_2) - \mu_1(x, \theta_1))^2}{2\sigma_2(x, \theta_2)^2}.$$

Since the MM model is a nested version of the MMM model, in this study, the true model is assumed to be the MMM model with known parameters. For example, let $\theta_1 = (V_1, K_1, F_1) = (1, 1, 1)$, and assume that both models share the same variance, i.e., $v_1^2(x) = v_2^2(x, \theta_2) = 1$. However, the literature does not specify the range of θ_2 , so we set $\theta_2 = (V_2, K_2) \in [0.1, 100] \times [0.1, 100]$. In this setting, the KL-optimal design is constructed under the constraint of using three support points, which defines the number of design locations to be allocated. Using the closed-form expression of the objective function derived earlier for computation, the resulting KL-optimal design is:

$$\xi_{KL-c}^* = \left\{ \begin{array}{ccc} 0.1 & 2.5 & 5 \\ 0.538 & 0.329 & 0.133 \end{array} \right\}.$$

The corresponding criterion value is 0.0149, with the parameter combination that minimizes the divergence criterion is identified as $\hat{\theta}_2(\xi_{KL-c}^*) = (18.200, 11.053)$. Additionally, the equivalence theorem is applied to verify whether this design is indeed optimal (Figure 4.1a), and the results confirm that it satisfies the optimality conditions, closely matching those reported in the literature. The specific settings for PSO-QN are as follows: PSO is run with 64 particles over 200 iterations, while L-BFGS is executed for 2 iterations. The total computation time is 39 seconds.

From the above example, it is evident that deriving a closed-form expression of the objective function for the KL-optimal design is highly complex, and in many cases, obtaining a closed-form solution may not be feasible, leading to several limitations. Therefore, we aim to perform numerical integration directly for computation. We apply the integration method described in Section 3.3 to directly evaluate the KL objective function given in Equation (4.1). The advantage of this approach is its ability to accommodate various model assumptions and distributions

without being restricted by closed-form derivations. However, its main drawback is that numerical integration requires significantly longer computation time compared to closed-form solutions. To address this, the following presents results obtained using numerical integration under the same scenario. The resulting KL-optimal design is:

$$\xi_{KL-n}^* = \begin{Bmatrix} 0.1 & 2.5 & 5 \\ 0.538 & 0.329 & 0.133 \end{Bmatrix}.$$

The corresponding criterion value is 0.0149, with the parameter combination that minimizes the divergence criterion is identified as $\hat{\theta}_2(\xi_{KL-n}^*) = (18.200, 11.053)$. Additionally, the equivalence theorem is applied to verify whether this design is indeed optimal (Figure 4.1b). The results confirm that it satisfies the optimality conditions and the outcome closely aligns with the results obtained from the closed-form objective function. This demonstrates the feasibility and reliability of the numerical integration method adopted in this study. The specific settings for PSO-QN are as follows: PSO is run with 64 particles over 200 iterations, while L-BFGS is executed for 2 iterations. The total computation time is 5165 seconds.

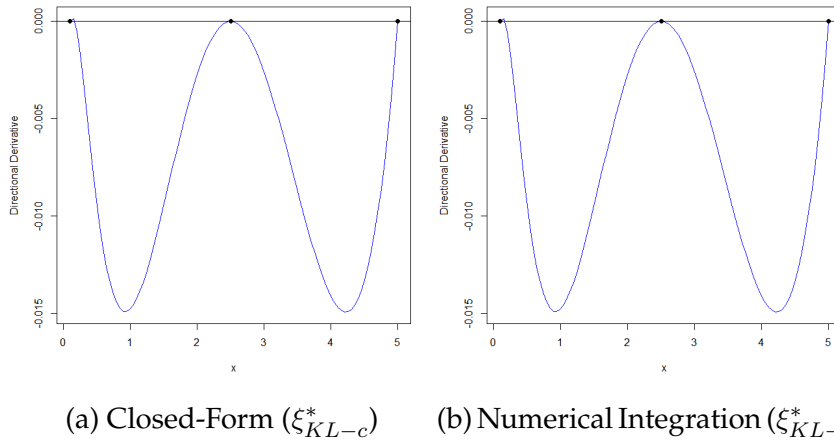


Figure 4.1: The directional derivative plots of the resulting designs discriminating for the MMM vs. MM case assuming Log-Normal response.

López-Fidalgo et al. (2007) explored the computation of KL-optimal design using the Log-Normal distribution and applied a closed-form solution for optimization. Their study primarily focused on pharmacokinetic models, where the error structure is well-suited for modeling with a Log-Normal distribution. However, in reliability testing, the Weibull distribution is widely used for modeling product lifespans, particularly in failure-time modeling within ALT. To extend the model discrimination design to the reliability domain, this study further investigates KL-optimal design under the same context but with a Weibull-distributed error structure. Following the same approach, we first derive a general KL divergence formula using fundamental mathematical notation and attempt to find the optimal design using its closed-form objective function.

Suppose that we have two random variables P and Q , which follow Weibull distributions with shape parameters k_1 and k_2 , and scale parameters λ_1 and λ_2 , respectively. Their probability density functions (PDF) are given by:

$$p(y) = \frac{k_1}{\lambda_1} \left(\frac{y}{\lambda_1} \right)^{k_1-1} e^{-\left(\frac{y}{\lambda_1}\right)^{k_1}},$$

$$q(y) = \frac{k_2}{\lambda_2} \left(\frac{y}{\lambda_2} \right)^{k_2-1} e^{-\left(\frac{y}{\lambda_2}\right)^{k_2}}.$$

For the following integral calculations, γ represents the Euler-Mascheroni constant, and we define the transformation:

$$u = \left(\frac{y}{\lambda_1} \right)^{k_1} \Rightarrow y = \lambda_1 u^{\frac{1}{k_1}} \Rightarrow du = \frac{k_1}{\lambda_1} \left(\frac{y}{\lambda_1} \right)^{k_1-1} dy.$$

Then, the Kullback–Leibler (KL) divergence can be expressed as:

$$\begin{aligned}
D_{KL}(P \parallel Q) &= \int_{-\infty}^{\infty} p(y) \log \left(\frac{p(y)}{q(y)} \right) dy \\
&= \int_0^{\infty} \frac{k_1}{\lambda_1} \left(\frac{y}{\lambda_1} \right)^{k_1-1} e^{-\left(\frac{y}{\lambda_1}\right)^{k_1}} \log \left(\frac{\frac{k_1}{\lambda_1} \left(\frac{y}{\lambda_1} \right)^{k_1-1} e^{-\left(\frac{y}{\lambda_1}\right)^{k_1}}}{\frac{k_2}{\lambda_2} \left(\frac{y}{\lambda_2} \right)^{k_2-1} e^{-\left(\frac{y}{\lambda_2}\right)^{k_2}}} \right) dy \\
&= \log \left(\frac{k_1}{k_2} \right) \underbrace{\int_0^{\infty} \frac{k_1}{\lambda_1} \left(\frac{y}{\lambda_1} \right)^{k_1-1} e^{-\left(\frac{y}{\lambda_1}\right)^{k_1}} dy}_1 + \log \left(\frac{\lambda_2}{\lambda_1} \right) \underbrace{\int_0^{\infty} \frac{k_1}{\lambda_1} \left(\frac{y}{\lambda_1} \right)^{k_1-1} e^{-\left(\frac{y}{\lambda_1}\right)^{k_1}} dy}_1 \\
&\quad + (k_1 - 1) \underbrace{\int_0^{\infty} \frac{k_1}{\lambda_1} \left(\frac{y}{\lambda_1} \right)^{k_1-1} e^{-\left(\frac{y}{\lambda_1}\right)^{k_1}} \log \left(\frac{y}{\lambda_1} \right) dy}_{-\frac{\gamma}{k_1}} - \underbrace{\int_0^{\infty} \frac{k_1}{\lambda_1} \left(\frac{y}{\lambda_1} \right)^{k_1-1} e^{-\left(\frac{y}{\lambda_1}\right)^{k_1}} \left(\frac{y}{\lambda_1} \right)^{k_1} dy}_1 \\
&\quad - (k_2 - 1) \underbrace{\int_0^{\infty} \frac{k_1}{\lambda_1} \left(\frac{y}{\lambda_1} \right)^{k_1-1} e^{-\left(\frac{y}{\lambda_1}\right)^{k_1}} \log \left(\frac{y}{\lambda_2} \right) dy}_{\log \left(\frac{\lambda_1}{\lambda_2} \right) - \frac{\gamma}{k_1}} + \underbrace{\int_0^{\infty} \frac{k_1}{\lambda_1} \left(\frac{y}{\lambda_1} \right)^{k_1-1} e^{-\left(\frac{y}{\lambda_1}\right)^{k_1}} \left(\frac{y}{\lambda_2} \right)^{k_2} dy}_{\left(\frac{\lambda_1}{\lambda_2} \right)^{k_2} \Gamma \left(\frac{k_2}{k_1} + 1 \right)} \\
&= \log \left(\frac{k_1}{k_2} \right) + \log \left(\frac{\lambda_2}{\lambda_1} \right) - \frac{k_1 - 1}{k_1} \gamma - 1 - (k_2 - 1) \log \left(\frac{\lambda_1}{\lambda_2} \right) + \frac{k_2 - 1}{k_1} \gamma + \left(\frac{\lambda_1}{\lambda_2} \right)^{k_2} \Gamma \left(\frac{k_2}{k_1} + 1 \right).
\end{aligned}$$

For the first and second terms of the integral evaluates to:

$$\int_0^{\infty} \frac{k_1}{\lambda_1} \left(\frac{y}{\lambda_1} \right)^{k_1-1} e^{-\left(\frac{y}{\lambda_1}\right)^{k_1}} dy = 1,$$

which follows from the fact that the probability density function of a Weibull distribution integrates to 1.

For the third term of the integral evaluates to:

$$\begin{aligned}
&\int_0^{\infty} \frac{k_1}{\lambda_1} \left(\frac{y}{\lambda_1} \right)^{k_1-1} e^{-\left(\frac{y}{\lambda_1}\right)^{k_1}} \log \left(\frac{y}{\lambda_1} \right) dy \\
&= \int_0^{\infty} e^{-u} \log \left(u^{\frac{1}{k_1}} \right) du \\
&= \frac{1}{k_1} \int_0^{\infty} e^{-u} \log(u) du \\
&= \frac{1}{k_1} - \gamma.
\end{aligned}$$

For the fourth term of the integral evaluates to:

$$\begin{aligned}
& \int_0^\infty \frac{k_1}{\lambda_1} \left(\frac{y}{\lambda_1} \right)^{k_1-1} e^{-\left(\frac{y}{\lambda_1}\right)^{k_1}} \left(\frac{y}{\lambda_1} \right)^{k_2} dy \\
&= \int_0^\infty u e^{-u} du \\
&= \int_0^\infty u^{2-1} e^{-u} du \\
&= \Gamma(2) \\
&= 1.
\end{aligned}$$

For the fifth term of the integral evaluates to:

$$\begin{aligned}
& \int_0^\infty \frac{k_1}{\lambda_1} \left(\frac{y}{\lambda_1} \right)^{k_1-1} e^{-\left(\frac{y}{\lambda_1}\right)^{k_1}} \log \left(\frac{y}{\lambda_2} \right) dy \\
&= \int_0^\infty e^{-u} \log \left(\frac{\lambda_1 u^{\frac{1}{k_1}}}{\lambda_2} \right) du \\
&= \int_0^\infty e^{-u} \log \lambda_1 du + \int_0^\infty e^{-u} \log \left(u^{\frac{1}{k_1}} \right) du - \int_0^\infty e^{-u} \log \lambda_2 du \\
&= \log \lambda_1 (-e^{-u} |_0^\infty) + \frac{1}{k_1} \int_0^\infty e^{-u} \log u du - \log \lambda_2 (-e^{-u} |_0^\infty) \\
&= \log \lambda_1 + \frac{1}{k_1} - \gamma - \log \lambda_2 \\
&= \log \left(\frac{\lambda_1}{\lambda_2} \right) - \frac{\gamma}{k_1}.
\end{aligned}$$

For the sixth term of the integral evaluates to:

$$\begin{aligned}
& \int_0^\infty \frac{k_1}{\lambda_1} \left(\frac{y}{\lambda_1} \right)^{k_1-1} e^{-\left(\frac{y}{\lambda_1}\right)^{k_1}} \left(\frac{y}{\lambda_2} \right)^{k_2} dy \\
&= \int_0^\infty e^{-u} \left(\frac{\lambda_1 u^{\frac{1}{k_1}}}{\lambda_2} \right)^{k_2} du \\
&= \left(\frac{\lambda_1}{\lambda_2} \right)^{k_2} \int_0^\infty u^{\frac{k_2}{k_1}+1-1} e^{-u} du \\
&= \left(\frac{\lambda_1}{\lambda_2} \right)^{k_2} \Gamma \left(\frac{k_2}{k_1} + 1 \right).
\end{aligned}$$

Suppose $\eta_j(x, \theta_j)$ represents the mean of two competing Weibull distribution models, where $j = 1, 2$. It is defined as follows:

$$\begin{aligned} E(y) &= \eta_j(x, \theta_j), \\ Var(y) &= v_j^2(x, \theta_j). \end{aligned}$$

Let $\theta_1 = (V_1, K_1, F_1) = (1, 1, 1)$, and assume that both models share the same variance, i.e., $v_1^2(x) = v_2^2(x, \theta_2) = 1$. Additionally, we assume that $\theta_2 = (V_2, K_2) \in [0.1, 100] \times [0.1, 100]$. We adopt a reparameterized form of the Weibull distribution, where the scale parameter is defined as $\lambda = \exp(\mu)$, and the shape parameter is specified as $k = 1/\sigma$, such that μ and σ approximately represent the log-mean and log-dispersion, respectively. This parameterization improves interpretability and numerical stability, and is conceptually related to the log-Weibull structure frequently used in extreme value theory (Coles et al., 2001). In this setting, we restrict the optimal design to consist of three support points, which defines the number of experimental conditions to be allocated. Using the previously derived closed-form objective function for computation, the resulting KL-optimal design is:

$$\xi_{KL-c}^* = \left\{ \begin{array}{ccc} 0.504 & 2.989 & 5 \\ 0.570 & 0.310 & 0.120 \end{array} \right\}.$$

The corresponding criterion value is 0.00392, with the parameter combination that minimizes the divergence criterion is identified as $\hat{\theta}_2(\xi_{KL-c}^*) = (22.502, 14.580)$. Furthermore, the equivalence theorem was applied to verify whether this design is indeed optimal (Figure 4.2a). The results confirm that it satisfies the optimality conditions. The specific settings for PSO-QN are as follows: PSO was run with 64 particles over 200 iterations, while L-BFGS was executed for 5 iterations. The total computation time was 40 seconds.

Compared to the first example, deriving a closed-form solution in this case is even more complex. To address this, we also provide results obtained via numerical integration under the same scenario and compare them with the closed-form expression of the objective function.

The resulting KL-optimal design is:

$$\xi_{KL-n}^* = \begin{Bmatrix} 0.507 & 2.991 & 5 \\ 0.570 & 0.310 & 0.120 \end{Bmatrix}.$$

The corresponding criterion value is 0.00389, with the parameter combination that minimizes the divergence criterion is identified as $\hat{\theta}_2(\xi_{KL-n}^*) = (22.548, 14.622)$. Additionally, the equivalence theorem was applied to verify whether this design is optimal (Figure 4.2b). The results confirm that it meets the optimality conditions and closely matches the results obtained using the closed-form objective function, further demonstrating the feasibility of our proposed approach. The specific settings for PSO-QN are as follows: PSO was run with 64 particles over 200 iterations, while L-BFGS was executed for 5 iterations. The total computation time was 102768 seconds.

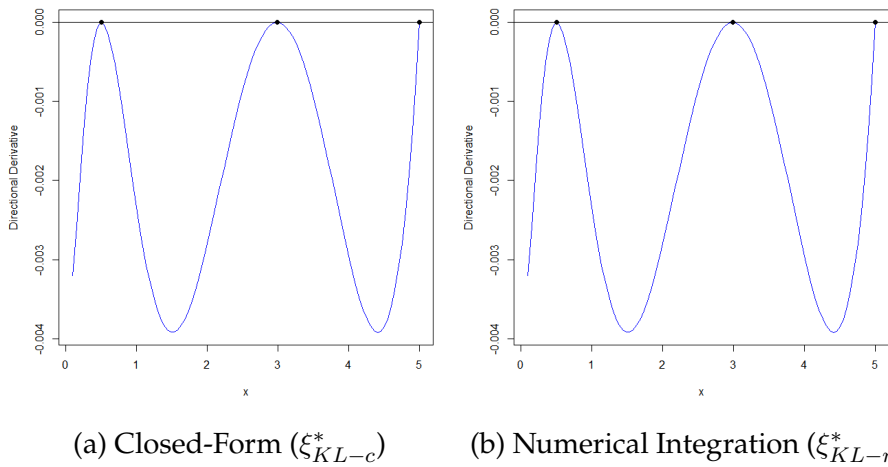


Figure 4.2: The directional derivative plots of the resulting designs discriminating for the MMM vs. MM case assuming Weibull response.

Through the two preceding examples, we have demonstrated the feasibility of using numerical integration in place of closed-form solutions for computing model discrimination criteria. By comparing the outcomes of our numerical approach with those derived from the closed-form expressions in the literature, we found that both methods yield highly consistent design points and criterion values. Additionally, since our computational approach may differ in certain details from the original authors, we conducted verification tests to ensure that our implementation could reliably reproduce published results. The experimental results confirm that our approach successfully replicates the KL-optimal design presented in the literature while exhibiting strong stability and applicability under different distributional assumptions. This suggests that our method is robust enough to handle a wide range of model discrimination problems and is suitable for most practical scenarios.

Having established the feasibility and stability of our approach, we now proceed to the core focus of this study: applying model discrimination design in Accelerated Life Testing (ALT) and optimizing experimental designs using different divergence measures.

4.2 Type I Censoring Model Discrimination Designs with Fixed Variance for Rival Model

Building upon the results validated in the previous section, we confirm the robustness and feasibility of the proposed method. In this section, we shift our focus to the core objective of this study: using the commonly adopted Arrhenius model in the field of reliability, together with Type I censored data- a typical feature in ALT, where the product has not failed at the end of the experiment- to compare the performance of four proposed optimal design strategies for discriminating between two com-

peting models. The two competing models considered in this section are defined as follows:

- The true model M_1 is a quadratic form:

$$\eta_{tr}(x, \theta_1) = \zeta_1 + \zeta_2 x + \zeta_3 x^2. \quad (4.2)$$

- The rival model M_2 is a linear form:

$$\eta_2(x, \theta_2) = \delta_1 + \delta_2 x. \quad (4.3)$$

Here, $\eta(x, \theta)$ represents the mean response function of the model, specifically the expected value of the transformed response variable $\log(t)$. This transformation follows from the Arrhenius model, where the original exponential relationship between lifespan t and temperature is linearized by taking the logarithm of t (see Equation 2.7). The error term ϵ is assumed to follow a log-location-scale distribution. Since the two models are nested, the true model is assumed to be M_1 , with the parameter vector θ corresponding to $(\zeta_1, \zeta_2, \zeta_3)$ for M_1 and (δ_1, δ_2) for M_2 .

To transform temperature into an accelerating variable suitable for modeling, we adopt the following link function based on the Arrhenius relationship:

$$x = \frac{11605}{\text{Temp}_C + 273.15}, \quad (4.4)$$

where Temp_C is temperature in degrees Celsius. This transformation reflects the physical principle that higher temperatures accelerate the failure process and reduce product lifespan.

Based on this foundation, we assume that the product lifespan t follows a Log-Normal distribution. Using maximum likelihood estimation and external real-world data (with a censoring time of 5000), the estimated standard deviation is obtained as $\hat{\sigma} = 0.9780103$. Therefore, the

following simulation scenarios will be based on this estimated parameter. The true model parameters are set as $\theta_{tr} = (\zeta_1, \zeta_2, \zeta_3) = (-5.0, -1.5, 0.05)$. The parameter space of the rival model is defined as $\theta_2 = (\delta_1, \delta_2) \in [-100, -10] \times [0.1, 5.0]$. The design space is set to $x \in [10, 80]$.

In the following simulations, the standard deviation parameter is based on the maximum likelihood estimate $\hat{\sigma} = 0.9780103$, with extended scenarios explored for comparative analysis. For simplicity of presentation, the values are referred to using their leading digits (e.g., 0.98, 1.48, 1.98), while the actual values used in computation retain full precision (e.g., 0.9780103, 1.4780103, 1.9780103). The specific settings for PSO-QN are as follows: PSO was run with 64 particles over 200 iterations, while L-BFGS was executed for 50 iterations.

In the following table 4.1 through 4.8, the column Dis. denotes the assumed model distribution type, including Log-Normal (LN) and Weibull (WB). Under four different divergence measures criteria, this study identifies the optimal experimental design for model discrimination, the parameter combination that minimizes the divergence criterion is identified as $\hat{\theta}$, and calculates the criterion value C^* to evaluate design performance. To assess the stability of the optimization process, the obtained design and the parameter combination are fed back into the algorithm to recompute the criterion value \hat{C} for consistency verification. The column Time records the CPU computation time for each scenario, measured in seconds, providing a basis for comparing computational efficiency across different designs.

Finally, the column Eqv. records the results of the equivalence theorem verification. To determine whether the design satisfies the optimality condition, we assess the following characteristics:

1. All support points in the approximate design have non-zero weights.
2. In the directional derivative plot, the blue function should lie entirely below zero, indicating that no other design point would improve the criterion.
3. The marked design points (black dots) must coincide exactly with the local maxima of the directional derivative function, and these maxima must equal zero—this is the key condition for confirming optimality.
4. The overall shape of the curve should be smooth and approximately parabolic, consistent with traditional optimal design geometry.

The optimality check results are classified into three levels:

- \checkmark indicates full satisfaction of the optimality conditions:

All four conditions are met, including: each support point has a non-zero weight; the directional derivative function lies entirely below zero; the design points correspond to local maxima of the function with value exactly zero; and the curve is smooth and continuous in shape.

- \triangle indicates partial satisfaction, typically arising in the following scenarios:
 - Although the function remains entirely below zero and the design points align with the local maxima of the directional derivative, only one point has non-zero weight.
 - A small portion of the directional derivative slightly exceeds zero, but the overall curve remains near zero, suggesting potential for achieving optimality.

- The function lies entirely below zero, but the local maxima do not coincide with the support points.
 - The directional derivative curve is not clearly displayed due to extremely small variation, making optimality difficult to assess visually; however, the structure suggests potential fulfillment of the conditions.
- \times indicates that the optimality conditions are not satisfied:

None of the above conditions are met.

Tables 4.1, 4.3, 4.5, and 4.7 summarize the performance of four divergence measures (CKL, CLW, CB, and $C\chi^2$) under the scenario where both competing models assume equal variance. In contrast, Tables 4.2, 4.4, 4.6, and 4.8 report the results when the models assume unequal variances.

1. CKL-optimal design (Tables 4.1 & 4.2): 18 simulation cases were conducted, with 12 fully satisfying optimality conditions (\checkmark), 3 partially satisfying (Δ), and 3 not satisfying (\times).
2. CLW-optimal design (Tables 4.3 & 4.4): Among 18 cases, only 4 achieved full optimality(\checkmark), 6 were partial(Δ), and 8 failed(\times).
3. CB-optimal design (Tables 4.5 & 4.6): None of the 18 designs fully satisfied the conditions(\checkmark); 14 were partial(Δ) and 4 failed(\times).
4. $C\chi^2$ -optimal design (Tables 4.7 & 4.8): Among 18 cases, 2 cases met full optimality(\checkmark), 7 were partial(Δ), and 9 failed(\times).

Notably, when a design fully satisfies the optimality conditions, the computed criterion value C^* is nearly identical to the re-evaluated value \hat{C} using the derived design and identified parameter combination—indicating algorithmic stability and robustness. It is worth emphasizing

that the CB-optimal designs, due to the nature of their divergence formula, often yield results where the criterion value C^* is either 1, 0, or an extremely small value. These results tend to be computed in very short time—suggesting that the optimization algorithm may have converged prematurely to an incorrect or suboptimal region, rather than locating a truly optimal design. Thus, although the computational time appears efficient, such rapid convergence often leads to designs that fail to satisfy optimality conditions and should be interpreted with caution.

As for the designs that partially or completely fail to meet optimality conditions, several possible explanations arise. The first relates to numerical instability during integration. While earlier validation confirmed the feasibility of the integration routine, the increased complexity introduced by Type I censored data and more intricate model structures may lead to localized numerical errors that distort the criterion evaluation. Another important consideration lies in the nature of the inner-loop optimization. Although the objective function is theoretically differentiable, it may not be sufficiently smooth in practice. In particular, if the function surface contains multiple local extrema—such as wave-like patterns—then quasi-Newton methods like L-BFGS, which rely on consistent curvature and a single basin of attraction, may perform poorly. This mismatch can lead to inaccurate gradients and hinder convergence, ultimately degrading design quality.

In conclusion, even under uniform initialization, the design outcomes remain sensitive to model assumptions, objective function properties, and numerical stability. Thus, each solution should be assessed not only by its computed criterion value but also through equivalence checks and the directional derivative plots, ensuring a more reliable and interpretable design process.

Table 4.1: Summary of CKL-optimal design results for cases of Quadratic vs. Linear means under with equal variance

Dis.	σ	ξ_{CKL}^*	$C^*(\hat{C})$	$\hat{\theta}_2(\xi_{CKL}^*)$	Eqv.	Opt?	Time
LN	0.98	$\begin{Bmatrix} 33.557 & 56.829 & 80 \\ 0.330 & 0.436 & 0.234 \end{Bmatrix}$	$\begin{matrix} 0.00927 \\ (0.00927) \end{matrix}$	$(-66.712, 2.017)$	A.1a	✓	18386
LN	1.48	$\begin{Bmatrix} 29.699 & 55.482 & 80 \\ 0.360 & 0.413 & 0.227 \end{Bmatrix}$	$\begin{matrix} 0.00517 \\ (0.00517) \end{matrix}$	$(-67.204, 2.031)$	A.1c	✓	58458
LN	1.98	$\begin{Bmatrix} 25.854 & 55.196 & 80 \\ 0.366 & 0.407 & 0.227 \end{Bmatrix}$	$\begin{matrix} 0.00385 \\ (0.00380) \end{matrix}$	$(-66.268, 2.006)$	A.1e	△	49577
WB	0.98	$\begin{Bmatrix} 32.545 & 57.686 & 80 \\ 0.368 & 0.415 & 0.217 \end{Bmatrix}$	$\begin{matrix} 0.00822 \\ (0.00822) \end{matrix}$	$(-66.459, 2.010)$	A.1b	△	59919
WB	1.48	$\begin{Bmatrix} 25.576 & 55.791 & 80 \\ 0.441 & 0.359 & 0.200 \end{Bmatrix}$	$\begin{matrix} 0.00489 \\ (0.00489) \end{matrix}$	$(-67.083, 2.028)$	A.1d	✓	68091
WB	1.98	$\begin{Bmatrix} 18.386 & 53.830 & 80 \\ 0.484 & 0.325 & 0.191 \end{Bmatrix}$	$\begin{matrix} 0.00386 \\ (0.00386) \end{matrix}$	$(-63.987, 1.944)$	A.1f	×	62045

Table 4.2: Summary of CKL-optimal design results for cases of Quadratic vs. Linear means under with unequal variance

Dis.	σ_1	σ_2	ξ_{CKL}^*	$C^*(\hat{C})$	$\hat{\theta}_2(\xi_{CKL}^*)$	Eqv.	Opt?	Time
LN	1.98	0.98	$\begin{Bmatrix} 76.132 & 80 & 80 \\ 0.000 & 0.000 & 1.000 \end{Bmatrix}$	$\begin{matrix} 0.841 \\ (0.841) \end{matrix}$	$(-52.575, 1.591)$	A.2a	△	62666
LN	0.98	1.98	$\begin{Bmatrix} 50.868 & 65.674 & 80 \\ 0.167 & 0.545 & 0.289 \end{Bmatrix}$	$\begin{matrix} 0.327 \\ (0.327) \end{matrix}$	$(-63.613, 1.925)$	A.2b	✓	53043
LN	0.98	1.48	$\begin{Bmatrix} 33.417 & 62.084 & 80 \\ 0.032 & 0.587 & 0.381 \end{Bmatrix}$	$\begin{matrix} 0.133 \\ (0.133) \end{matrix}$	$(-64.846, 1.962)$	A.2c	✓	54685
LN	1.48	0.98	$\begin{Bmatrix} 52.007 & 67.791 & 80 \\ 0.085 & 0.577 & 0.338 \end{Bmatrix}$	$\begin{matrix} 0.230 \\ (0.230) \end{matrix}$	$(-62.900, 1.904)$	A.2d	✓	65978
LN	0.48	0.98	$\begin{Bmatrix} 43.412 & 61.109 & 80 \\ 0.213 & 0.521 & 0.266 \end{Bmatrix}$	$\begin{matrix} 0.339 \\ (0.339) \end{matrix}$	$(-65.183, 1.972)$	A.2e	×	23744
LN	0.98	0.48	$\begin{Bmatrix} 47.75 & 64.187 & 80 \\ 0.161 & 0.547 & 0.292 \end{Bmatrix}$	$\begin{matrix} 0.885 \\ (0.885) \end{matrix}$	$(-64.115, 1.940)$	A.2f	✓	30497
WB	1.98	0.98	$\begin{Bmatrix} 58.678 & 69.702 & 80 \\ 0.154 & 0.551 & 0.295 \end{Bmatrix}$	$\begin{matrix} 0.600 \\ (0.600) \end{matrix}$	$(-61.542, 1.884)$	A.3a	✓	109772
WB	0.98	1.98	$\begin{Bmatrix} 46.469 & 62.717 & 80 \\ 0.215 & 0.525 & 0.261 \end{Bmatrix}$	$\begin{matrix} 0.292 \\ (0.292) \end{matrix}$	$(-64.861, 1.955)$	A.3b	✓	76696
WB	0.98	1.48	$\begin{Bmatrix} 32.393 & 59.119 & 80 \\ 0.064 & 0.597 & 0.339 \end{Bmatrix}$	$\begin{matrix} 0.117 \\ (0.117) \end{matrix}$	$(-66.032, 1.992)$	A.3c	✓	79644
WB	1.48	0.98	$\begin{Bmatrix} 49.573 & 64.735 & 80 \\ 0.181 & 0.549 & 0.270 \end{Bmatrix}$	$\begin{matrix} 0.176 \\ (0.600) \end{matrix}$	$(-63.807, 1.939)$	A.3d	✓	102226
WB	0.48	0.98	$\begin{Bmatrix} 41.993 & 58.347 & 76.142 \\ 0.231 & 0.526 & 0.244 \end{Bmatrix}$	$\begin{matrix} 0.303 \\ (0.227) \end{matrix}$	$(-70.313, 2.112)$	A.3e	×	62836
WB	0.98	0.48	$\begin{Bmatrix} 45.473 & 62.576 & 80 \\ 0.189 & 0.551 & 0.260 \end{Bmatrix}$	$\begin{matrix} 0.635 \\ (0.635) \end{matrix}$	$(-64.316, 1.957)$	A.3f	✓	81337

Table 4.3: Summary of CLW-optimal design results for cases of Quadratic vs. Linear means under with equal variance

Dis.	σ	ξ_{CLW}^*	$C^*(\hat{C})$	$\hat{\theta}_2(\xi_{CLW}^*)$	Eqv.	Opt?	Time
LN	0.98	$\begin{Bmatrix} 10 & 31.597 & 31.714 \\ 0.000 & 0.999 & 0.001 \end{Bmatrix}$	$\begin{matrix} 0.00551 \\ (0.00551) \end{matrix}$	$(-94.530, 3.277)$	A.4a	×	793
LN	1.48	$\begin{Bmatrix} 79.410 & 80 & 80 \\ 1.000 & 0.000 & 0.000 \end{Bmatrix}$	$\begin{matrix} 0.693 \\ (-2.675 \times 10^{-6}) \end{matrix}$	$(-86.830, 2.632)$	A.4c	×	3239
LN	1.98	$\begin{Bmatrix} 80 & 80 & 80 \\ 0.066 & 0.143 & 0.791 \end{Bmatrix}$	$\begin{matrix} 0.693 \\ (-7.356 \times 10^{-6}) \end{matrix}$	$(-73.661, 2.232)$	A.4e	×	3299
WB	0.98	$\begin{Bmatrix} 66.764 & 69.61 & 80 \\ 0.001 & 0.998 & 0.001 \end{Bmatrix}$	$\begin{matrix} 0.694 \\ (0.694) \end{matrix}$	$(-67.984, 2.751)$	A.4b	\triangle	3175
WB	1.48	$\begin{Bmatrix} 58.379 & 59.356 & 80 \\ 0.001 & 0.989 & 0.010 \end{Bmatrix}$	$\begin{matrix} 0.693 \\ (-8.071 \times 10^{-6}) \end{matrix}$	$(-62.162, 1.883)$	A.4d	×	5288
WB	1.98	$\begin{Bmatrix} 16.897 & 53.487 & 80 \\ 0.482 & 0.311 & 0.207 \end{Bmatrix}$	$\begin{matrix} 0.00107 \\ (-0.000827) \end{matrix}$	$(-62.796, 1.907)$	A.4f	✓	32163

Table 4.4: Summary of CLW-optimal design results for cases of Quadratic vs. Linear means under with unequal variance

Dis.	σ_1	σ_2	ξ_{CLW}^*	$C^*(\hat{C})$	$\hat{\theta}_2(\xi_{CLW}^*)$	Eqv.	Opt?	Time
LN	1.98	0.98	$\begin{Bmatrix} 52.005 & 57.073 & 80 \\ 0.000 & 1.000 & 0.000 \end{Bmatrix}$	$\begin{matrix} 0.0751 \\ (0.0732) \end{matrix}$	$(-66.588, 2.010)$	A.5a	×	4343
LN	0.98	1.98	$\begin{Bmatrix} 57.022 & 68.893 & 72.433 \\ 0.000 & 0.000 & 1.000 \end{Bmatrix}$	$\begin{matrix} 0.705 \\ (0.705) \end{matrix}$	$(-82.884, 4.692)$	A.5b	\triangle	2592
LN	0.98	1.48	$\begin{Bmatrix} 61.118 & 62.214 & 80 \\ 0.726 & 0.126 & 0.148 \end{Bmatrix}$	$\begin{matrix} 0.0475 \\ (0.0451) \end{matrix}$	$(-62.081, 1.880)$	A.5c	✓	3316
LN	1.48	0.98	$\begin{Bmatrix} 57.404 & 61.771 & 80 \\ 0.288 & 0.217 & 0.495 \end{Bmatrix}$	$\begin{matrix} 0.0315 \\ (0.0307) \end{matrix}$	$(-62.481, 1.892)$	A.5d	✓	3583
LN	0.48	0.98	$\begin{Bmatrix} 69.351 & 76.607 & 80 \\ 0.856 & 0.031 & 0.113 \end{Bmatrix}$	$\begin{matrix} 0.695 \\ (0.131) \end{matrix}$	$(-84.952, 2.556)$	A.5e	×	2608
LN	0.98	0.48	$\begin{Bmatrix} 45.006 & 50.316 & 80 \\ 0.436 & 0.000 & 0.564 \end{Bmatrix}$	$\begin{matrix} 0.0858 \\ (0.686) \end{matrix}$	$(-71.609, 2.537)$	A.5f	\triangle	3455
WB	1.98	0.98	$\begin{Bmatrix} 76.217 & 80 & 80 \\ 1.000 & 0.000 & 0.000 \end{Bmatrix}$	$\begin{matrix} 0.693 \\ (0.0664) \end{matrix}$	$(-66.549, 2.020)$	A.6a	\triangle	2497
WB	0.98	1.98	$\begin{Bmatrix} 49.129 & 63.954 & 80 \\ 0.230 & 0.513 & 0.257 \end{Bmatrix}$	$\begin{matrix} 0.496 \\ (0.496) \end{matrix}$	$(-65.295, 1.943)$	A.6b	×	666111
WB	0.98	1.48	$\begin{Bmatrix} 31.711 & 59.803 & 80 \\ 0.203 & 0.533 & 0.265 \end{Bmatrix}$	$\begin{matrix} 0.0386 \\ (0.0366) \end{matrix}$	$(-70.211, 2.114)$	A.6c	\triangle	5097
WB	1.48	0.98	$\begin{Bmatrix} 62.798 & 65.451 & 80 \\ 0.583 & 0.330 & 0.087 \end{Bmatrix}$	$\begin{matrix} 0.0284 \\ (0.693) \end{matrix}$	$(-59.234, 2.380)$	A.6d	✓	4659
WB	0.48	0.98	$\begin{Bmatrix} 74.778 & 75.283 & 75.604 \\ 0.030 & 0.477 & 0.493 \end{Bmatrix}$	$\begin{matrix} 0.351 \\ (0.693) \end{matrix}$	$(-40.068, 1.937)$	A.6e	\triangle	3694
WB	0.98	0.48	$\begin{Bmatrix} 41.785 & 60.771 & 80 \\ 0.462 & 0.538 & 0.000 \end{Bmatrix}$	$\begin{matrix} 0.0703 \\ (0.596) \end{matrix}$	$(-73.372, 2.611)$	A.6f	×	4721

Table 4.5: Summary of CB-optimal design results for cases of Quadratic vs. Linear means under with equal variance

Dis.	σ	ξ_{CB}^*	$C^*(\hat{C})$	$\hat{\theta}_2(\xi_{CB}^*)$	Eqv.	Opt?	Time
LN	0.98	$\begin{Bmatrix} 10 & 10 & 10 \\ 0.001 & 0.210 & 0.789 \end{Bmatrix}$	$\begin{matrix} 1 \\ (1) \end{matrix}$	$(-83.787, 3.896)$	A.7a	\triangle	319
LN	1.48	$\begin{Bmatrix} 21.036 & 37.942 & 43.839 \\ 1.000 & 0.000 & 0.000 \end{Bmatrix}$	$\begin{matrix} 4.661 \times 10^{-75} \\ (1.000) \end{matrix}$	$(-50.864, 2.922)$	A.7c	\triangle	336
LN	1.98	$\begin{Bmatrix} 10 & 10 & 10 \\ 0.037 & 0.225 & 0.738 \end{Bmatrix}$	$\begin{matrix} 1.000 \\ (1.807 \times 10^{-43}) \end{matrix}$	$(-65.133, 0.757)$	A.7e	\times	308
WB	0.98	$\begin{Bmatrix} 13.011 & 31.319 & 72.62 \\ 0.715 & 0.020 & 0.265 \end{Bmatrix}$	$\begin{matrix} 0 \\ (0) \end{matrix}$	$(-98.112, 1.771)$	A.7b	\triangle	549
WB	1.48	$\begin{Bmatrix} 11.236 & 16.331 & 51.198 \\ 0.127 & 0.102 & 0.771 \end{Bmatrix}$	$\begin{matrix} 0 \\ (0) \end{matrix}$	$(-60.391, 0.729)$	A.7d	\triangle	443
WB	1.98	$\begin{Bmatrix} 11.969 & 22.932 & 40.06 \\ 0.432 & 0.001 & 0.567 \end{Bmatrix}$	$\begin{matrix} 0 \\ (0) \end{matrix}$	$(-77.064, 1.004)$	A.7f	\triangle	1871

Table 4.6: Summary of CB-optimal design results for cases of Quadratic vs. Linear means under with unequal variance

Dis.	σ_1	σ_2	ξ_{CB}^*	$C^*(\hat{C})$	$\hat{\theta}_2(\xi_{CB}^*)$	Eqv.	Opt?	Time
LN	1.98	0.98	$\begin{Bmatrix} 10 & 10 & 10 \\ 0.018 & 0.328 & 0.654 \end{Bmatrix}$	$\begin{matrix} 1.000 \\ (9.038 \times 10^{-60}) \end{matrix}$	$(-80.856, 1.492)$	A.8a	\triangle	320
LN	0.98	1.98	$\begin{Bmatrix} 10 & 10 & 10 \\ 0.042 & 0.058 & 0.900 \end{Bmatrix}$	$\begin{matrix} 1 \\ (1) \end{matrix}$	$(-62.980, 3.691)$	A.8b	\times	2592
LN	0.98	1.48	$\begin{Bmatrix} 10 & 10 & 10 \\ 0.004 & 0.355 & 0.641 \end{Bmatrix}$	$\begin{matrix} 1 \\ (1.761 \times 10^{-116}) \end{matrix}$	$(-77.233, 0.903)$	A.8c	\times	333
LN	1.48	0.98	$\begin{Bmatrix} 15.502 & 40.168 & 76.326 \\ 0.088 & 0.276 & 0.637 \end{Bmatrix}$	$\begin{matrix} 0 \\ (0.256) \end{matrix}$	$(-43.561, 2.292)$	A.8d	\times	443
LN	0.48	0.98	$\begin{Bmatrix} 10 & 10 & 13.664 \\ 0.336 & 0.527 & 0.137 \end{Bmatrix}$	$\begin{matrix} 1 \\ (1) \end{matrix}$	$(-12.408, 4.678)$	A.8e	\triangle	333
LN	0.98	0.48	$\begin{Bmatrix} 29.672 & 67.096 & 74.092 \\ 0.621 & 0.198 & 0.180 \end{Bmatrix}$	$\begin{matrix} 0 \\ (2.069 \times 10^{-20}) \end{matrix}$	$(-88.604, 2.237)$	A.8f	\triangle	316
WB	1.98	0.98	$\begin{Bmatrix} 34.337 & 71.517 & 79.083 \\ 0.118 & 0.545 & 0.338 \end{Bmatrix}$	$\begin{matrix} 0 \\ (0) \end{matrix}$	$(-78.484, 1.190)$	A.9a	\triangle	1120
WB	0.98	1.98	$\begin{Bmatrix} 25.219 & 33.485 & 72.658 \\ 0.127 & 0.763 & 0.110 \end{Bmatrix}$	$\begin{matrix} 0 \\ (0) \end{matrix}$	$(-63.610, 0.858)$	A.9b	\triangle	1452
WB	0.98	1.48	$\begin{Bmatrix} 22.499 & 23.034 & 43.321 \\ 0.144 & 0.322 & 0.534 \end{Bmatrix}$	$\begin{matrix} 0 \\ (0) \end{matrix}$	$(-67.238, 0.887)$	A.9c	\triangle	445
WB	1.48	0.98	$\begin{Bmatrix} 10 & 10 & 10 \\ 0.057 & 0.419 & 0.524 \end{Bmatrix}$	$\begin{matrix} 0.999 \\ (0.999) \end{matrix}$	$(-58.774, 3.780)$	A.9d	\triangle	706
WB	0.48	0.98	$\begin{Bmatrix} 48.499 & 55.901 & 62.657 \\ 0.007 & 0.823 & 0.170 \end{Bmatrix}$	$\begin{matrix} 0 \\ (2.870 \times 10^{-17}) \end{matrix}$	$(-43.884, 3.505)$	A.9e	\triangle	518
WB	0.98	0.48	$\begin{Bmatrix} 10 & 46.047 & 70.919 \\ 1.000 & 0.000 & 0.000 \end{Bmatrix}$	$\begin{matrix} 1.000 \\ (1.000) \end{matrix}$	$(-52.593, 3.173)$	A.9f	\triangle	551

Table 4.7: Summary of $C\chi^2$ -optimal design results for cases of Quadratic vs. Linear means under with equal variance

Dis.	σ	$\xi_{C\chi^2}^*$	$C^*(\hat{C})$	$\hat{\theta}_2(\xi_{C\chi^2}^*)$	Eqv.	Opt?	Time
LN	0.98	$\begin{Bmatrix} 80 & 80 & 80 \\ 0.014 & 0.449 & 0.537 \end{Bmatrix}$	4.938×10^{11} (-1.698×10^{-10})	(-75.507, 2.289)	A.10a	×	3394
LN	1.48	$\begin{Bmatrix} 41.953 & 46.694 & 47.929 \\ 0.000 & 0.000 & 1.000 \end{Bmatrix}$	726.370 (-9.216×10^{-6})	(-65.563, 1.983)	A.10c	×	2277
LN	1.98	$\begin{Bmatrix} 22.557 & 28.732 & 34.66 \\ 0.000 & 1.000 & 0.000 \end{Bmatrix}$	0.0230 (0.0233)	(-64.951, 1.967)	A.10e	△	1353
WB	0.98	$\begin{Bmatrix} 11.049 & 16.362 & 34.388 \\ 0.000 & 0.000 & 1.000 \end{Bmatrix}$	0.0296 (-4.966×10^{-9})	(-59.045, 1.819)	A.10b	△	25836
WB	1.48	$\begin{Bmatrix} 29.181 & 46.269 & 61.937 \\ 0.999 & 0.000 & 0.001 \end{Bmatrix}$	0.0196 (-4.332×10^{-9})	(-71.474, 2.151)	A.10d	×	65818
WB	1.98	$\begin{Bmatrix} 12.069 & 23.116 & 31.719 \\ 0.000 & 1.000 & 0.000 \end{Bmatrix}$	0.0146 (-4.941×10^{-9})	(-62.198, 1.919)	A.10f	×	47360

Table 4.8: Summary of $C\chi^2$ -optimal design results for cases of Quadratic vs. Linear means under with unequal variance

Dis.	σ_1	σ_2	$\xi_{C\chi^2}^*$	$C^*(\hat{C})$	$\hat{\theta}_2(\xi_{C\chi^2}^*)$	Eqv.	Opt?	Time
LN	1.98	0.98	$\begin{Bmatrix} 80 & 80 & 80 \\ 0.000 & 0.005 & 0.995 \end{Bmatrix}$	457251.8 (-0.969)	(-59.428, 1.893)	A.11a	×	5395
LN	0.98	1.98	$\begin{Bmatrix} 45.597 & 61.641 & 64.68 \\ 0.000 & 1.000 & 0.000 \end{Bmatrix}$	0.532 (0.526)	(-59.442, 1.804)	A.11b	△	2931
LN	0.98	1.48	$\begin{Bmatrix} 30.879 & 61.575 & 69.17 \\ 0.000 & 1.000 & 0.000 \end{Bmatrix}$	0.219 (0.218)	(-64.922, 1.967)	A.11c	△	2413
LN	1.48	0.98	$\begin{Bmatrix} 43.696 & 45.881 & 66.72 \\ 0.000 & 0.000 & 1.000 \end{Bmatrix}$	13.689 (13.692)	(-62.586, 1.890)	A.11d	△	4297
LN	0.48	0.98	$\begin{Bmatrix} 54.039 & 80 & 80 \\ 0.000 & 0.004 & 0.996 \end{Bmatrix}$	8.422×10^{11} (-1.000)	(-69.759, 2.146)	A.11e	×	3450
LN	0.98	0.48	$\begin{Bmatrix} 80 & 80 & 80 \\ 0.022 & 0.380 & 0.598 \end{Bmatrix}$	4.938×10^{15} (167714.9)	(-75.719, 2.287)	A.11f	×	3560
WB	1.98	0.98	$\begin{Bmatrix} 10 & 34.502 & 53.741 \\ 1.000 & 0.000 & 0.000 \end{Bmatrix}$	-51105.61 (-163214.6)	(-45.631, 2.366)	A.12a	×	72416
WB	0.98	1.98	$\begin{Bmatrix} 56.336 & 58.701 & 76.992 \\ 0.000 & 1.000 & 0.000 \end{Bmatrix}$	0.494 (0.487)	(-58.049, 1.761)	A.12b	×	26184
WB	0.98	1.48	$\begin{Bmatrix} 30.746 & 61.381 & 80 \\ 0.000 & 0.361 & 0.639 \end{Bmatrix}$	0.192 (0.189)	(-62.108, 1.878)	A.12c	×	94295
WB	1.48	0.98	$\begin{Bmatrix} 80 & 80 & 80 \\ 0.002 & 0.005 & 0.993 \end{Bmatrix}$	1.152 (1.152)	(-56.581, 1.735)	A.12d	△	154226
WB	0.48	0.98	$\begin{Bmatrix} 41.312 & 57.184 & 74.433 \\ 0.228 & 0.526 & 0.246 \end{Bmatrix}$	0.507 (0.507)	(-66.715, 2.013)	A.12e	△	92497
WB	0.98	0.48	$\begin{Bmatrix} 10 & 32.163 & 46.132 \\ 0.000 & 0.005 & 0.995 \end{Bmatrix}$	4996.081 (-12323.91)	(-55.175, 2.385)	A.12f	×	5097

4.3 Type I Censoring Model Discrimination Designs with Parameterized Variance for Rival Model

Based on the results from the previous section, only the CKL-optimal design exhibited stable performance under censoring. Therefore, in the following simulation study, we focus solely on the CKL-optimal design. Unlike the previous setting where variances of both models were fixed, we now incorporate variance as part of the parameter search to enable a more flexible and realistic analysis framework.

4.3.1 Competing Mean Responses, Equal Distribution Assumption with Parameterized Variance

To investigate the scenario where the variance of the rival model must also be included in parameter search, this section continues the previous experimental design setting. The true model parameters are specified as $\theta_{tr} = (\zeta_1, \zeta_2, \zeta_3) = (-5.0, -1.5, 0.05)$, with the variance fixed at the previously well-performing values (0.9780103 and 1.4780103). The rival model parameters are set as $(\delta_1, \delta_2) \in [-100, -10] \times [0.1, 5.0]$, with an additional unknown constant variance parameter σ_2 assumed to lie within the range $\sigma_2 \in [0.4780103, 4.9780103]$. The censoring time is 5000. The experimental design space is $x \in [10, 80]$. The PSO-QN settings are as follows: PSO uses 64 particles and 200 iterations, while L-BFGS is set to 50 iterations.

In this section, we investigate the CKL-optimal designs under two scenarios: when both models assume a Log-Normal distribution and when both assume a Weibull distribution.

The current model settings are as follows:

- The true model M_1 is a quadratic form:

$$\eta_{tr}(x, \theta_1) = \zeta_1 + \zeta_2 x + \zeta_3 x^2. \quad (4.5)$$

- The rival model M_2 is a linear form:

$$\eta_2(x, \theta_2) = \delta_1 + \delta_2 x. \quad (4.6)$$

The key difference from previous settings is that the parameter vectors are now defined as $\theta_{tr} = (\zeta_1, \zeta_2, \zeta_3)$ for the true model and $\theta_2 = (\delta_1, \delta_2, \sigma_2)$ for the rival model, meaning that M_2 additionally includes an unknown variance parameter σ_2 that is treated as a search variable in the optimization process.

- Both models follow the Log-Normal distribution:

1. True model variance is 0.9780103 :

$$\xi_{CKL}^* = \begin{Bmatrix} 33.799 & 57.185 & 80 \\ 0.317 & 0.443 & 0.240 \end{Bmatrix}.$$

The corresponding criterion value is 9.116×10^{-3} , and the parameter combination is identified as $\hat{\theta}_2(\xi_{CKL}^*) = (\hat{\delta}_1, \hat{\delta}_2, \hat{\sigma}_2) = (-66.584, 2.013, 0.965)$. Furthermore, the equivalence theorem confirms the optimality of this design (Figure 4.3a). The results confirm that it satisfies the optimality conditions. The total computation time is 144836 seconds.

2. True model variance is 1.4780103 :

$$\xi_{CKL}^* = \begin{Bmatrix} 29.974 & 56.272 & 80 \\ 0.339 & 0.423 & 0.238 \end{Bmatrix}.$$

The corresponding criterion value is 0.00501, and the parameter combination is identified as $\hat{\theta}_2(\xi_{CKL}^*) = (\hat{\delta}_1, \hat{\delta}_2, \hat{\sigma}_2) = (-66.986, 2.025, 1.457)$.

Again, the optimality of this design is verified via the equivalence theorem (Figure 4.3b). The results confirm that it satisfies the optimality conditions. The total computation time is 149893 seconds.

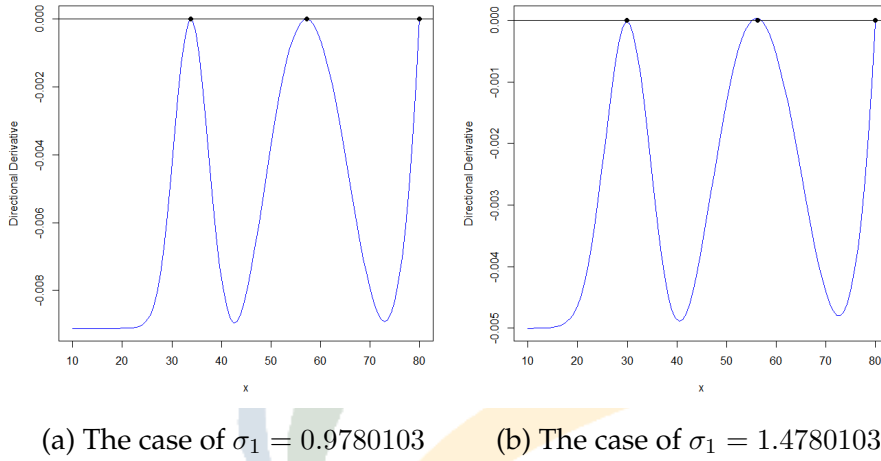


Figure 4.3: The directional derivative plots of the resulting designs ξ_{CKL}^* discriminating for the cases of Quadratic vs. Linear means assuming Log-Normal response.

- Both models follow the Weibull distribution:

1. True model variance is 0.9780103 :

$$\xi_{CKL}^* = \left\{ \begin{array}{ccc} 33.531 & 58.185 & 80 \\ 0.340 & 0.434 & 0.226 \end{array} \right\}.$$

The corresponding criterion value is 0.00784, and the parameter combination is identified as $\hat{\theta}_2(\xi_{CKL}^*) = (\hat{\delta}_1, \hat{\delta}_2, \hat{\sigma}_2) = (-66.207, 2.002, 0.957)$. Furthermore, the equivalence theorem confirms the optimality of this design (Figure 4.4a). The results confirm that it satisfies the optimality conditions. The total computation time is 134408 seconds.

2. True model variance is 1.4780103 :

$$\xi_{CKL}^* = \begin{Bmatrix} 26.713 & 57.032 & 80 \\ 0.396 & 0.382 & 0.222 \end{Bmatrix}.$$

The corresponding criterion value is 4.491×10^{-3} , and the parameter combination is identified as $\hat{\theta}_2(\xi_{CKL}^*) = (\hat{\delta}_1, \hat{\delta}_2, \hat{\sigma}_2) = (-66.560, 2.013, 1.441)$. Furthermore, the equivalence theorem confirms the optimality of this design (Figure 4.4b). The results confirm that it satisfies the optimality conditions. The total computation time is 85551 seconds.

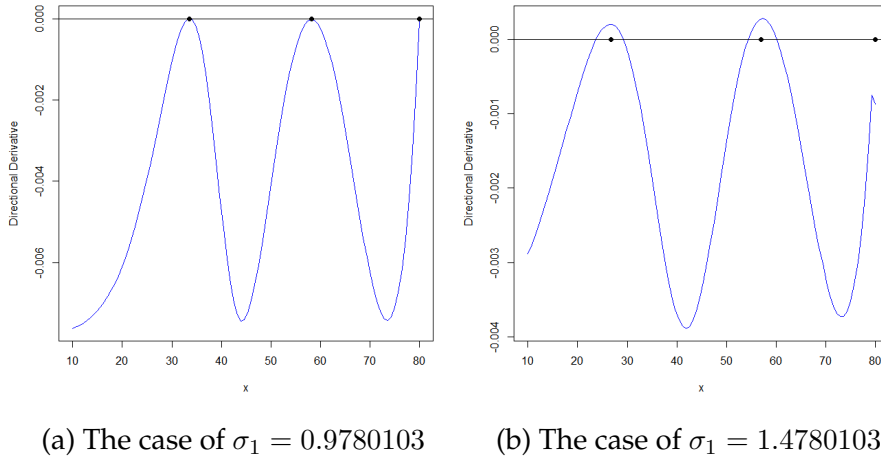


Figure 4.4: The directional derivative plots of the resulting designs ξ_{CKL}^* discriminating for the cases of Quadratic vs. Linear means assuming Weibull response.

In this extended design setting, the variance of the rival model is treated as an unknown parameter and jointly optimized alongside the location parameters. The directional derivative plots shown in Figures 4.3 and 4.4 illustrate the results of the resulting designs. While not all designs fully satisfy the optimality conditions, they demonstrate strong potential. With additional algorithm iterations, these designs are expected

to converge further and fully meet the theoretical criteria. Interestingly, the identified parameter combination's variance $\hat{\sigma}_2$ consistently converge to values close to the true model's variance σ_1 . Rather than suggesting that the rival model is recovering the true variance, this outcome reflects a deeper implication: to achieve maximal model separation under the CKL criterion, the rival model's variance tends to align with that of the true model. This alignment likely amplifies differences in the mean structure, which is where model discrimination power is most pronounced.

To compare the design differences between fixed-variance and variance-search scenarios, the information from Table 4.1 has been consolidated into Tables 4.9 and 4.10, showing support points, weights, and cumulative failure probabilities before the censoring time C . This facilitates both visual and numerical evaluation.

Results from both distribution types indicate that once variance search is introduced, the first two support points tend to shift toward higher stress levels. The shift is moderate in Log-Normal cases but more pronounced in Weibull cases, suggesting greater sensitivity to tail behavior and censoring effects.

To assess practical feasibility, we compute the cumulative failure probability before C for each support point to ensure sufficient failure observations within the testing period. Low probabilities would result in excessive censoring, reducing the informativeness of the data.

The outcomes show that cumulative failure probabilities mostly range from 5% to 100%, implying that all design points yield observable failures, helping avoid data loss due to censoring. These CKL-optimal designs thus demonstrate strong feasibility and discrimination capability under censoring scenarios.

Table 4.9: Comparison of design points, weights, and cumulative failure probabilities under different model assumptions ($\sigma = 0.9780103$)

Model	Point	Weight	Cumulative Probability
Log-Normal (fixed θ_2)			
	33.557	0.330	0.0902
	56.829	0.436	1.000
	80	0.234	1
Log-Normal (unknown θ_2)			
	33.799	0.317	0.102
	57.185	0.443	1.000
	80	0.226	1
Weibull (fixed θ_2)			
	32.545	0.368	0.177
	57.686	0.415	1
	80	0.217	1
Weibull (unknown θ_2)			
	33.531	0.340	0.229
	58.185	0.434	1
	80	0.226	1

Table 4.10: Comparison of design points, weights, and cumulative failure probabilities under different model assumptions ($\sigma = 1.4780103$)

Model	Point	Weight	Cumulative Probability
Log-Normal (fixed θ_2)			
	29.699	0.360	0.0506
	55.482	0.413	0.997
	80	0.227	1
Log-Normal (unknown θ_2)			
	29.974	0.339	0.0566
	56.272	0.423	0.998
	80	0.238	1
Weibull (fixed θ_2)			
	25.576	0.441	0.0801
	55.791	0.359	1
	80	0.200	1
Weibull (unknown θ_2)			
	26.713	0.396	0.100
	57.032	0.382	1
	80	0.222	1

4.3.2 Equal Mean Response, Competing Distribution Assumptions with Stress-Dependent Variance

This section follows the fatigue life modeling framework proposed by Pascual and Meeker (1997), which considers fatigue life data under the presence of a fatigue limit and allows the standard deviation to vary with stress levels. Traditional fatigue life models often assume the absence of a fatigue limit and a constant standard deviation; however, such assumptions frequently lead to modeling errors when applied to real-world data. Incorporating a stress-dependent standard deviation structure enables a more accurate representation of the curvature observed in S-N curves and better captures the dispersion characteristics of fatigue life data.

To construct the life distribution more precisely, this study adopts the mean response model and stress-dependent variance structure suggested by Pascual and Meeker (1997). The parameter settings are initially based on the estimates obtained through maximum likelihood estimation (MLE) and profile likelihood confidence intervals from their analysis. Additional simulation scenarios are independently defined but must satisfy two essential conditions: first, the mean response function $\eta(x, \theta)$ must be a decreasing function of stress, and it must remain strictly positive to ensure numerical stability; second, the variation of the standard deviation with stress must be controlled within reasonable bounds to prevent numerical overflow caused by excessively large exponential terms. Notably, their study estimated the parameter $\gamma = 75.71$, which appears in both the mean response function and the variance structure, and this value is retained in the subsequent simulations.

Based on these principles, a series of numerical simulations and model discrimination analyzes are conducted. The detailed simulation

scenarios are summarized in Table 4.11 (with a censoring time of 1000), and the structures of the true model M_1 and the rival model M_2 are specified below, each comprising a mean response function and a stress-dependent standard deviation function.

- The true model M_1 is:

$$\eta_{tr}(x, \theta) = \zeta_1 + \zeta_2 \log(x - \gamma) \quad (4.7)$$

$$\sigma_1 = \exp\{\phi_1 + \phi_2 \log(x - \gamma)\} \quad (4.8)$$

- The rival model M_2 :

$$\eta_2(x, \theta) = \delta_1 + \delta_2 \log(x - \gamma) \quad (4.9)$$

$$\sigma_2 = \exp\{\kappa_1 + \kappa_2 \log(x - \gamma)\} \quad (4.10)$$

It is also noted that in the result tables, the searched parameter vector is expressed as $\hat{\theta}_2(\xi_{CKL}^*) = (\hat{\delta}_1, \hat{\delta}_2, \hat{\kappa}_1, \hat{\kappa}_2)$, corresponding to the parameters in the mean response and stress-dependent variance models, respectively.

In the final simulation scenarios of this study, although most results were numerically unstable or the directional derivative plots were difficult to interpret, some cases still demonstrated potential feasibility. Specifically, several designs—though degenerate in form with only a single support point—exhibited directional derivatives that remained strictly below zero across the entire design region, indicating stability under the equivalence theorem. Additionally, some non-degenerate designs showed directional derivative curves with slight local positivity; however, the magnitude of these positive values was extremely small (e.g., around 10^{-9}), and the overall trend quickly returned below zero. These observations suggest that such designs have room for improvement and the

potential to evolve into optimal solutions. A summary of the full simulation outcomes under different settings is provided in Table 4.12.

The numerical integration process may be another contributing factor to the observed instability. In particular, the log terms associated with the censoring component of the objective function can produce non-finite values under certain parameter and support point combinations, resulting in integration failure. These errors not only compromise the accuracy of the criterion function but may also cause the optimization process to terminate prematurely or converge to suboptimal regions. Future research could explore ways to improve the structure of the integrand, such as reformulating the log expressions via numerical approximation, refining the integration bounds, or incorporating error-handling mechanisms to recover from integration failures.

Table 4.11: Simulation settings for Meeker cases including mean and dispersion parameters of the true and rival models

Case	Dis.		M_1				M_2			
	M_1	M_2	ζ_1	ζ_2	ϕ_1	ϕ_2	δ_1	δ_2	κ_1	κ_2
(1)	LN	WB	14.75	-1.39	10.97	-2.5	[12.06,17.44]	[-2.02,-0.76]	[10,20]	[-3,-0.01]
(2)			14.75	-1.39	10.97	-2.5	[15.9,21.45]	[-2.81,-0.92]	[10,20]	[-3,-0.01]
(3)			10	-2	0.63	-0.91	[9.5,15]	[-2.1,-1]	[0.5,1]	[-1,-0.81]
(4)			43	-0.63	4.32	-0.88	[5,50]	[-1,-0.05]	[3.12,5.32]	[-1,-0.5]
(5)			458	-53	4.32	-0.88	[432,480]	[-100,-1]	[3.12,5.32]	[-1,-0.5]
(6)			53.39	-7.81	4.32	-0.88	[50,60]	[-10,-5]	[3.12,5.32]	[-1,-0.5]
(7)	WB	LN	14.75	-1.39	10.97	-2.5	[12.06,17.44]	[-2.02,-0.76]	[10,20]	[-3,-0.01]
(8)			14.75	-1.39	10.97	-2.5	[15.9,21.45]	[-2.81,-0.92]	[10,20]	[-3,-0.01]
(9)			10	-2	0.63	-0.91	[9.5,15]	[-2.1,-1]	[0.5,1]	[-1,-0.81]
(10)			43	-0.63	4.32	-0.88	[5,50]	[-1,-0.05]	[3.12,5.32]	[-1,-0.5]
(11)			458	-53	4.32	-0.88	[432,480]	[-100,-1]	[3.12,5.32]	[-1,-0.5]
(12)			53.39	-7.81	4.32	-0.88	[50,60]	[-10,-5]	[3.12,5.32]	[-1,-0.5]

Table 4.12: Summary of CKL-optimal design results for Meeker cases, under the same mean response structure but assuming the true model follows a Weibull distribution with variance depending on stress.

Case	ξ_{CKL}^*	$C^*(\hat{C})$	$\hat{\theta}_2(\xi_{CKL}^*)$	Eqv.	Opt?	Time
(1)	$\begin{Bmatrix} 88.245 & 115.191 & 122.132 & 123.571 \\ 1.000 & 0.000 & 0.000 & 0.000 \end{Bmatrix}$	2.023×10^{-8} (4.956×10^{-9})	(14.918, -1.350, 11.824, -2.942)	A.13a	\triangle	4083
(2)	$\begin{Bmatrix} 76.389 & 86.024 & 94.240 & 112.132 \\ 0.000 & 1.000 & 0.000 & 0.000 \end{Bmatrix}$	6.725×10^{-8} (2.136×10^{-8})	(20.968, -2.056, 10, -2.397)	A.13b	\triangle	5043
(3)	$\begin{Bmatrix} 111.009 & 112.296 & 113.75 & 150 \\ 0.000 & 0.000 & 1.000 & 0.000 \end{Bmatrix}$	27.167 (6.275×10^{-5})	(10.597, -1.873, 0.723, -0.922)	A.13c	\times	4245
(4)	$\begin{Bmatrix} 77.297 & 78.038 & 109.932 & 132.334 \\ 1.000 & 0.000 & 0.000 & 0.000 \end{Bmatrix}$	2.449×10^{-12} (5.462×10^{-14})	(36.931, -0.523, 3.791, -0.878)	A.13d	\times	3897
(5)	$\begin{Bmatrix} 90.99 & 98.775 & 108.941 & 116.822 \\ 0.464 & 0.231 & 0.271 & 0.035 \end{Bmatrix}$	0 (0)	(455.318, -49.116, 4.219, -0.533)	A.13e	\triangle	1376
(6)	$\begin{Bmatrix} 123.238 & 123.969 & 125.026 & 127.373 \\ 0.022 & 0.977 & 0.000 & 0.000 \end{Bmatrix}$	2.265×10^{-14} (-4.305×10^{-49})	(55.951, -6.358, 3.846, -0.928)	A.13f	\triangle	7386
(7)	$\begin{Bmatrix} 76 & 86.748 & 126.815 & 150 \\ 0.476 & 0.247 & 0.000 & 0.277 \end{Bmatrix}$	1.235×10^{-4} (1.208×10^{-4})	(17.44, -1.638, 10, -2.028)	A.14a	\triangle	48506
(8)	$\begin{Bmatrix} 76 & 87.744 & 97.631 & 150 \\ 0.469 & 0.242 & 0.000 & 0.289 \end{Bmatrix}$	1.173×10^{-4} (1.156×10^{-4})	(18.350, -1.781, 10.011, -2.012)	A.14b	\triangle	54794
(9)	$\begin{Bmatrix} 80.622 & 94.153 & 94.67 & 127.625 \\ 0.259 & 0.519 & 0.000 & 0.221 \end{Bmatrix}$	0.0907 (0.0872)	(9.972, -1.995, 0.882, -0.839)	A.14c	\times	217023
(10)	$\begin{Bmatrix} 76 & 76.879 & 76.950 & 118.382 \\ 0.000 & 0.000 & 1.000 & 0.000 \end{Bmatrix}$	3.197×10^{-9} (3.808×10^{-10})	(27.531, -0.658, 4.374, -0.728)	A.14d	\triangle	1487
(11)	$\begin{Bmatrix} 79.235 & 94.878 & 110.173 & 150 \\ 0.000 & 1.000 & 0.000 & 0.000 \end{Bmatrix}$	1.808×10^{-91} (1.534×10^{-92})	(473.842, -9.458, 4.621, -0.364)	A.14e	\triangle	1436
(12)	$\begin{Bmatrix} 104.273 & 113.865 & 130.105 & 150 \\ 0.982 & 0.000 & 0.000 & 0.018 \end{Bmatrix}$	8.222×10^{-8} (4.220×10^{-8})	(54.974, -7.423, 4.200, -0.586)	A.14f	\triangle	6743

Moreover, previous simulations using the CKL-, CLW-, CB-, and $C\chi^2$ -optimal criteria revealed that the inner objective function, though theoretically differentiable, may lack sufficient smoothness in practice. When the function exhibits multiple local extrema or wave-like structures, solvers like L-BFGS, which rely on local curvature, may fail to converge and yield poor gradient searches. Given the increased complexity here, such issues are more likely, suggesting the need to revisit the function's structure and consider alternative solvers.



Chapter 5

Conclusion and Future Works

5.1 Summary and Key Contributions

This thesis focuses on model discrimination design in the context of reliability modeling and offers an alternative to traditional Bayesian and sampling-based approaches. While these conventional methods are theoretically sound, they often suffer from high computational cost and limited reproducibility. To address these limitations, we focus on the approximation design and adopt the Particle Swarm Optimization (PSO) algorithm—widely recognized in the literature—as the core of our optimization framework. To better accommodate the Type I censored data commonly observed in Accelerated Life Testing, we propose four divergence measures-based design criteria: CKL-, CLW-, CB-, and $C\chi^2$ -optimal designs. Furthermore, recognizing that the variance and dispersion structures in reliability models may depend on stress levels, we further modify the PSO-QN algorithm in [Chen et al. \(2020\)](#) by allowing the stress-dependent variance settings into the objective function evaluation. Detailed user manual and the configuration of the new PSO-QN algorithm are provided in Appendix B. We also develop a user-friendly app using Shiny to better describe our work in the appendix C. Overall, the pro-

posed optimization methodology and enhanced criteria provide a robust and scalable solution for model discrimination design in reliability experiments.

The numerical study begins by reproducing results from a reference study to validate the feasibility of our proposed approach. While the original work obtains optimal designs through closed-form expression of the objective function, we adopt a numerical integration-based method. The results reveal that both approaches yield nearly identical designs, confirming the stability and correctness of our method. The subsequent numerical experiments center on the core of this research—the Arrhenius model, which is widely used in reliability studies. Under the assumption of known variance for both the true and rival models, and incorporating Type I censored data, we search for optimal designs using four proposed divergence measures criteria. The results suggest that CKL-optimal criterion consistently outperforms the others in most scenarios. Motivated by this, the following numerical results focus on the CKL divergence, extending the analysis to cases where the variance of the rival model is unknown and must be searched. Finally, to address practical situations where the variance structure may vary with stress level, we design several illustrative simulation cases to preliminarily examine the algorithm’s behavior under such conditions, highlighting the challenges encountered and identifying directions for future refinement.

In summary, this study integrates multiple divergence measures with numerical integration techniques and a hybrid optimization framework to construct stable and effective model discrimination designs under Type I censored reliability data. Numerical results show that the CKL-optimal design consistently outperforms others in most scenarios, demonstrating its potential in model discrimination for reliability stud-

ies.

More importantly, this study is among the first to propose a design framework that considers stress-dependent variance structures in model discrimination. Although initial numerical results under such settings did not yield strong performance, they reveal critical challenges both theoretically and computationally. This opens a promising direction for future research to enhance algorithmic robustness and design strategies under complex modeling assumptions. Overall, this work not only extends the scope of existing optimal design methodologies but also provides new insights and tools for more realistic and flexible reliability test planning.

5.2 Limitations and Future Directions

While the proposed optimization framework in this study demonstrates feasibility and robustness, several limitations remain. Future research may address these challenges from the following three aspects:

First, during numerical integration, issues such as non-finite values or overflow may arise due to logarithmic terms in the integrand (e.g., $\log(1 - F(y))$), especially when the tail probability becomes extremely small. Future work may consider reformulating the censoring term using more stable approximations or optimizing the integration approach (e.g., adjusting bounds or resolution) to enhance numerical stability and computational reliability.

Second, while this study assumes that the inner-loop objective function is differentiable and therefore adopts gradient-based methods such as L-BFGS, differentiability alone does not guarantee smoothness. In practice, the objective function may exhibit irregular behavior—such as

sharp curvature or multiple local extrema—which can mislead gradient-based solvers into premature convergence. Further investigation into the structure of the objective function is warranted, and alternatives such as subgradient methods, nonsmooth optimization techniques, or heuristic algorithms may be more robust under these conditions.

Finally, the current design strategy identifies the parameter combination in the rival model that minimizes divergence (e.g., KL divergence) from the true model and constructs the optimal design based on this configuration. However, the resulting parameter values may not be the most representative or precise due to estimation uncertainty, potentially limiting the effectiveness of the discrimination design. Future research may consider performing parameter-level optimization prior to discrimination design. For example, a compound approach that combines CKL-optimal and D-optimal designs could simultaneously enhance model discriminability and parameter estimability, thereby improving the practical utility and interpretability of the resulting designs.

References

- Abd El-Raheem, A. (2020). Optimal design of multiple accelerated life testing for generalized half-normal distribution under type-i censoring. *Journal of Computational and Applied Mathematics*, 368:112539.
- Arrhenius, S. (1889). Über die reaktionsgeschwindigkeit bei der inversion von rohrzucker durch säuren. *Zeitschrift für physikalische Chemie*, 4(1):226–248.
- Atkinson, A. C. and Fedorov, V. (1975a). The design of experiments for discriminating between two rival models. *Biometrika*, 62(1):57–70.
- Atkinson, A. C. and Fedorov, V. V. (1975b). Optimal design: Experiments for discriminating between several models. *Biometrika*, 62(2):289–303.
- Chen, R.-B., Chang, S.-P., Wang, W., Tung, H.-C., and Wong, W. K. (2015). Minimax optimal designs via particle swarm optimization methods. *Statistics and Computing*, 25:975–988.
- Chen, R.-B., Chang, S.-P., Wang, W., and Wong, W. (2011). Optimal experimental designs via particle swarm optimization methods. *Preprint, Department of Mathematics, National Taiwan University*, 3.
- Chen, R.-B., Chen, P.-Y., Hsu, C.-L., and Wong, W. K. (2020). Hybrid algorithms for generating optimal designs for discriminating multiple nonlinear models under various error distributional assumptions. *PloS one*, 15(10):e0239864.

- Coles, S., Bawa, J., Trenner, L., and Dorazio, P. (2001). *An introduction to statistical modeling of extreme values*, volume 208. Springer.
- Davis, P. J. and Rabinowitz, P. (2007). *Methods of numerical integration*. Courier Corporation.
- Eberhart, R. and Kennedy, J. (1995). A new optimizer using particle swarm theory. In *MHS'95. Proceedings of the sixth international symposium on micro machine and human science*, pages 39–43. Ieee.
- Guideline, I. et al. (2003). Stability testing of new drug substances and products. *Q1A (R2), current step*, 4(1-24).
- López-Fidalgo, J., Tommasi, C., and Trandafir, P. C. (2007). An optimal experimental design criterion for discriminating between non-normal models. *Journal of the Royal Statistical Society Series B: Statistical Methodology*, 69(2):231–242.
- López-Fidalgo, J. and Wong, W. K. (2002). Design issues for the michaelis–menten model. *Journal of Theoretical Biology*, 215(1):1–11.
- Lu, L., Lee, I.-C., and Hong, Y. (2019). Bayesian sequential design based on dual objectives for accelerated life tests. *Statistical Quality Technologies: Theory and Practice*, pages 257–275.
- Lukemire, J., Mandal, A., and Wong, W. K. (2016). Using particle swarm optimization to search for locally d -optimal designs for mixed factor experiments with binary response. *arXiv preprint arXiv:1602.02187*.
- Nasir, E. A. and Pan, R. (2015). Simulation-based bayesian optimal alt designs for model discrimination. *Reliability Engineering & System Safety*, 134:1–9.
- Newer, H. A., Abd-El-Monem, A., Al-Shbeil, I., Emam, W., and Nower, M. (2024). Optimal test plans for accelerated life tests based on progressive

- type-i censoring with engineering applications. *Alexandria Engineering Journal*, 87:604–621.
- Pakgohar, A., Habibirad, A., and Yousefzadeh, F. (2019). Lin-wong divergence and relations on type i censored data. *Communications in Statistics-Theory and Methods*, 48(19):4804–4819.
- Park, S. and Shin, M. (2014). Kullback–leibler information of a censored variable and its applications. *Statistics*, 48(4):756–765.
- Pascual, F. G. and Meeker, W. Q. (1997). Analysis of fatigue data with runouts based on a model with nonconstant standard deviation and a fatigue limit parameter. *Journal of testing and evaluation*, 25(3):292–301.
- Shannon, C. E. (1948). A mathematical theory of communication. *The Bell system technical journal*, 27(3):379–423.
- Silvey, S. (2013). *Optimal design: an introduction to the theory for parameter estimation*, volume 1. Springer Science & Business Media.
- Stoer, J., Bulirsch, R., Bartels, R., Gautschi, W., and Witzgall, C. (1980). *Introduction to numerical analysis*, volume 1993. Springer.
- Uddin, K., Jackson, T., Widanage, W. D., Chouchelamane, G., Jennings, P. A., and Marco, J. (2017). On the possibility of extending the life-time of lithium-ion batteries through optimal v2g facilitated by an integrated vehicle and smart-grid system. *Energy*, 133:710–722.
- Walsh, S. J. and Borkowski, J. J. (2022). Fast computation of highly g-optimal exact designs via particle swarm optimization. *arXiv preprint arXiv:2206.06498*.

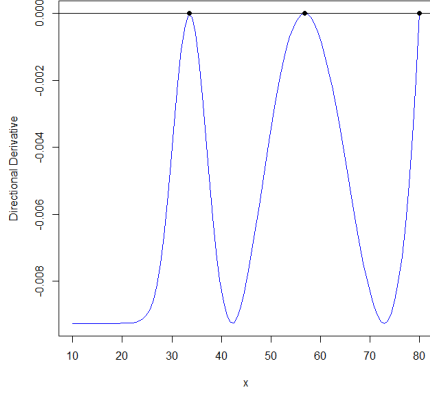


Appendix A

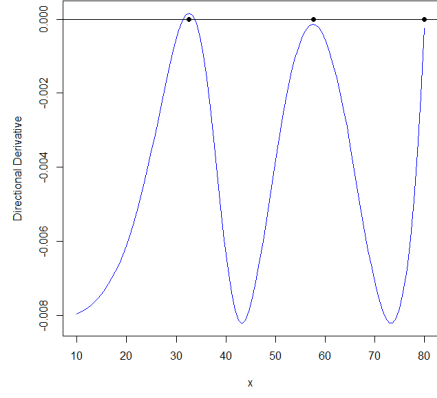
The Directional Derivative Plots of the Resulting Model Discrimination Designs

This section presents the directional derivative plots corresponding to the model discrimination designs discussed in Sections 4.2 and 4.3.2, which are used to verify whether the proposed designs satisfy the optimality conditions outlined by the equivalence theorem. According to theoretical criteria, an optimal design must ensure that the directional derivative remains less than or equal to zero throughout the design region, and that the support points align with the local maxima of the directional derivative, each attaining a value of zero.

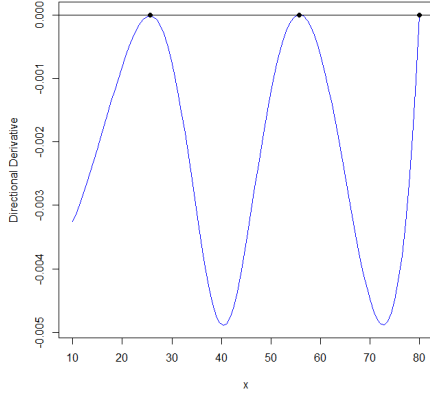
The plots are grouped into two major scenarios. The first scenario, from Section 4.2, assumes both models have fixed variance, and explores four divergence measures (CKL, CLW, CB, and $C\chi^2$), with results summarized in Tables 4.1 to 4.8. The second scenario, from Section 4.3.2, considers CKL-optimal designs under a stress-dependent variance structure, with corresponding results shown in Table 4.12. These visualizations provide supportive evidence for evaluating whether the identified designs achieve both theoretical optimality and numerical stability.



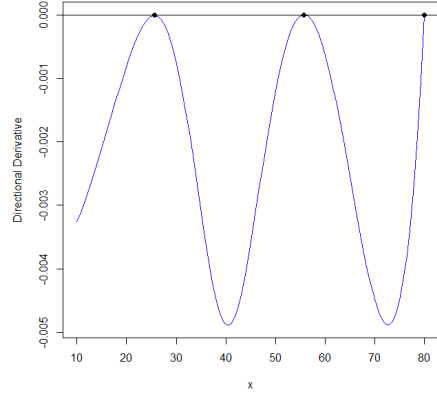
(a) $\sigma_1 = \sigma_2 = 0.98$ (LN)



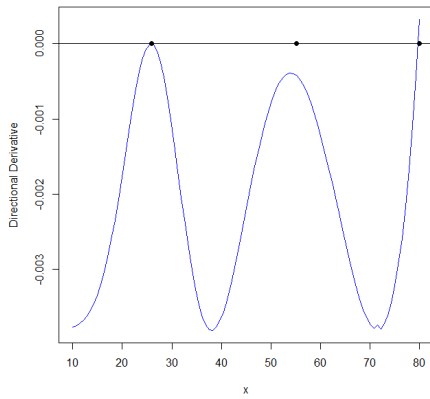
(b) $\sigma_1 = \sigma_2 = 0.98$ (Weibull)



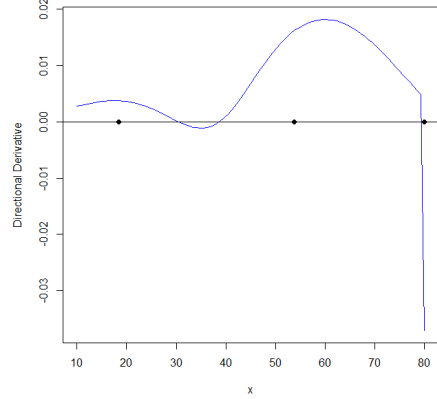
(c) $\sigma_1 = \sigma_2 = 1.48$ (LN)



(d) $\sigma_1 = \sigma_2 = 1.48$ (Weibull)

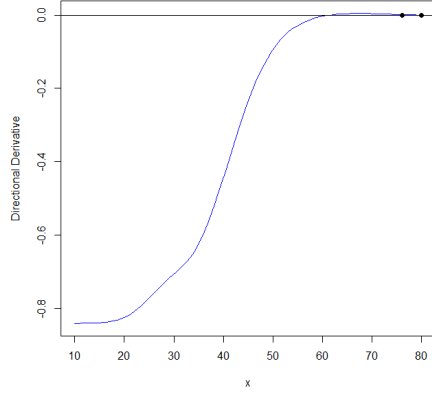


(e) $\sigma_1 = \sigma_2 = 1.98$ (LN)

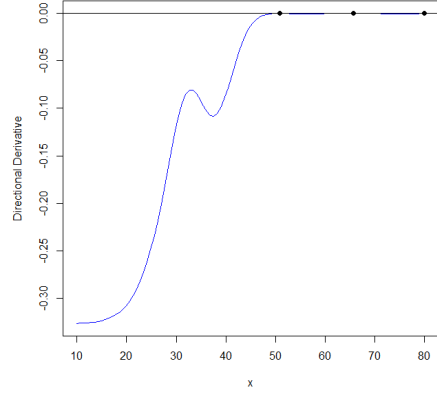


(f) $\sigma_1 = \sigma_2 = 1.98$ (Weibull)

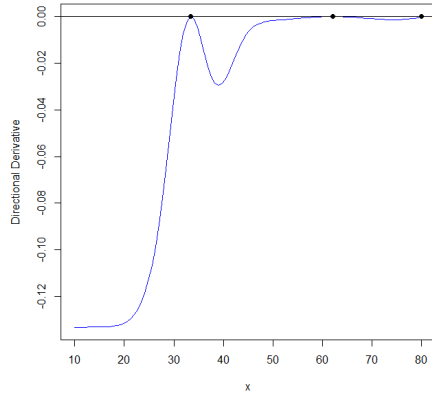
Figure A.1: The directional derivative plots of the resulting ξ_{CKL}^* designs discriminating for cases of Quadratic vs. Linear means with equal variance. Results are shown in Table 4.1.



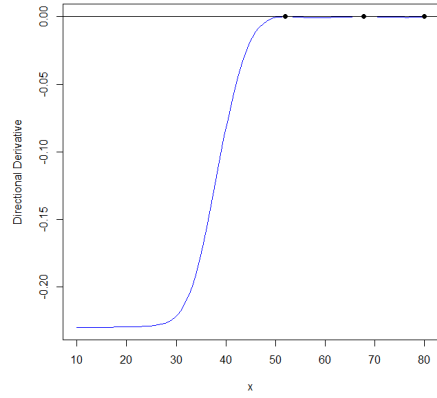
(a) $\sigma_1 = 1.98, \sigma_2 = 0.98$



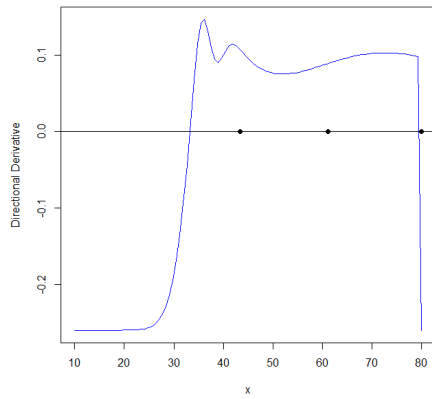
(b) $\sigma_1 = 0.98, \sigma_2 = 1.98$



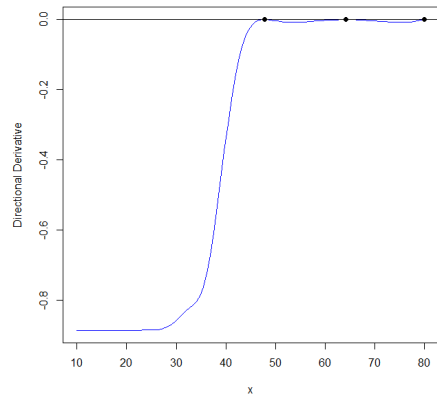
(c) $\sigma_1 = 0.98, \sigma_2 = 1.48$



(d) $\sigma_1 = 1.48, \sigma_2 = 0.98$

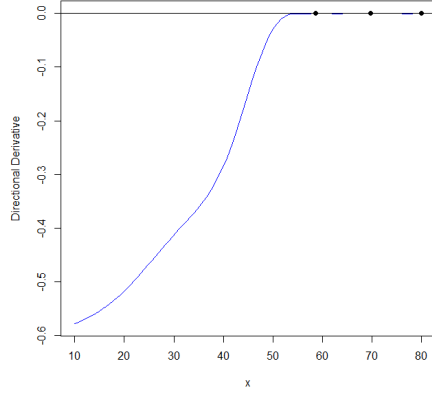


(e) $\sigma_1 = 0.48, \sigma_2 = 0.98$

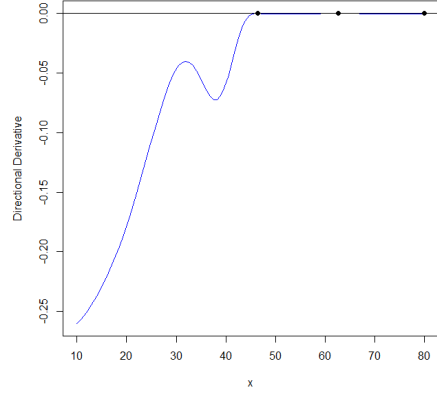


(f) $\sigma_1 = 0.98, \sigma_2 = 0.48$

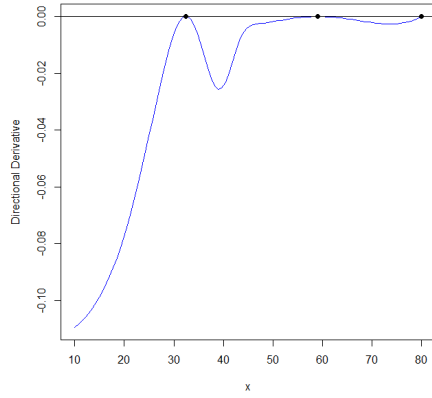
Figure A.2: The directional derivative plots of the resulting ξ_{CKL}^* designs discriminating for cases of Quadratic vs. Linear means with unequal variance assuming Log-Normal response. Results are shown in Table 4.2.



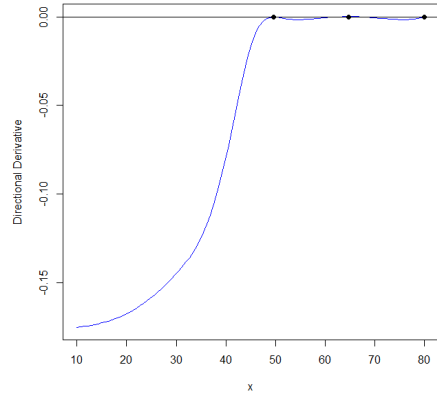
(a) $\sigma_1 = 1.98, \sigma_2 = 0.98$



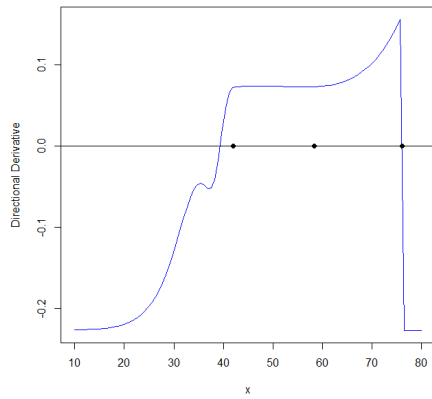
(b) $\sigma_1 = 0.98, \sigma_2 = 1.98$



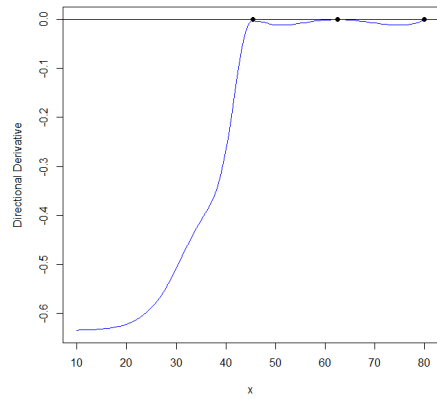
(c) $\sigma_1 = 0.98, \sigma_2 = 1.48$



(d) $\sigma_1 = 1.48, \sigma_2 = 0.98$

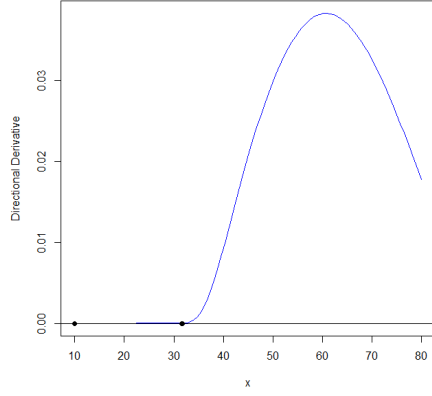


(e) $\sigma_1 = 0.48, \sigma_2 = 0.98$

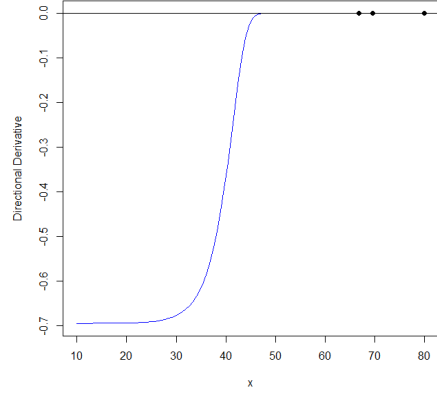


(f) $\sigma_1 = 0.98, \sigma_2 = 0.48$

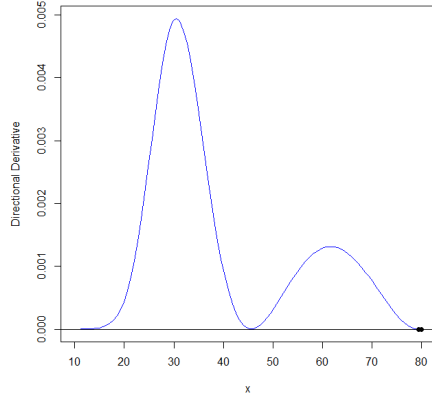
Figure A.3: The directional derivative plots of the resulting ξ_{CKL}^* designs discriminating for cases of Quadratic vs. Linear means with unequal variance assuming Weibull response. Results are shown in Table 4.2.



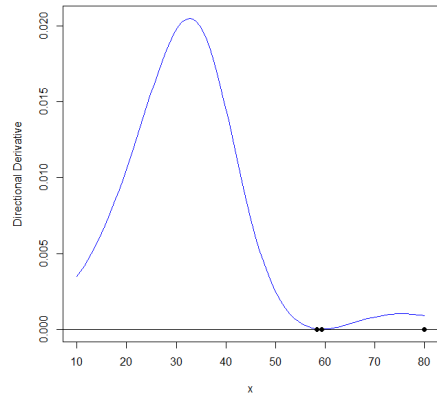
(a) $\sigma_1 = \sigma_2 = 0.98(\text{LN})$



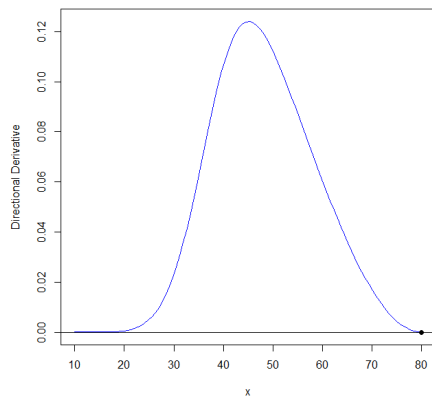
(b) $\sigma_1 = \sigma_2 = 0.98(\text{Weibull})$



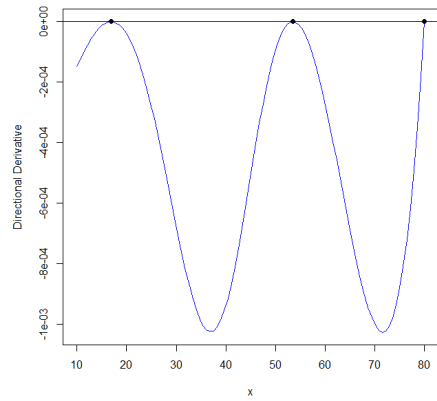
(c) $\sigma_1 = \sigma_2 = 1.48(\text{LN})$



(d) $\sigma_1 = \sigma_2 = 1.48(\text{Weibull})$

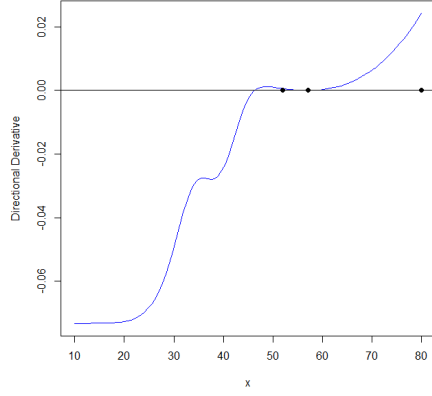


(e) $\sigma_1 = \sigma_2 = 1.98(\text{LN})$

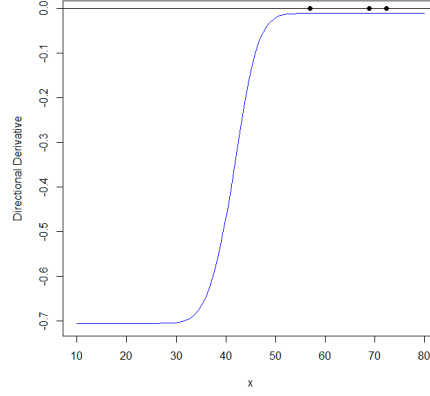


(f) $\sigma_1 = \sigma_2 = 1.98(\text{Weibull})$

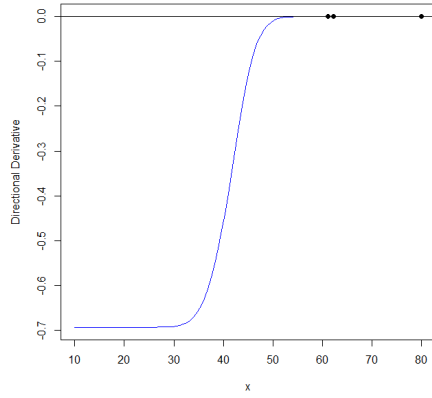
Figure A.4: The directional derivative plots of the resulting ξ_{CLW}^* designs discriminating for cases of Quadratic vs. Linear means with equal variance. Results are shown in Table 4.3.



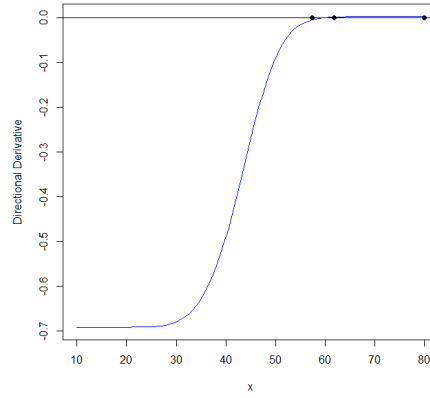
(a) $\sigma_1 = 1.98, \sigma_2 = 0.98$



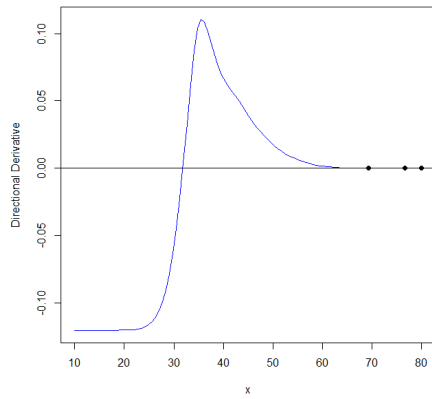
(b) $\sigma_1 = 0.98, \sigma_2 = 1.98$



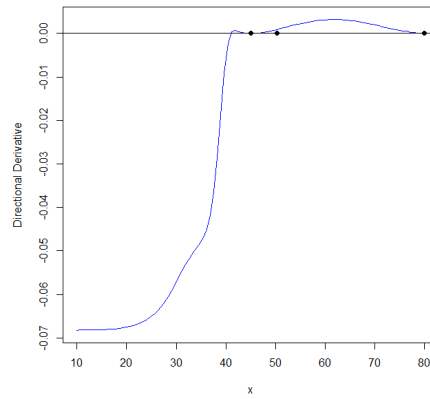
(c) $\sigma_1 = 0.98, \sigma_2 = 1.48$



(d) $\sigma_1 = 1.48, \sigma_2 = 0.98$

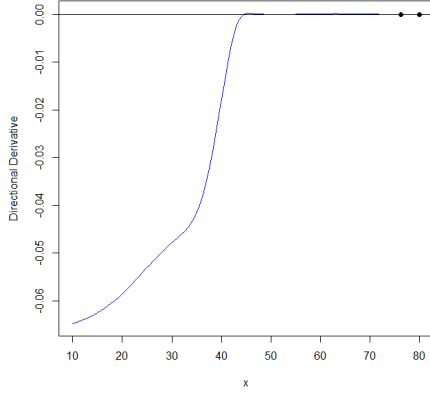


(e) $\sigma_1 = 0.48, \sigma_2 = 0.98$

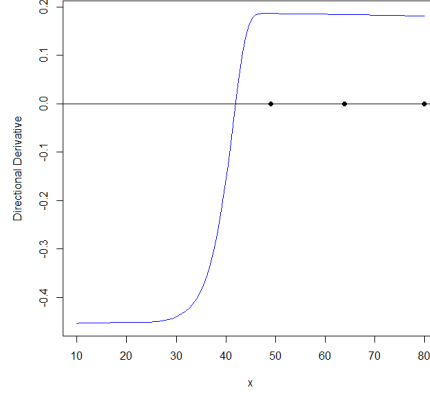


(f) $\sigma_1 = 0.98, \sigma_2 = 0.48$

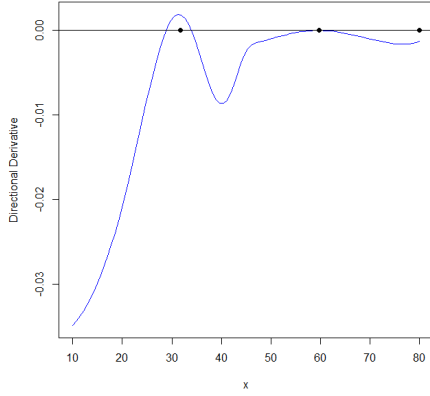
Figure A.5: The directional derivative plots of the resulting ξ_{CLW}^* designs discriminating for cases of Quadratic vs. Linear means with unequal variance assuming Log-Normal response. Results are shown in Table 4.4.



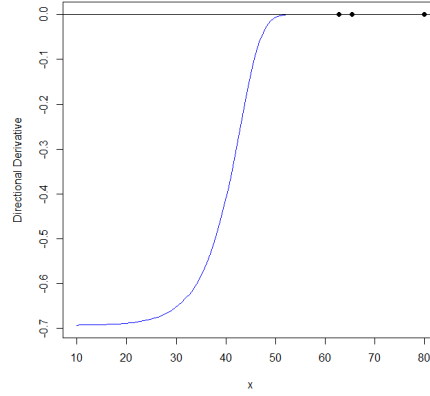
(a) $\sigma_1 = 1.98, \sigma_2 = 0.98$



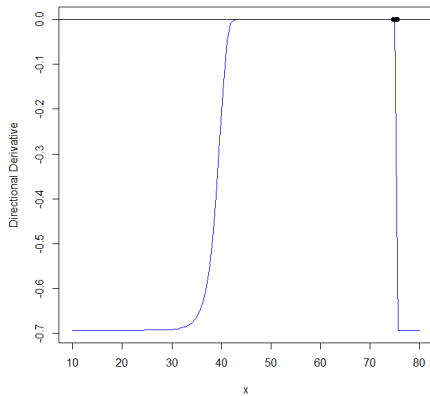
(b) $\sigma_1 = 0.98, \sigma_2 = 1.98$



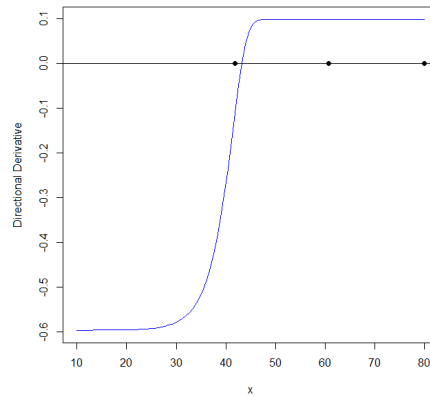
(c) $\sigma_1 = 0.98, \sigma_2 = 1.48$



(d) $\sigma_1 = 1.48, \sigma_2 = 0.98$

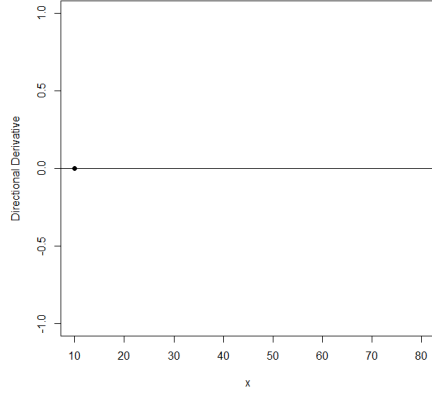


(e) $\sigma_1 = 0.48, \sigma_2 = 0.98$

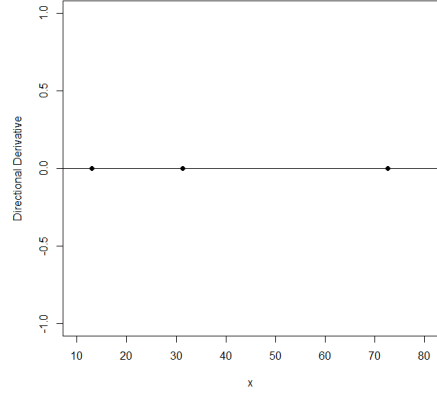


(f) $\sigma_1 = 0.98, \sigma_2 = 0.48$

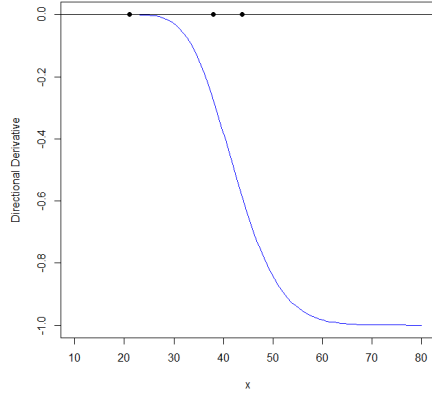
Figure A.6: The directional derivative plots of the resulting ξ_{CLW}^* designs discriminating for cases of Quadratic vs. Linear means with unequal variance assuming Weibull response. Results are shown in Table 4.4.



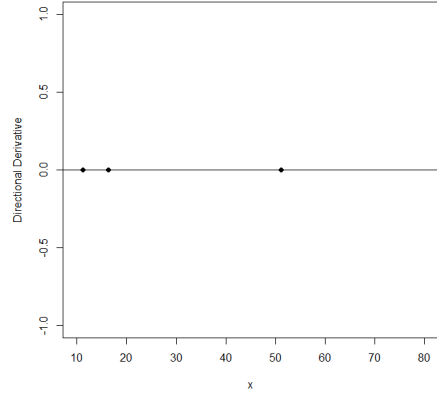
(a) $\sigma_1 = \sigma_2 = 0.98(\text{LN})$



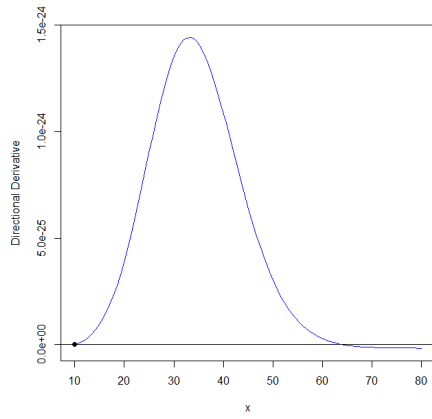
(b) $\sigma_1 = \sigma_2 = 0.98(\text{Weibull})$



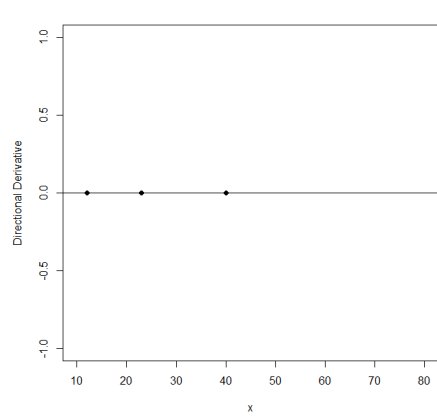
(c) $\sigma_1 = \sigma_2 = 1.48(\text{LN})$



(d) $\sigma_1 = \sigma_2 = 1.48(\text{Weibull})$

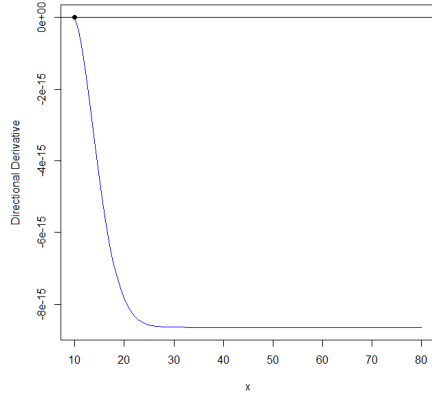


(e) $\sigma_1 = \sigma_2 = 1.98(\text{LN})$

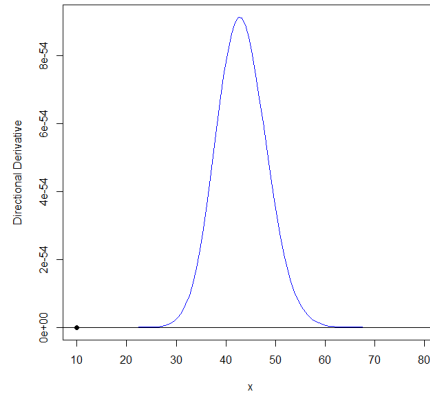


(f) $\sigma_1 = \sigma_2 = 1.98(\text{Weibull})$

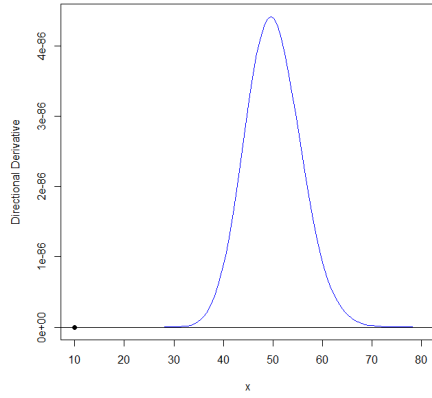
Figure A.7: The directional derivative plots of the resulting ξ_{CB}^* designs discriminating for cases of Quadratic vs. Linear means with equal variance. Results are shown in Table 4.5.



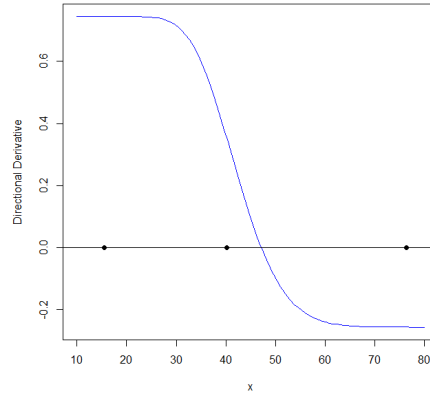
(a) $\sigma_1 = 1.98, \sigma_2 = 0.98$



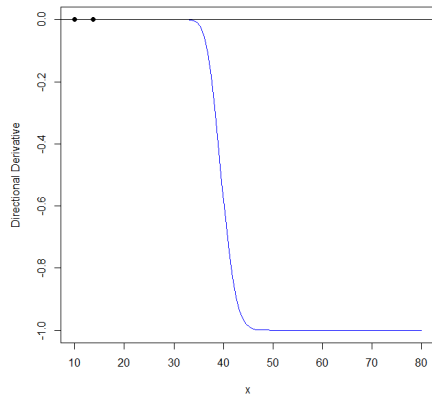
(b) $\sigma_1 = 0.98, \sigma_2 = 1.98$



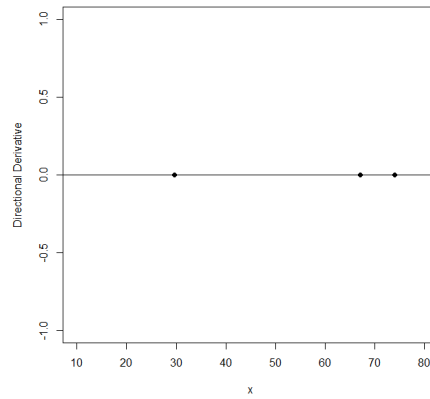
(c) $\sigma_1 = 0.98, \sigma_2 = 1.48$



(d) $\sigma_1 = 1.48, \sigma_2 = 0.98$

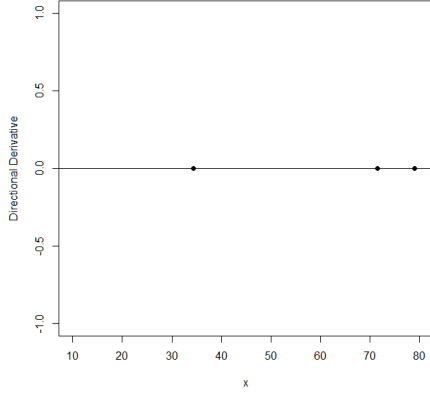


(e) $\sigma_1 = 0.48, \sigma_2 = 0.98$

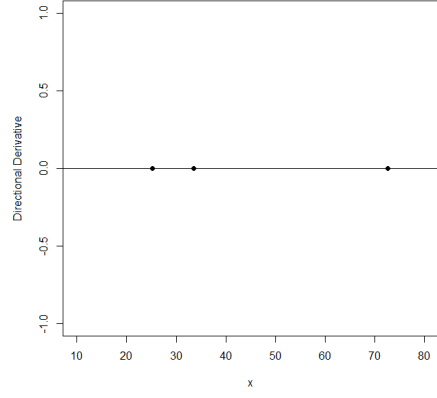


(f) $\sigma_1 = 0.98, \sigma_2 = 0.48$

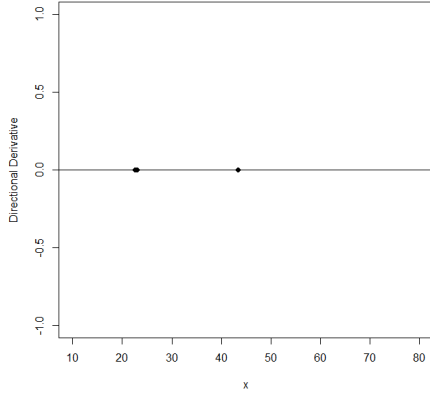
Figure A.8: The directional derivative plots of the resulting ξ_{CB}^* designs discriminating for cases of Quadratic vs. Linear means with unequal variance assuming Log-Normal response. Results are shown in Table 4.6.



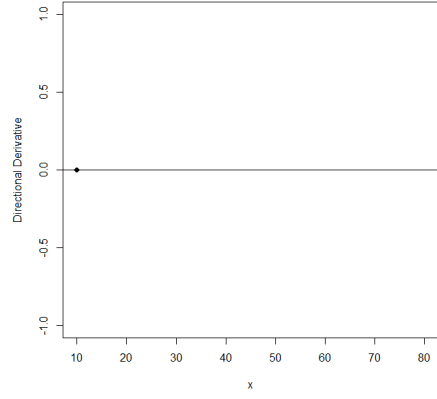
(a) $\sigma_1 = 1.98, \sigma_2 = 0.98$



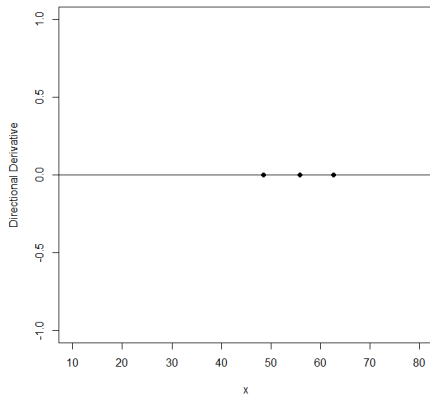
(b) $\sigma_1 = 0.98, \sigma_2 = 1.98$



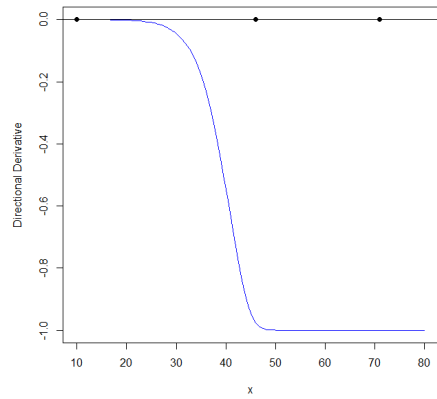
(c) $\sigma_1 = 0.98, \sigma_2 = 1.48$



(d) $\sigma_1 = 1.48, \sigma_2 = 0.98$

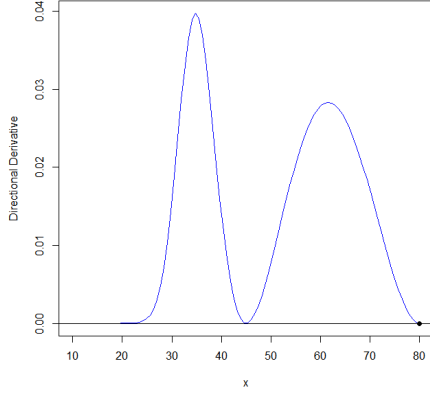


(e) $\sigma_1 = 0.48, \sigma_2 = 0.98$

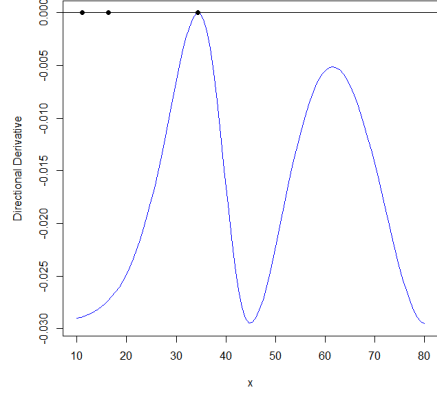


(f) $\sigma_1 = 0.98, \sigma_2 = 0.48$

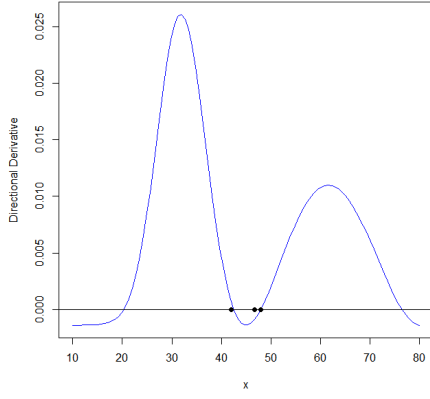
Figure A.9: The directional derivative plots of the resulting ξ_{CB}^* designs discriminating for cases of Quadratic vs. Linear means with unequal variance assuming Weibull response. Results are shown in Table 4.6.



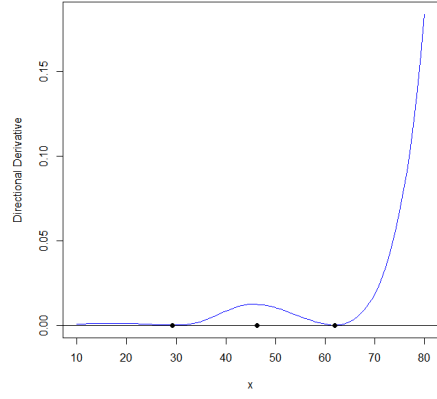
(a) $\sigma_1 = \sigma_2 = 0.98(\text{LN})$



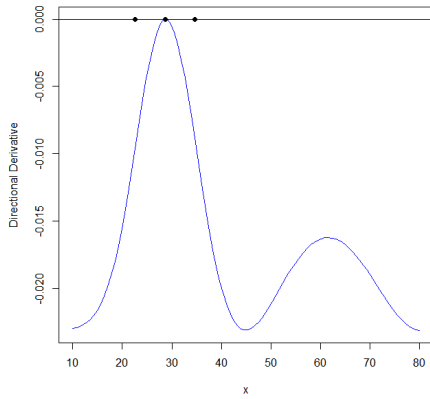
(b) $\sigma_1 = \sigma_2 = 0.98(\text{Weibull})$



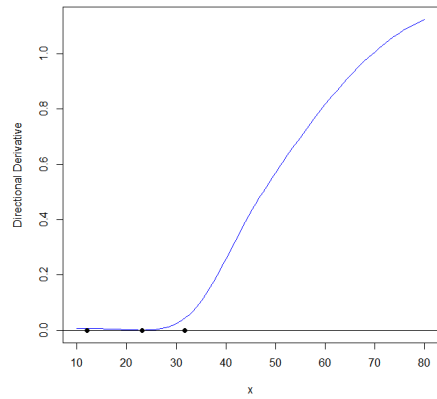
(c) $\sigma_1 = \sigma_2 = 1.48(\text{LN})$



(d) $\sigma_1 = \sigma_2 = 1.48(\text{Weibull})$

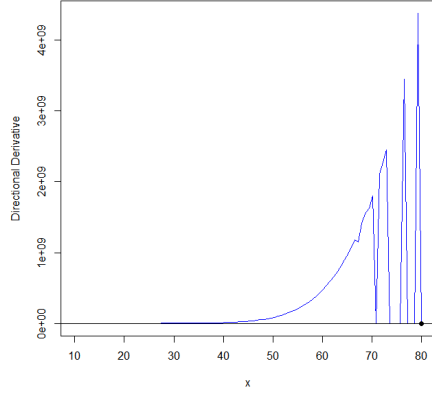


(e) $\sigma_1 = \sigma_2 = 1.98(\text{LN})$

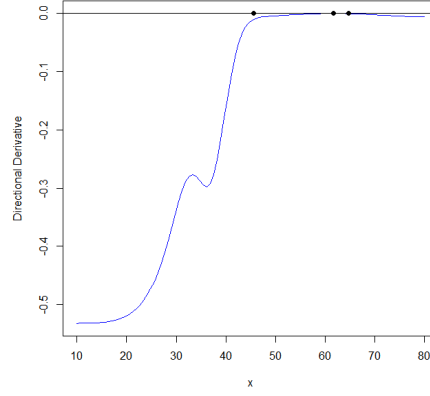


(f) $\sigma_1 = \sigma_2 = 1.98(\text{Weibull})$

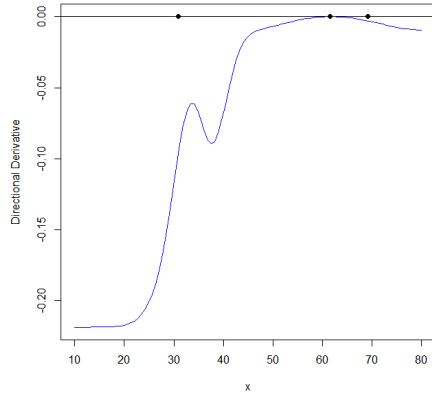
Figure A.10: The directional derivative plots of the resulting $\xi_{C\chi^2}^*$ designs discriminating for cases of Quadratic vs. Linear means with equal variance. Results are shown in Table 4.7.



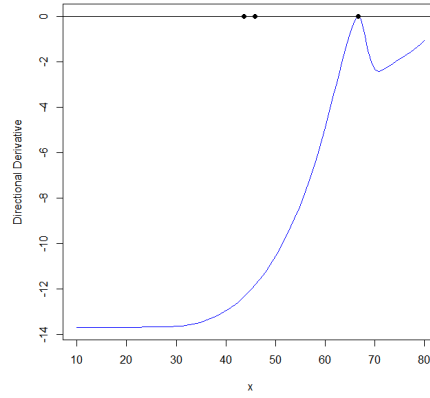
(a) $\sigma_1 = 1.98, \sigma_2 = 0.98$



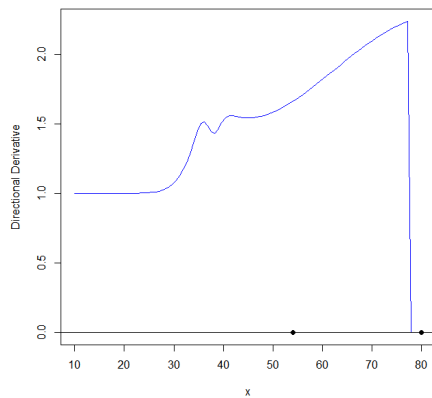
(b) $\sigma_1 = 0.98, \sigma_2 = 1.98$



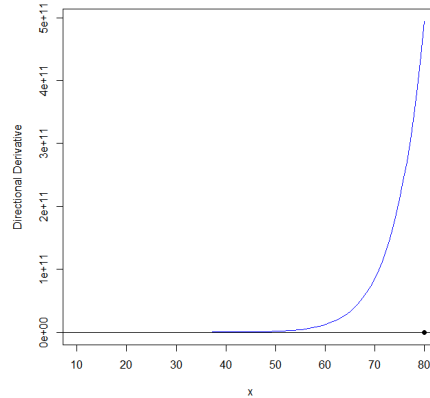
(c) $\sigma_1 = 0.98, \sigma_2 = 1.48$



(d) $\sigma_1 = 1.48, \sigma_2 = 0.98$

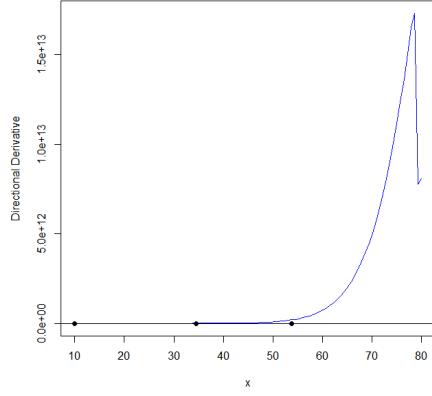


(e) $\sigma_1 = 0.48, \sigma_2 = 0.98$

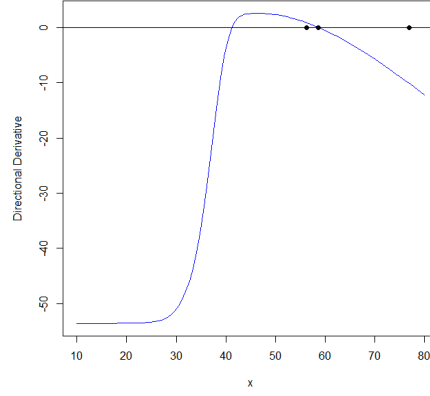


(f) $\sigma_1 = 0.98, \sigma_2 = 0.48$

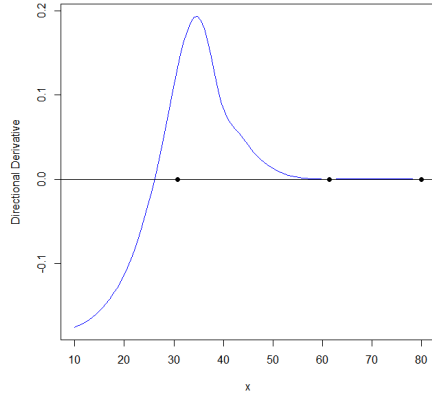
Figure A.11: The directional derivative plots of the resulting $\xi_{C\chi^2}^*$ designs discriminating for cases of Quadratic vs. Linear means with unequal variance assuming Log-Normal response. Results are shown in Table 4.8.



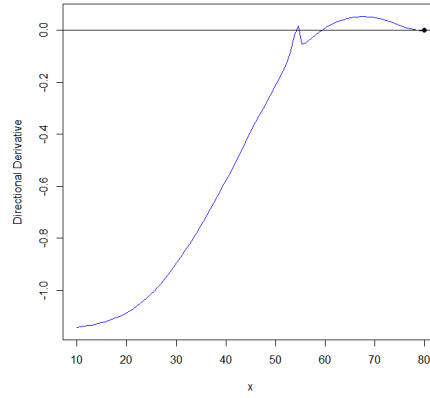
(a) $\sigma_1 = 1.98, \sigma_2 = 0.98$



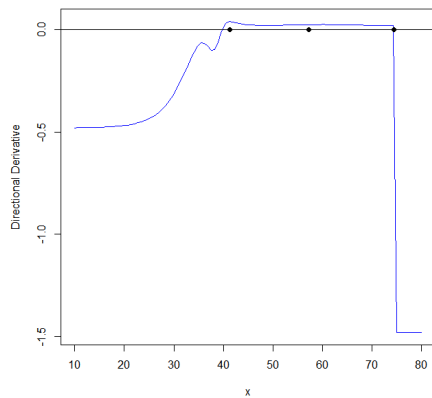
(b) $\sigma_1 = 0.98, \sigma_2 = 1.98$



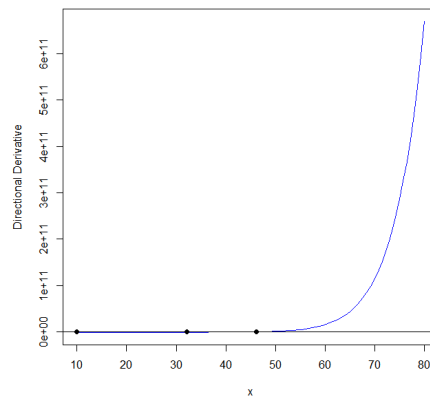
(c) $\sigma_1 = 0.98, \sigma_2 = 1.48$



(d) $\sigma_1 = 1.48, \sigma_2 = 0.98$

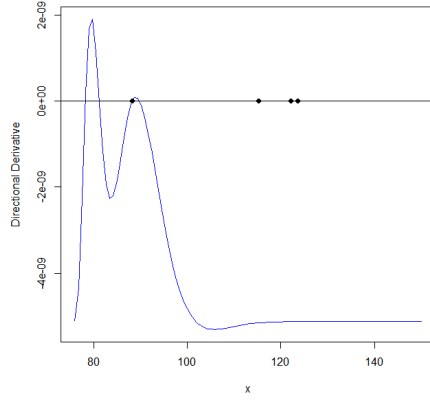


(e) $\sigma_1 = 0.48, \sigma_2 = 0.98$

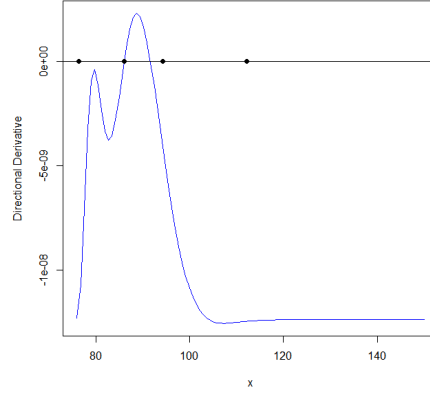


(f) $\sigma_1 = 0.98, \sigma_2 = 0.48$

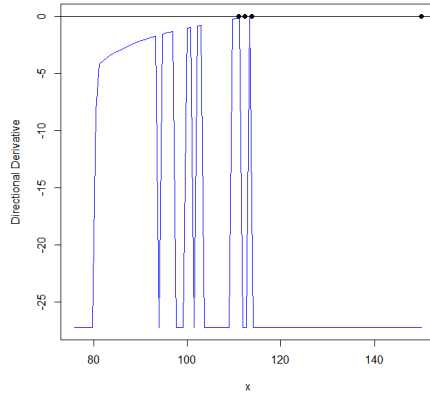
Figure A.12: The directional derivative plots of the resulting $\xi_{C\chi^2}^*$ designs discriminating for cases of Quadratic vs. Linear means with unequal variance assuming Weibull response. Results are shown in Table 4.8.



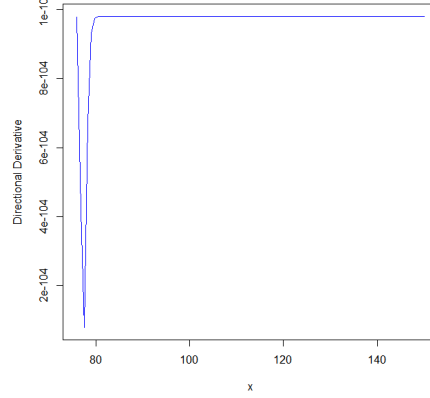
(a) Meeker Case (1)



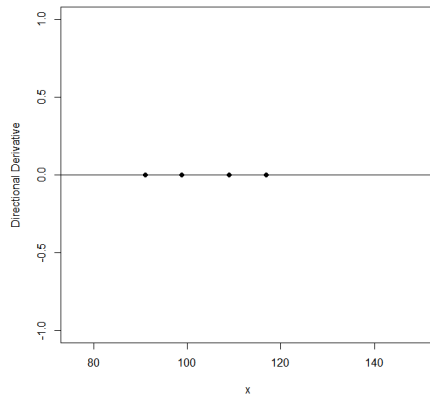
(b) Meeker Case (2)



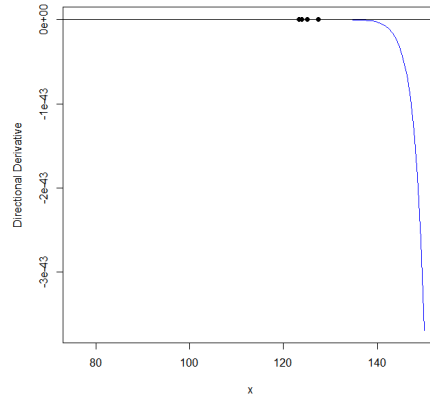
(c) Meeker Case (3)



(d) Meeker Case (4)

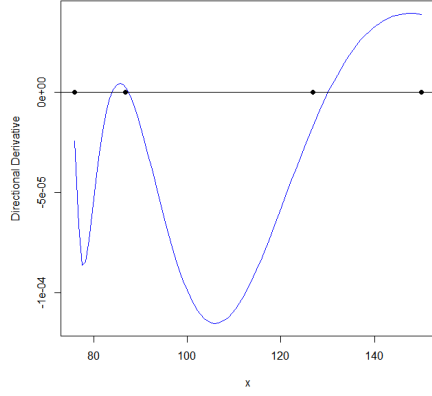


(e) Meeker Case (5)

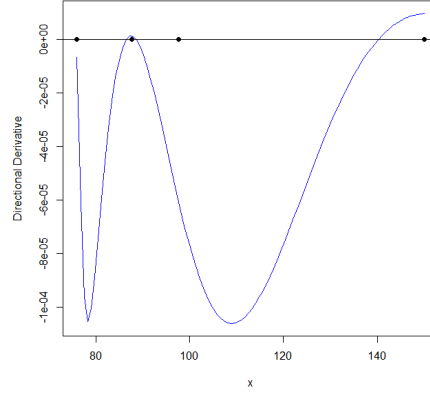


(f) Meeker Case (6)

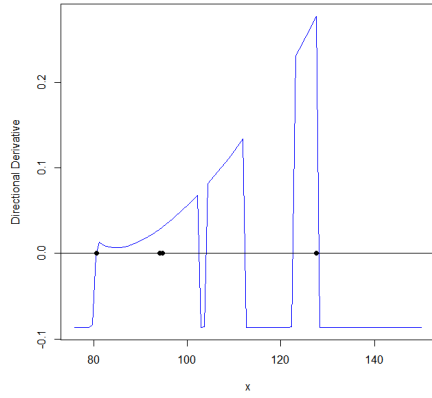
Figure A.13: The directional derivative plots of the resulting ξ_{CKL}^* designs for Meeker cases, under the same mean response structure but assuming the true model follows a Log-Normal distribution with variance depending on stress. Results are shown in Table 4.12.



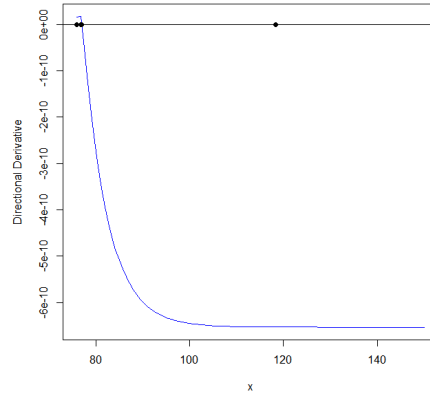
(a) Meeker Case (7)



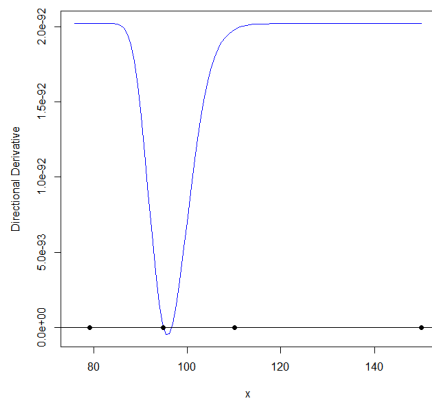
(b) Meeker Case (8)



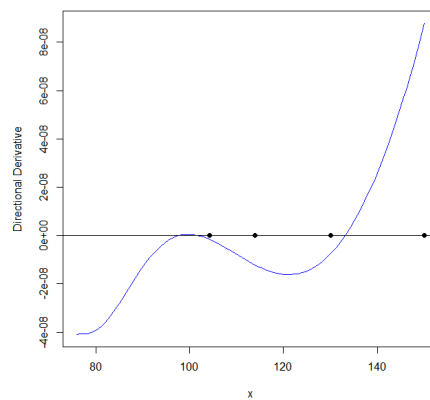
(c) Meeker Case (9)



(d) Meeker Case (10)



(e) Meeker Case (11)



(f) Meeker Case (12)

Figure A.14: The directional derivative plots of the resulting ξ_{CKL}^* designs for Meeker cases, under the same mean response structure but assuming the true model follows a Weibull distribution with variance depending on stress. Results are shown in Table 4.12.



Appendix B

R Implementation Example

The source code used in this study is available at: [GitHub/GPLIN514](https://github.com/GPLIN514). This appendix provides a brief explanation of the code used for the simulation and optimal design of the KL divergence under the Arrhenius model framework.

The following code defines the mean response and dispersion functions for both the true model and the rival model under Arrhenius assumptions:

Listing B.1: Model structure settings

```
af1_mean <- function(x, p) p[1] + p[2] * (11605/(x+273.15))  
          + p[3] * (11605/(x+273.15))^2  
af2_mean <- function(x, p) p[1] + p[2] * (11605/(x+273.15))  
af1_disp <- function(x, p) rep(p[1], length(x))  
af2_disp <- function(x, p) rep(p[1], length(x))
```

In this design setup:

- The true model M_1 adopts a quadratic form of the Arrhenius function, expressed as:

$$\eta_{tr}(x, \theta_1) = \zeta_1 + \zeta_2 x + \zeta_3 x^2$$

- The rival model M_2 uses a linear form:

$$\eta_2(x, \theta_2) = \delta_1 + \delta_2 x$$

Both models assume constant dispersion that is independent of the stress level, as defined in the `af1_disp_Arrhenius` and `af2_disp_Arrhenius` functions. These functions provide the foundation for calculating KL divergence and constructing the corresponding optimal design.

Before searching for the max-min CKL-optimal design, the structures of the true model $\eta_{tr}(x, \theta_1)$ and the rival model $\eta_2(x, \theta_2)$ must be defined, along with a bounded parameter space for the rival model. It is important to ensure that the rival parameter space is finite. Users can define the range based on prior knowledge or regions where the KL divergence is expected to attain its minimum. If the dispersion of the rival model is to be fixed, this can be achieved by setting its upper and lower bounds to the same value, thereby excluding it from search. The relevant setup is shown in the following code.

Listing B.2: Setting Model Parameters

```
# Set the nominal values for the true model
af1_para <- c(-5, -1.5, 0.05)
model_info <- list(
  # The first list should be the true model and the specified nominal
  # values
  list(mean = af1_mean, disp = af1_disp, meanPara = af1_para, dispPara =
    0.9780103),
  # Then the rival models are listed accordingly. We also need to
  # specify the model space.
  list(mean = af2_mean, disp = af2_disp,
    meanParaLower = c(-100, 0.1), meanParaUpper = c(-10, 5),
    dispParaLower = c(0.9780103), dispParaUpper = c(0.9780103) )
)
```

To perform CKL-optimal design, the divergence measure must be explicitly defined. In this study, the measure is based on the Kullback-Leibler divergence as described in Equation (3.8), and its computation is divided into two parts: one for observed (non-censored) data and another for Type I censored data, assuming a censoring time of $t_c = 5000$.

In the R implementation, three functions are defined to handle these

computations. The `kl_lnl_n_observed` function computes the integral over the observed data, while the `kl_lnl_n_censored` function evaluates the adjustment term for Type I censored data. The `kldiv_lnl_n_censored5000` function combines both components to obtain the overall KL divergence. This framework effectively incorporates both censored and uncensored data contributions, enabling a more accurate evaluation of model discrimination. The corresponding R code is shown below.

Listing B.3: Defining the KL Divergence Function

```
# xt is the mean values of the true model
# xr is the mean values of the rival model
kl_lnl_n_observed <- function(y, m1, m2, s1, s2) {
  lpdf1 <- dlnorm(y, m1, s1, log = TRUE)
  lpdf2 <- dlnorm(y, m2, s2, log = TRUE)
  pdf1 <- exp(lpdf1)
  val <- pdf1*(lpdf1 - lpdf2)
  return(val)
}
kl_lnl_n_censored <- function(y, m1, m2, s1, s2) {
  lcdf1 <- log(1 - plnorm(y, m1, s1) + 1e-12)
  lcdf2 <- log(1 - plnorm(y, m2, s2) + 1e-12)
  cdf1 <- exp(lcdf1)
  val <- cdf1*(lcdf1 - lcdf2)
  return(val)
}
kldiv_lnl_n_censored5000 <- function(xt, xr, st, sr) {
  tc <- 5000
  intVec <- rep(0, length(xt))
  for (i in 1:length(xt)) {
    intg_part <- integrate(kl_lnl_n_observed, 0, tc,
                          m1 = xt[i], m2 = xr[i],
                          s1 = st[i], s2 = sr[i],
                          subdivisions = 100,
                          stop.on.error = FALSE)$value
    cens_part <- kl_lnl_n_censored(tc, m1 = xt[i], m2 = xr[i],
                                   s1 = st[i], s2 = sr[i])
    intVec[i] <- intg_part + cens_part
  }
  return(intVec)
}
```

In this example, we utilize the DiscrimOD software package to perform optimal experimental design searches. As DiscrimOD is currently in the alpha testing phase, it is only available to the development team and

must be installed via a specific method.

Before installation, ensure that you are using R version 3.4.0. Then, install the `devtools` package along with two necessary dependencies: `Rcpp` and `RcppArmadillo`. After setting up these prerequisites, use the `devtools::install_github()` function from the `devtools` package to install `DiscrimOD` directly from Ping-Yang Chen's GitHub repository. The R code is shown below:

Listing B.4: Installing the DiscrimOD Package

```
install.packages(c("devtools", "Rcpp", "RcppArmadillo"))
devtools::install_github("PingYangChen/DiscrimOD")
```

Once the installation is complete, load the package using the `library()` function:

Listing B.5: Loading the DiscrimOD Package

```
library(DiscrimOD)
```

The optimal discrimination design search algorithm in the `DiscrimOD` package involves two types of algorithms, PSO and L-BFGS. The PSO and L-BFGS settings are defined through `getPSOInfo()` function. Here, we list the most influential tuning parameters of PSO below:

- `nSwarm`: The size of the particle swarm. Typically, we set 32 or 64 particles.
- `dsRange`: The number of maximal iterations.
- `IF_INNER_LBFGS`: The logical input TRUE/FALSE to turn on/off the L-BFGS algorithm for the inner optimization problem (minimizing the distance among parameter space). If specified `IF_INNER_LBFGS = FALSE`, the `DiscrimOD` package will run the NestedPSO algorithm in [Chen et al. \(2015\)](#).

- **LBFGS_RETRY**: The maximal times of trails of L-BFGS algorithm. This parameter is used to prevent failures due to poor initial vectors, and it is commonly recommended to set it to 2 or 3 attempts. However, in our simulation studies, we observed inconsistencies between the criterion value C^* and the recomputed value \hat{C} based on the estimated parameters and design, which is suspected to be caused by instability in the inner L-BFGS computation. To improve robustness and consistency of the results, we uniformly set this parameter to 50 in our study.

The codes shown below are the algorithm settings used in this example. First, for PSO-QN algorithm working on discrimination design for two models, we set 64 particles and 200 iterations for PSO, and for each computation for the inner loop, we repeat L-BFGS algorithm 50 times. The remaining settings in both algorithms are set as default values.

Listing B.6: Configuring Algorithm Parameters (PSO and L-BFGS)

```
PSO_INFO <- getPSOInfo(nSwarm = 64, maxIter = 200)
LBFGS_INFO <- getLBFGSInfo(LBFGS_RETRY = 50)
```

Note: Although the main example in this study adopts the L-BFGS method for the inner optimization routine, the DiscrimOD package also supports using Particle Swarm Optimization (PSO) for solving the inner optimization problem. This approach is referred to as the NestedPSO algorithm ([Chen et al., 2015](#)).

To configure the NestedPSO algorithm, each setting in the `getPSOInfo()` function must be a vector of length 2. The first element specifies the configuration for the outer PSO loop, while the second is for the inner loop. For instance, in the example below, 64 particles and 200 iterations are used for the outer loop, and 32 particles and 100 iterations for the inner loop. Most importantly, the L-BFGS algorithm must be dis-

abled when using NestedPSO by setting `IF_INNER_LBFGS = FALSE` in the `getLBFGSInfo()` function. The following code illustrates how to implement this setup (note: not used in the current example, shown for demonstration purposes only):

Listing B.7: Alternative Setup Using NestedPSO

```
# Set NestedPSO options. The length of setting indicates the number of
  loops
NESTEDPSO_INFO <- getPSOInfo(nSwarm = c(64, 32), maxIter = c(200, 100))
# Turn off L-BFGS implementation for the inner optimization loop
LBFGS_NOTRUN <- getLBFGSInfo(IF_INNER_LBFGS = FALSE)
```

Next, we apply the `DiscrimOD()` function and invoke the PSO-QN algorithm to search for the CKL-optimal design for pairwise model discrimination. In this example, we illustrate the procedure using the true model $\eta_{tr}(x, \theta_1)$ versus the rival model $\eta_2(x, \theta_2)$.

In addition to specifying the model list, the divergence function, and the algorithm settings, it is also necessary to define the type of discrimination criterion using the argument `crit_type = "pair_fixed_true"` for pairwise discrimination. Furthermore, the number of support points must be specified (here, `nSupp = 3`), along with the lower and upper bounds of the design space, set as `dsLower = 10` and `dsUpper = 80`, respectively.

Listing B.8: Running DiscrimOD to Obtain the Optimal Design

```
nSupp <- 3
dsRange <- c(10, 80)
res <- DiscrimOD(MODEL_INFO = model_info, DISTANCE = kldiv_lnl_n_
  censored5000,
  nSupp = nSupp, dsLower = dsRange[1], dsUpper = dsRange
    [2],
  crit_type = "pair_fixed_true",
  PSO_INFO = PSO_INFO, LBFGS_INFO = LBFGS_INFO,
  seed = 100, verbose = TRUE)
```

After completing the optimal design search, the `DiscrimOD()` function returns a list object with several key outputs. The three most relevant

fields include:

- Best Design and Weights(\$BESTDESIGN):

This component stores the final design matrix identified by the PSO-QN algorithm. The matrix contains two columns: the first for support points and the second for the associated weights. The R code is shown below:

Listing B.9: Best design and weights

```
round(res$BESTDESIGN, 3)
```

Output:

Listing B.10: The Output of Best design and weights

```
dim_1 weight
obs_1 33.557 0.330
obs_2 56.829 0.436
obs_3 80.000 0.234
```

- Criterion Value(\$BESTVAL):

This is the minimized KL divergence corresponding to the best design. It serves as the criterion value used to evaluate design quality. The R code is shown below:

Listing B.11: KL criterion value of the best design

```
res$BESTVAL
```

Output:

Listing B.12: The Output of KL criterion value of the best design

```
[1] 0.009265602
```

- Computation Time(\$CPUTIME):

This field records the elapsed CPU time (in seconds) during the optimization process, which can be used to assess algorithm efficiency:

Listing B.13: CPU time of the optimization

```
res$CPUTIME
```

Output:

Listing B.14: The Output of CPU time of the optimization

```
elapsed  
42714.86
```

To further examine the accuracy and stability of the identified design, we employ the `designCriterion()` function to recompute the criterion value based on the specified models and parameters, while also obtaining the searched parameters of the rival model.

This function accepts the design result (e.g., `res$BESTDESIGN`), the model configuration (`MODEL_INFO`), the divergence function (`kldiv_lnl_n_censored5000`), the bounds of the design space, the type of discrimination criterion (e.g., `"pair_fixed_true"`), and the optimization settings (`PSO_INFO` and `LBFGS_INFO`).

The output consists of:

- `$cri_val`:

the recomputed criterion value \hat{C} based on the current design and model settings. This value can be compared with the original optimal value C^* to check consistency.

- `$theta2`:

the searched parameters of the rival model obtained under the current design, including both the true and rival model parameter vectors (with the true model often held fixed).

This verification step is crucial for assessing the numerical stability of the optimization process, especially whether parameter search issues may

cause discrepancies in the criterion values. The R code is shown below:

Listing B.15: Verifying Design Stability and Parameter Search

```
designCriterion(res$BESTDESIGN, MODEL_INFO = model_info,
              DISTANCE = kldiv_lnl_n_censored5000,
              dsLower = dsRange[1], dsUpper = dsRange[2],
              crit_type = "pair_fixed_true", MaxMinStdVals = NULL,
              PSO_INFO = PSO_INFO, LBFGS_INFO = LBFGS_INFO)
```

Output:

Listing B.16: The Output of Verifying Design Stability and Parameter Search

```
$cri_val
[1] 0.009265599

$theta2
      [,1] [,2] [,3] [,4]
model_1 -5.000000 -1.500000 0.0500000 0.9780103
model_2 -66.71046 2.016919 0.9780103 0.0000000
```

To verify whether the resulting design is optimal or not, we use the equivalence theorem. In the `DiscrimOD` package, we implement the equivalence function. In this function, we need to input the numerical result object, `res`, obtain by the `DiscrimOD` function. Based on the numerical result, the equivalence function computes the values of directional derivative function on the grid of length `ngrid`. One can plot the curve of the directional derivative function by R utility function `plot`. The x -axis is the grid vector of design space which can be found in the `$Grid_1` tag. The y -axis is the values of directional derivative function in `$DirDeriv` tag. We can also pin the support points on the curve by `points` function. To make a better visualization, we use the horizontal line at $y = 0$ to show the resulting design is CKL-optimal, that is, the values of directional derivative function are smaller than zero, and at the support points, the values should be zero (at least close to zero).

Listing B.17: Equivalence Theorem and Graphical Verification of Optimality

```
eqv <- equivalence(ngrid = 100, PSO_RESULT = res,
  MODEL_INFO = model_info,
  DISTANCE = kldiv_lnl_n_censored5000,
  dsLower = dsRange[1], dsUpper = dsRange[2],
  crit_type = "pair_fixed_true",
  PSO_INFO = PSO_INFO, LBFGS_INFO = LBFGS_INFO)
# Draw the directional derivative curve
plot(eqv$Grid_1, eqv_Arrhenius$DirDeriv, type = "l",
  col = "blue", main = "",
  xlab = "x", ylab = "Directional_Derivative"); abline(h = 0)
points(res$BESTDESIGN[,1], rep(0, nrow(res$BESTDESIGN)), pch = 16)
```

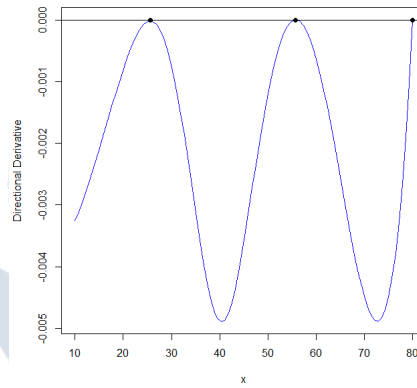


Figure B.1: Directional derivative plot generated from the example code to verify design optimality

Through the above codes and visualizations, we can not only confirm whether the resulting design is optimal but also examine whether the support points correspond to the zero-crossings of the directional derivative. This procedure plays a crucial role in verifying the correctness and numerical stability of the design, thereby enhancing the reliability of model discrimination.

Appendix C

Demonstration of the Shiny Interface

This appendix presents the R Shiny user interface developed for this study, which serves as an interactive platform to configure model discrimination designs, execute optimization routines, and interpret results. The interface design aligns closely with the simulation settings discussed throughout earlier chapters, allowing users to flexibly adjust design conditions based on various modeling assumptions and objectives.

The interface supports an intuitive workflow that enables configuration of key elements such as divergence criteria, model distribution assumptions, parameter ranges, and algorithm-specific settings.

The full Shiny source code used in this study is openly available at: [GitHub/GPLIN514](#). Additionally, an online interactive version is hosted on `shinyapps.io`, allowing users to directly access and explore the interface without local setup: [shinyapps.io/MSGPLIN](#).

The following provides a walkthrough of the interface's core components, supported by screenshots to demonstrate how each element contributes to the model discrimination design and evaluation process.

Kuan-Yuan Lin
Department of Statistics, National Taipei University, Taiwan

MMM vs. MM under pharmacokinetic model (López-Fidalgo et al., 2007)

◊ Maintainer: Kuan-Yuan Lin (a0921129003@gmail.com)

108

Figure C.1 displays the Shiny interface designed based on the simulation setup in Section 4.1. The following describes each configuration item, with the red box highlighting the user-defined input area:

1. Model Structure (Preloaded):

The interface preloads the mathematical structures of the two competing models to help users align the required parameter settings below.

2. Divergence Calculation Method:

As shown in Figure C.2, users can choose between a closed-form solution and numerical integration for computing the objective function.

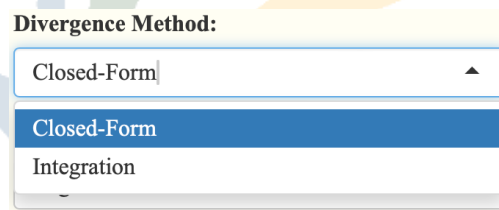


Figure C.2: Divergence calculation method selection

3. Distribution Assumption:

As illustrated in Figure C.3, users can specify whether both models follow a Log-Normal or Weibull distribution.

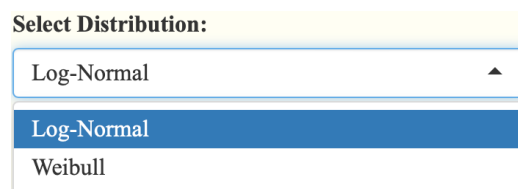


Figure C.3: Distribution assumption selection

4. Design Space Settings:

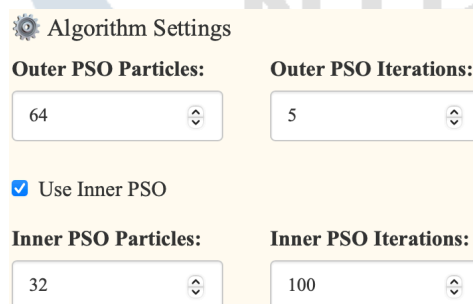
Users define the number of support points in the approximation design and adjust the bounds of the design variable.

5. Parameter Settings:

The true model parameters are specified directly by the user, based on prior knowledge or expert input, while ranges are provided for the rival model. By default, the variance is assumed to be the same for both models, but users may modify this setting if needed.

6. Algorithm Configuration:

The outer loop uses Particle Swarm Optimization (PSO), requiring the number of particles and iterations. The inner loop is set by default to use the L-BFGS method, where users must specify the number of repetitions. If the Use Inner PSO option is selected (as shown in Figure C.4), the inner optimization will switch to PSO, and an additional set of particle and iteration settings will be required.



The image shows a dialog box titled "Algorithm Settings" with a gear icon. It contains four input fields and one checkbox. The "Outer PSO Particles" field is set to 64, and the "Outer PSO Iterations" field is set to 5. The "Use Inner PSO" checkbox is checked. The "Inner PSO Particles" field is set to 32, and the "Inner PSO Iterations" field is set to 100. The fields are arranged in a 2x2 grid, with the checkbox centered below the top row.

Algorithm Settings	
Outer PSO Particles:	Outer PSO Iterations:
64	5
<input checked="" type="checkbox"/> Use Inner PSO	
Inner PSO Particles:	Inner PSO Iterations:
32	100

Figure C.4: Algorithm configuration options

The area highlighted by the blue box represents the output results generated by the algorithm. The meaning of each section is described below:

1. Approximation Design: This part lists the final optimal design configuration, including the locations of the support points and their

corresponding weights. These constitute the approximation design ξ^* .

2. Criterion Value and CPU Time: This part presents the criterion value (C^*) associated with the design, as well as the total computation time (in seconds) required to obtain it. This information is used to assess the efficiency and performance of the optimization algorithm.

3. Searched Parameter Values:

Since the adopted model discrimination design follows a maximin structure—finding the design that maximizes the criterion under the worst-case (minimum) parameter setting—the searched parameter combination is critical for understanding the behavior and robustness of the obtained design.

4. Directional Derivative Plot:

To verify whether the selected design satisfies the optimality conditions, a directional derivative plot is generated. This plot helps confirm whether the support points correspond to the local maxima of the function and whether the curve remains entirely below 0, as required by the equivalence theorem.

Additionally, if the Setting tab is selected, users can view the inputs they manually configured during the current analysis—such as model assumptions, parameter ranges, and algorithm settings—as shown in Figure C.5. Please note that default system values are not displayed in this section.

Setting	Value
Outer PSO Particles	64
Outer PSO Iterations	5
Use Inner PSO	FALSE
Inner PSO Particles	N/A
Inner PSO Iterations	N/A
BFGS Retries	2
Support Points	3
Design Bounds	[0.1, 5]
True Model Parameters	(1, 1, 1)
Model Dispersion	1

Figure C.5: Summary table of User-Defined settings

Finally, several interface components in the Arrhenius and Meeker tabs differ from Fidalgo tab. The following explains their unique settings:

- Censoring Threshold Setting (both tabs): This input corresponds to the Type I censoring scenario, which addresses situations where some products have not failed by the end of the test. Users can specify the censoring threshold directly, as shown in Figure C.6.

Censoring Threshold Setting

Censoring Threshold (tc):

5000

Figure C.6: Censoring threshold configuration

- Divergence Method (Arrhenius tab only): This dropdown menu allows users to choose among four divergence criteria: KL diver-

gence, LW divergence, Bhattacharyya distance, and Chi-square distance. These options enable flexibility for various modeling goals. The options are shown in Figure C.7. For the Meeker tab, the divergence method is pre-set to KL divergence and cannot be changed.

Divergence Method:

KL Divergence ▲

KL Divergence

LW Divergence

Bhattacharyya Distance

Chi-square Distance

Figure C.7: Selection of divergence criteria in Arrhenius tab

- **Model Distribution Assumptions (Meeker tab only):** In this case, the aim is to evaluate the identifiability of two models with the same structural form but different distributional assumptions. Therefore, users can only specify the distribution for the true model (Log-Normal or Weibull), while the rival model's distribution is automatically assigned to be the other type. See Figure C.8 for examples.

Select Model Distributions

True Model: Log-Normal ▼ **Rival Model:** Weibull ▼

(a) True model follow Log-Normal distribution

Select Model Distributions

True Model: Weibull ▼ **Rival Model:** Log-Normal ▼

(b) True model follow Weibull distribution

Figure C.8: Model distribution options in Meeker tab



著作權聲明

論文題目：以合成最佳化演算法生成加速壽命試驗之模型辨識設計

論文頁數：115 頁

系所組別：統計學系

研究生：林貫原

指導教授：陳秉洋

畢業年月：一一四年六月

本論文著作權為林貫原所有，並受中華民國著作權法保護。

